UNIVERSIDADE FEDERAL DE SANTA CATARINA
CENTRO TECNOLÓGICO
PROGRAMA DE PÓS-GRADUAÇÃO EM CIÊNCIA E ENGENHARIA DE MATERIAIS

Bianca Constante Guedert

A COMPARATIVE ASSESSMENT OF BIOACTIVE GLASSES 45S5, S53P4, 58S AND MBG 58S: PHYSICAL, CHEMICAL, BIOACTIVE, AND BIOLOGICAL PROPERTIES

Florianópolis
2023

Bianca Constante Guedert

A comparative assessment of bioactive glasses 45S5, S53P4, 58s and MBG 58S: Physical, chemical, bioactive, and biological properties

Master thesis presented to the Graduate Program in Materials Science and Engineering at the Federal University of Santa Catarina, as a requirement to obtain a master's degree in Materials Science and Engineering, concentration area: ceramics.

Advisor: Prof. Bruno Alexandre P. C. Henriques, Dr.

Florianópolis

2023

Guedert, Bianca Constante
A comparative assessment of bioactive glasses 45S5, S53P4, 58s and MBG 58S : Physical, chemical, bioactive, and biological properties / Bianca Constante Guedert ; orientador, Bruno Alexandre Pacheco de Castro Henriques, 2023.
105 p.

Dissertação (mestrado) - Universidade Federal de Santa Catarina, Centro Tecnológico, Programa de Pós-Graduação em Ciência e Engenharia de Materiais, Florianópolis, 2023.

Inclui referências.

1. Ciência e Engenharia de Materiais. 2. Vidros bioativos. 3. Regeneração óssea. I. Henriques, Bruno Alexandre Pacheco de Castro . II. Universidade Federal de Santa Catarina. Programa de Pós-Graduação em Ciência e Engenharia de Materiais. III. Título.

Bianca Constante Guedert

A comparative assessment of bioactive glasses 45S5, S53P4, 58S and MBG 58S: Physical, chemical, bioactive, and biological properties

The present work at the Master's level was evaluated and approved on August 21, 2023, by the examining board composed of the following members:

Prof.(a) Sabrina Arcaro, Dr.(a)
South Extremity University of Santa Catarina, UNESC

Prof. Antonio Pedro Novaes de Oliveira, Dr.Ing.
Federal University of Santa Catarina, UFSC

We certify that this is the original and final version of the conclusion paper, which has been deemed suitable for obtaining the Master's degree in Materials Science and Engineering

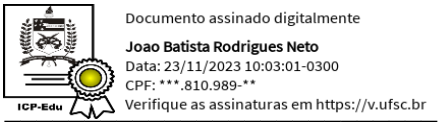

Coordination of the Graduate Program in Materials Science and Engineering

_____

Prof. Bruno Alexandre P. C. Henriques, Dr.
Advisor

Florianópolis, 2023.

Dedicated to all those who have suffered due to COVID-19.

ACKNOWLEDGEMENT

I thank, first and foremost, all those who indirectly encourage the pursuit of knowledge through research and science, and who believe in the progress these fields provide. To those who maintained hope and persevered through the challenging periods faced throughout the development of this work, by my side and enduring a tragedy that spanned two long years of this journey, demanding adaptation, and the hope for better times ahead. I extend my gratitude especially to my partner, Matheus Leite Dettmar.

I also thank my family - my mother, Luciani Farias Constante; my grandmother, Maria da Glória Constante; my mother-in-law, Ana Cristina Leite; the women in my life - and my brothers, Patrick Constante Guedert and Nicolas Constante Guedert, for being present and for all the encouragement, assistance, and support in this phase of my life, as well as in all others. I am grateful to have you in my life.

My thanks also go to old friends and those who crossed my path, remaining in my support network during moments of leisure and exchange, making the journey lighter. I thank Bianca Vieira, Bruno Ribas, Carlos Alexandre, Duda Movimenta, Eli Batista, Felix Li Han Huang, Francielle Pinheiro, Gabriel Bernardo, Gabriel Campos, Gabriela Eller, Jaciara de Melo, Laura Ma, Letícia Sampaio, Luis Schiavo, Morgana Machado, and Rodrigo Neves.

I also thank everyone from Mutama, School of Movement and Expression, for their welcome and teachings.

I would also like to express my gratitude to Professor Bruno Henriques for the opportunity, trust, and support provided to me during the execution of this work. To my colleague Rafael Matos, my appreciation for his willingness, commitment, and clarifications that greatly contributed to this research.

I am thankful to the Graduate Program in Materials Science and Engineering and to the University for the opportunity granted. Finally, my thanks to CAPES and CNPq for the encouragement and support of scientific development programs that enabled the realization of the CNPq/INOVA/441457/2018-5 project "Development of Bioactive Glasses for Application in Bone Defects," as well as this work.

AGRADECIMENTOS

Agradeço, em primeiro lugar, a todos aqueles que indiretamente incentivam a busca pelo conhecimento por meio da pesquisa e da ciência, e que acreditam nos progressos que esses campos proporcionam. Aos que mantiveram a esperança e perseveraram durante os períodos difíceis enfrentados ao longo do desenvolvimento deste trabalho, ao meu lado e resistindo a uma tragédia que atravessou dois longos anos desta jornada, exigindo readaptação e a esperança de tempos melhores que estavam por vir. Agradeço especialmente ao meu companheiro, Matheus Leite Dettmar.

Agradeço também à minha família - minha mãe, Luciani Farias Constante; minha avó, Maria da Glória Constante; minha sogra, Ana Cristina Leite; as mulheres da minha vida - e a meus irmãos, Patrick Constante Guedert e Nicolas Constante Guedert, por estarem presentes e por todo o incentivo, auxílio e apoio nesta etapa da minha vida, assim como em todas as outras. Sou grata por tê-los em minha vida.

Meus agradecimentos se estendem aos amigos antigos e aqueles que cruzaram o meu caminho, permanecendo em minha rede de apoio nos momentos de descontração e trocas, tornando o trajeto mais leve. Agradeço a Bianca Vieira, Bruno Ribas, Carlos Alexandre, Duda Movimenta, Eli Batista, Felix Li Han Huang, Francielle Pinheiro, Gabriel Bernardo, Gabriel Campos, Gabriela Eller, Jaciara de Melo, Laura Ma, Letícia Sampaio, Luis Schiavo, Morgana Machado e Rodrigo Neves.

Agradeço também a todos da Mutama, escola de movimento e expressão pelo acolhimento e ensinamentos.

Gostaria de expressar também meus agradecimentos ao Professor Bruno Henriques pela oportunidade, confiança e apoio proporcionados a mim durante a realização deste trabalho. Ao colega de trabalho Rafael Matos, minha gratidão por sua disposição, comprometimento e esclarecimentos que muito contribuíram para esta pesquisa.

Agradeço ao Programa de Pós-Graduação em Ciência e Engenharia de Materiais e à Universidade pela oportunidade concedida. Por fim, meus agradecimentos à CAPES e ao CNPq pelo estímulo e suporte aos programas de desenvolvimento científico que possibilitaram a concretização do projeto CNPq/INOVA/441457/2018-5 "Desenvolvimento de Vidros Bioativos para Aplicação em Defeitos Ósseos", assim como deste trabalho.

“Quero ser apenas um entre os milhões de brasileiros que resistem.
Não tenho tempo para ter medo.”
Marighella, Carlos.

ABSTRACT

Bioactive glasses (BG) have been investigated as synthetic grafts for bone regeneration due to their favorable osteoconductive, angiogenic, osteogenic, and antibacterial properties. These traits are inherently connected to their chemical composition and morphology, and traditional methods for producing bioglasses include melting and sol-gel processes. The purpose of this work was to conduct a systematic review providing an overview of the *in vivo* application of various compositions of bioactive glasses as grafts for critical bone defects, along with evaluating the chemical reactivity of four different bioactive glasses: BG 45S5 and S53P4 produced through the melt-derived process, and BG 58S and Mesoporous 58S through the sol-gel technique. The literature review followed the Preferred Reporting Items for Systematic Reviews and Meta-Analyses (PRISMA) guidelines and covered articles published until April 30, 2023, in two electronic databases: PubMed/Medline and Web of Science. Among the 20 included papers, a total of 547 animal subjects (433 rats and 107 rabbits) were enrolled in the *in vivo* studies, with an average follow-up period of 12 weeks. Two main groups of bioactive glasses were identified: scaffolds (13 studies) and particles (7 studies). For the laboratory analysis, samples underwent physicochemical characterization using SEM and N_2 adsorption/desorption analysis for MBG powder. Chemical reactivity was assessed through SEM, EDS, FTIR, and Ca/P analysis after immersion in simulated body fluid (SBF) for 8, 24, and 72 h. MBG particles displayed a pore volume of 0.20 cm^3/g, a pore diameter of approximately 14.29 nm, and a surface area of 77.20 m^2/g, as determined by BJH and BET analyses. All samples exhibited the anticipated chemical composition and exhibited notable Si wt.% loss and significant P wt.% increase after 72 h of SBF immersion. After 72 h in SBF, all samples achieved a Ca/P ratio of approximately 2.00, closely aligning with the reference value of the non-stoichiometric biological apatite molar ratio of 1.67 Ca/P. Biological behavior was evaluated using the MTS metabolic assay, and cell viability was assessed using the murine fibroblast cell line L929 over 24, 48, and 72 h. The biological tests revealed a non-cytotoxic behavior for the melt-derived bioactive glasses, whereas the sol-gel-derived bioactive glasses suggest a concentration and time-dependent cytotoxic behavior.

Keywords: Bioactive glass, bioglass, melt-derived, sol-gel

RESUMO EXPANDIDO

A comparative assessment of bioactive glasses 45S5, S53P4, 58S and MBG 58S: Physical, chemical, bioactive, and biological properties

Introdução

Quando defeitos ósseos ultrapassam 2 a 2,5 vezes o diâmetro do osso afetado, a capacidade regenerativa diminui, apresentando desafios na reparação tecidual. Esses defeitos significativos frequentemente resultam de traumas, ressecções tumorais e infecções [1]. Globalmente, os defeitos relacionados a tumores atingem 3,4 milhões de casos anualmente [2], enfatizando a necessidade de abordar a regeneração óssea comprometida. Conforme a população envelhece, tratamentos eficazes para defeitos ósseos ganham maior importância, especialmente para os idosos, que enfrentam questões relacionadas a ossos. Tratar defeitos ósseos grandes, especialmente com danos nos tecidos, permanece um desafio; os enxertos autólogos são o "padrão-ouro" para a cicatrização de fraturas, mas a disponibilidade é uma preocupação [3]. Biomateriais sintéticos, como os vidros bioativos (BGs), oferecem uma solução como enxertos ósseos. O pioneiro 45S5 Bioglass®, com base em composição pertencente ao sistema Na_2O-CaO-SiO_2, tem sido amplamente utilizado, e diversas outras composições de vidros bioativos surgiram [4,5]. Vidros bioativos obtidos por meio de processos de fusão, como os vidros 45S5 e S53P4, possuem boas propriedades mecânicas [6–8]. Vidros obtidos via sol-gel apresentam rápida formação de camada de apatita em exposição a fluido corporal simulado [9–11]. O vidro 58S apresenta melhor biodegradação e liberação de íons, enquanto os Vidros Bioativos Mesoporosos (MBV) 58S oferecem potencial em entrega de medicamentos e engenharia de tecidos [12–15]. A dissolução da rede de vidro, formando uma camada rica em sílica e deposição de apatita-similar, promove a ligação entre vidro e tecido [10]. A avaliação *in vitro* possui limitações para simular condições *in vivo*, mas continua valiosa para estudos preliminares de biomateriais [16]. Modelos animais de defeitos ósseos oferecem insights sob diversas condições, auxiliando na integração de implantes e comparações antes de estudos *in vivo* [17]. A pesquisa é crucial para o desenvolvimento de biomateriais adaptados a esses desafios, melhorando a assistência médica e avançando na medicina regenerativa [3].

Objetivos

Este estudo tem como objetivo produzir quatro composições distintas de vidros bioativos e avaliar suas propriedades físicas e químicas, bioativas e biológicas. Para atender o objetivo geral foram definidos alguns objetivos específicos:

- Produzir vidros bioativos de composições contendo 45% em massa de SiO_2, 24,5% em massa de Na_2O, 24,5% em massa de CaO, 6% em massa de P_2O_5 (45S5), 53% em massa de SiO_2, 23% em massa de Na_2O, 20% em massa de CaO, 4% em massa de P_2O_5 (S53P4), 58% em massa de SiO_2, 33% em massa de CaO, 9% em massa de P_2O_5 (BG 58S e MBG 58S) através dos métodos de fusão e sol-gel para verificar a viabilidade de produção desses materiais e servir como matéria prima para os objetivos seguintes.
- Analisar as propriedades físicas e químicas, a estrutura e a microestrutura dos vidros produzidos utilizando técnicas como microscopia eletrônica de varredura (MEV), espectrômetro de raios X por dispersão de energia (EDS), difração de raios X (DRX), espectroscopia de infravermelho por transformada de Fourier (FTIR), microscopia óptica de aquecimento, dispersão laser de partículas e densidade por picnometria para todas as composições buscando entender melhor o comportamento desses materiais e comparar os resultados obtidos nas diferentes rotas de processamento (fusão e sol-gel).
- Investigar o comportamento bioativo dos vidros produzidos a partir da formação de camada de hidroxiapatita (HA) em contato com fluido corporal simulado por 8, 24 e 72 horas para determinar a capacidade de formação dessa camada e posterior análise morfológica da camada obtida.
- Avaliar o comportamento biológico por meio de análises de biocompatibilidade, adesão celular e bioatividade para compreender o comportamento dos vidros quando em contato com células.

Metodologia

O presente trabalho foi estruturado em quatro capítulos. O primeiro capítulo abrange uma introdução aos temas relevantes relacionados ao estudo. O segundo capítulo, intitulado "Literature review – *In vivo* evaluation of bioactive glasses applied to large bone defects: where are we?" a qual consiste em uma revisão sistemática da literatura que descreve o panorama atual da avaliação *in vivo* dos vidros bioativos, com foco na sua aplicação em grandes defeitos ósseos. A pesquisa abrangeu o período até 2023 e foi conduzida seguindo as diretrizes da "Preferred Reporting Items for Systematic Reviews and Meta-Analyses" (PRISMA). Foi realizada uma busca abrangente em duas bases de dados eletrônicas, PubMed/Medline e Web of Science, utilizando diversas combinações de termos relevantes. Os critérios de inclusão abarcaram artigos em inglês publicados até 30 de abril de 2023, que reportassem a aplicação *in vivo* de vidros bioativos como enxertos para defeitos ósseos. Após uma seleção minuciosa dos dados utilizando o Mendeley como gerenciador de referências, um total de 20 estudos foram

incluídos e utilizados como base para esta revisão. O terceiro capítulo, intitulado "A comparative assessment of bioactive glasses 45S5, S53P4, 58S and MBG 58S: Physical, chemical, bioactive and biological properties", aborda o desenvolvimento de quatro composições distintas de vidros bioativos denominados 45S5, S53P4, 58S e MBG 58S, derivados tanto da rota de fusão quanto da rota sol-gel. As propriedades físicas e químicas foram caracterizadas por meio de microscopia eletrônica de varredura (MEV), espectrômetro de raios X com dispersão de energia (EDS), difração de raios X (DRX), espectroscopia de infravermelho por transformada de Fourier (FTIR), microscopia óptica de aquecimento, dispersão laser de partículas e densidade por picnometria. A bioatividade foi analisada pela capacidade de formação de camada de HA quando em contato com fluido corporal simulado (SBF) por 8, 24 e 72 h, enquanto o comportamento biológico foi avaliado por meio de medidas colorimétricas (espectrofotometria, MTS), utilizando a linhagem celular de fibroblastos murinos L929 por 24, 48 e 72 h. Por fim, o quinto e último capítulo apresenta as conclusões gerais e as perspectivas para trabalhos futuros.

Resultados e Discussão

Os vidros bioativos têm sido explorados como enxertos sintéticos para a regeneração óssea devido às suas propriedades osteocondutoras, angiogênicas, osteogênicas e antibacterianas, ligadas à sua composição química e morfologia. O primeiro capítulo apresenta uma revisão abrangente composta por 20 artigos relevantes que reportam as aplicações *in vivo* dos vidros bioativos. A busca inicial resultou em 234 artigos, que foram refinados para 221 após a remoção de duplicatas. Após a triagem de títulos e resumos, 131 artigos foram excluídos, restando 90 para avaliação em texto completo. Desses, 70 artigos foram posteriormente excluídos, resultando na seleção final de 20 artigos. Os estudos *in vivo* envolveram 547 sujeitos animais (433 ratos e 107 coelhos) com um período médio de acompanhamento de 12 semanas. Os defeitos ósseos induzidos variaram, tendo como alvos predominantes o fêmur dos animais (11 estudos) e a região da calvária (7 estudos). A revisão classificou as pesquisas em duas categorias principais: scaffolds (13 estudos) e partículas (7 estudos). A revisão fornece um panorama atual sobre estudos *in vivo* dos vidros bioativos para a regeneração óssea, enfatizando o uso prevalente de ratos e coelhos nestes testes e a importância de explorar modelos alternativos que sejam mais próximos as condições humanas. Além disso, ela reforça a confiabilidade de testes *in vitro* na previsão do comportamento *in vivo* desses materiais. O capítulo dois envolve uma análise extensa das composições nomeadas 45S5, S53P4, 58S e MBG 58S, revelando que todas atingiram os resultados esperados. A reatividade química foi avaliada usando MEV, EDS, FTIR

e análise de Ca/P após imersão em fluido corporal simulado (SBF) por 8, 24 e 72 h. As análises BJH e BET revelaram que as partículas de MBG exibiram um volume de poros de 0,20 cm^3/g, diâmetro de poro em torno de 14,29 nm e área de superfície específica de 77,20 m^2/g. Todas as amostras exibiram a composição química esperada, perda de Si (% em massa) e aumento significativo de P (% em massa) após imersão durante 72 h em SBF. As amostras alcançaram uma relação Ca/P de aproximadamente 2,00 após 72 h, se aproximando do valor de referência, isto é, da relação molar de apatita biológica não estequiométrica (1,67 Ca/P). Os testes biológicos revelaram um comportamento não citotóxico para os biovidros derivados da rota de fusão, enquanto os biovidros derivados da rota sol-gel sugerem um comportamento citotóxico dependente da concentração e do tempo.

Considerações Finais

É necessário ter uma compreensão abrangente das propriedades dos vidros bioativos para atender às necessidades de ligação de tecidos e suas aplicações específicas. Vidros bioativos têm sido desenvolvidos para atender a essas necessidades, o que exige um entendimento mais detalhado de suas propriedades para aplicações específicas e fabricação de produtos. Para lidar com as complexas e imprevisíveis condições de carga, foram desenvolvidas estruturas 3D. Otimizações foram desenvolvidas para aplicações locais de fármacos, incorporando vidros bioativos com medicamentos ou até mesmo uma combinação de ambas as aplicações, desenvolvendo estruturas 3D revestidas com biovidros. A seleção da composição do vidro requer um profundo entendimento de como os principais componentes influenciam propriedades relevantes, considerando tanto o uso final quanto a fabricação. Estudos *in vitro* oferecem um meio confiável para prever o comportamento do vidro bioativo *in vivo*. Apesar das limitações estudos *in vivo* em modelos animais adequados para conectar aplicações pré-clínicas e clínicas devem ser melhor explorados. Este estudo apresenta uma revisão sistemática detalhada de cenários de avaliação *in vivo* para vidros bioativos, com foco em defeitos ósseos críticos. Além disso, uma análise comparativa de quatro vidros bioativos distintos, 45S 5, S53P4, 58S e MBG 58S produzidos por fusão e por sol-gel foi conduzida. Todas as composições mostraram capacidade de desenvolver uma camada de hidroxiapatita (HCAp) e apresentaram resultados biológicos positivos, como não citotoxicidade *in vitro*. No entanto, investigações adicionais são essenciais para avaliar o comportamento de dissolução e conduzir estudos *in vivo* para um entendimento mais abrangente.

Palavras-chave: vidros bioativos, biovidros, fusão, sol-gel, *in vitro*, *in vivo*, hidroxiapatita.

LISTA DE FIGURAS

LISTA DE TABELAS

TABLE OF CONTENTS

CHAPTER 1– INTRODUCTION AND OBJECTIVES

1.1 INTRODUCTION

When bone defects surpass 2 - 2.5 times the diameter of the affected bone, bone tissue's regenerative capacity diminishes, posing tissue repair challenges. These substantial defects often result from high-energy trauma, aggressive tumor resections, and bone infections [1]. Globally, the incidence of tumor-related defects annually reaches 3.4 million cases [2], emphasizing the importance of addressing compromised bone regeneration.

As the population ages, effective bone defect treatments gain greater significance. The elderly are particularly vulnerable to bone-related issues, highlighting the need for advanced restoration and repair strategies. Research in this context is crucial, driving the development of biomaterials tailored to these specific challenges. These endeavors enhance healthcare for the aging population and contribute to broader regenerative medicine [4].

The treatment of large bone defects, especially those involving significant soft tissue damage, remains a challenge. Autografts are considered the "gold standard" for fracture healing, yet their availability remains a concern [3]. The pursuit of healthcare materials and devices has led to significant biomaterial development, with biomaterials defined as substances, whether synthetic or natural, used to treat, enhance, or replace tissues, organs, or body functions [18].

Among synthetic biomaterials used as bone grafts, bioactive glasses (BGs) stand out for their biodegradability. Discovered by Larry Hench in 1969, they were the first materials to chemically bond with bone, creating stable and active implants that facilitate the healthy restoration of damaged bone tissue [4,5]. The pioneering BG, referred to as 45S5, is based on the Na_2O-CaO-SiO_2 ternary system. Over approximately three decades, FDA approved from 1985 to 2016, 45S5 Bioglass® which was implanted in 1.5 million patients to repair bone and dental defects [5]. Over time, numerous other bioactive glass compositions have emerged, proposed for innovative biomedical applications, including soft tissue repair and drug delivery [19].

The melt-derived route, a well-established method, produced compositions like 45S5 and S53P4 bioglass, developed in the 1990s, with heightened silica content, improved mechanical properties, and heightened bioactivity [6–8]. Moreover, textural attributes' influence on bioactivity gained prominence with sol-gel-derived bioactive glasses, leveraging the porous nature for superior bioactivity compared to melt-derived counterparts [20,21]. Rapid apatite layer development on sol-gel glasses in various systems upon simulated body fluid exposure is well-

documented [9–11]. Sol-gel technique offers benefits like lower processing temperatures and improved control over textural traits. In this context, 58S bioglass emerged, marked by enhanced biodegradation and ion release [22–24]. Additionally, Mesoporous Bioactive Glasses (MBG) 58S, recognized for their unique mesoporous structure, exhibit potential in drug delivery and tissue engineering [12–15].

The dissolution of the glass network, resulting in the formation of a silica-rich gel layer and subsequent apatite-like layer deposition, is integral to establishing a bond between glass and living tissue *in vivo* [25]. This phenomenon is also observed in *in vitro* tests, in which bioactive glasses immersed in simulated body fluids display similar behavior [25]. The degree of bioactivity, indicated by apatite layer formation rate and thickness, depends on the glass's chemical composition and morphological traits, including surface area, pore size, and pore volume [20,21].

In vitro assessment of biomaterials is limited by the simplified *in vitro* environment, lacking immune and inflammatory responses present *in vivo*. These limitations include interactions with blood components, clot formation, vascularization, and recruitment of wound-healing-related cells [26]. Moreover, *in vitro* studies tend to overestimate material toxicity and address only acute toxicity effects due to the limited lifespan of cultured cells [17]. However, they serve as preliminary steps before *in vivo* studies, aiding understanding of implant integration and initial biomaterial comparisons. Extensively reviewed bone defect animal models facilitate biomaterial research, enabling evaluation under diverse conditions [17]. Selection of a suitable test species considers physiological similarities to humans, controllability, adherence to international standards, costs, availability, acceptability, durability, and housing ease [16].

This work is part of a national health innovation project within regenerative medicine, under the CNPq/INOVA/441457/2018-5 initiative. The project aims to develop diverse bioactive glass compositions for treating large bone defects. Aligned with the pressing need to address bone-related challenges in an aging population, this study explores advanced solutions through an extensive material examination. It reviews *in vivo* assessments of bioactive glasses for critical bone defects and conducts a comparative analysis of four bioactive glasses—45S5, S53P4, 58S, and MBG 58S—in a dual-focused approach.

The primary objective of this research is to address the evolving trends in the application of bioactive glass, marking the first-time comprehensive literature review of in vivo bioactive glass development. By identifying trends and limitations, it aims to provide novel insights into the evolving utilization of biomaterials. This research also furnishes literature support for the produced bioactive glasses and offers a comprehensive assessment of their

viability for national development. This work is motivated by the need to enhance our understanding of the properties and limitations associated with bioactive glasses.

1.2 RESEARCH OBJECTIVES

This work aims to produce four different compositions of bioactive glasses and evaluate their physical, chemical, bioactive, and biological properties. In order to meet the general objective, the following specific objectives were defined:

- To produce bioactive glasses with the following compositions: 45wt.% SiO_2, 24.5wt.% Na_2O, 24.5wt.% CaO, 6wt.% P_2O_5 (45S5), 53wt.% SiO_2, 23wt.% Na_2O, 20wt.% CaO, 4wt.% P_2O_5 (S53P4), 58wt.% SiO_2, 33wt.% CaO, 9wt.% P_2O_5 (BG 58S and MBG 58S) through melting and sol-gel routes to verify the production feasibility of these materials and serve as raw material for the subsequent objectives;
- To characterize the physical and chemical properties of the produced glass compositions using techniques such as scanning electron microscopy (SEM), X-ray diffraction (XRD), Fourier-transform infrared spectroscopy (FTIR), optical heating microscopy, particle size analysis (Laser Diffraction), and density for all compositions to gain a better understanding of the behavior of these materials and compare the results obtained from different processing routes (melting and sol-gel);
- To investigate the bioactive behavior through hydroxyapatite (HAp) layer formation when in contact with simulated body fluid for 8, 24, and 72 h to determine the capability of forming this layer and conduct subsequent morphological analysis of the obtained layer.
- To evaluate the biological behavior of the produced glasses through biocompatibility analysis according to ISO 10.993/5 to comprehend the behavior of the glasses when in contact with cells.

1.3 THESIS STRUCTURE

This thesis is organized into four chapters. Chapter 1 is related to an introduction to pertinent topics concerned to this work. Chapter 2 provides a comprehensive literature review that delves into the *in vivo* application of bioactive glasses for critical bone defects. The research section is housed in Chapter 3, which is further divided into the following segments: introduction, materials and methods, results, discussion, and conclusions. In this case, four different bioactive glasses were synthesized, i.e., 45S5 and S53P4 produced by the melt-derived process, and 58S and MBG 58S produced by the sol-gel method.

These glasses were systematically evaluated to compare their physical, chemical, bioactive, and biological properties. The references are consolidated at the end of this document. Finally, Chapter 4 describes general conclusions and offers insights into possible directions for future research on topics of scientific and technological interest.

CHAPTER 2 – LITERATURE REVIEW – *IN VIVO* EVALUATION OF BIOACTIVE GLASSES APPLIED TO LARGE BONE DEFECTS: WHERE ARE WE?

2.1 INTRODUCTION

Bone is a highly specialized connective tissue with remarkable remodeling and regenerative capabilities. It has the inherent capacity to heal fractures and bone defects, particularly in younger individuals, often without the need for extensive interventions. However, when the defect exceeds 2-2.5 times the diameter of the affected bone, the body's ability to repair the damaged tissue is overwhelmed. Large bone defects commonly result from high-energy trauma, infected bones, or the resection of aggressive tumors [1]. The global incidence of the latter is approximately 3.4 million individuals per year [2]. The treatment of large bone defects, especially those involving significant soft tissue damage, remains a challenge. A critical bone defect is characterized as a type of bone damage or loss that fails to achieve substantial healing, with less than 10% new bone formation occurring within the expected lifespan of the patient [26]. In this context, tissue engineering (TE) has emerged as a potential alternative for repairing such defects.

Autografts continue to be the "gold standard" for fracture healing, but their availability remains a concern. Research in the search for materials and devices applicable to healthcare has significantly increased in recent years, stimulating the development of biomaterials. Biomaterials can be defined as any synthetic or natural substance or combinations thereof that can be used, either completely or partially, for a period as part of a system that treats, enhances, or replaces any tissue, organ, or body function [18].

One widely used synthetic biomaterial for bone grafting is bioactive glasses (BGs), which are biodegradable and were first discovered by Larry Hench in 1969. They were the first materials to form a chemical bond with bone, resulting in stable and active implants that promote the healthy restoration of damaged bone tissues[4]. The first bioactive glass, known as 45S5, has a ternary composition belonging to the Na_2O-CaO-Si_2O system which has been implanted in 1.5 million patients for bone and dental defect repair between 1985 (FDA approval) and 2016 [5]. Over the years, numerous other compositions of bioactive glasses have been proposed for innovative biomedical applications, such as soft tissue repair and drug delivery [19].

The "bioreactivity" of bioactive glasses, characterized by their ability to partially dissolve in physiological solutions and release ions, has attracted research related to drug

administration. Furthermore, the incorporation of biological molecules that stimulate cell differentiation and proliferation enhances the osteogenic potential bioglasses [27–29]. Growth factors such as bone morphogenetic proteins (BMPs), transforming growth factor-β (TGF-β), platelet-derived growth factor (PDGF), vascular endothelial growth factor (VEGF), and insulin-like growth factors (IGF), when applied in conjunction with bioactive glass, can enhance the bone formation ability [28].

In vitro evaluation of biomaterials is subject to specific limitations due to the reduced complexity of the *in vitro* environment. *In vitro* studies lack immune and inflammatory responses observed *in vivo*, including interactions with blood components, clot formation, vascularization, and recruitment of various cells involved in the wound healing response [26]. Moreover, *in vitro* studies often overestimate material toxicity levels and are limited to investigating acute toxicity effects due to the relatively short lifespan of cultured cells [17]. Nevertheless, *in vitro* studies are frequently performed as a preliminary step before conducting *in vivo* studies, aiming to better understand the future integration of implants and provide an initial comparison between biomaterials.

Bone defect animal models have been extensively discussed and reviewed in the literature for biomaterials research [17]. *In vivo* animal models allow the assessment of biomaterials under different loading conditions, over extended durations, and in different tissue qualities (e.g., normal healthy or osteogenic bone) and ages. The selection of a specific animal species as a testing model should consider several factors, including physiological and pathophysiological resemblances to humans, controllability for observation and operation of various post-surgery testing criteria within a relatively short timeframe, adherence to international standards regarding implant size, number of implants per animal, and test duration. Other considerations include costs of acquisition and care, animal availability, social acceptability, the ability of the animal to withstand testing, and ease of housing. Understanding the bone characteristics specific to the chosen species, such as microstructure, composition, and remodeling characteristics, as well as the similarity between the animal model and the human clinical situation, is crucial for investigating bone-scaffold interactions and translating results to humans [17].

The ideal bone defect model should closely resemble the intended clinical application and can include calvaria, long bone, or maxillofacial defects, categorized as non-critical or critical-sized bone defects for assessing osteocompatibility and osteogenesis, respectively. Calvaria defects are commonly used as non-load-bearing models for investigating bioactive glasses with inferior mechanical properties compared to bone. Load-bearing long bone defect

models (e.g., femur, tibia, radius, and humerus) are frequently used to evaluate the osteoregenerative capacity of scaffolds with properties similar to bone [30].

This systematic review aims to investigate the current scenario of *in vivo* applications of bioactive glasses. It serves as a pioneering effort to consolidate and synthesize dispersed information from various studies conducted over time. By analyzing existing literature, we seek to provide a comprehensive overview of the performance of bioactive glasses in living organisms, evaluating their efficacy, biocompatibility, and long-term outcomes for the first time. We will explore the *in vivo* applications of bioactive glasses in bone regeneration. Through this review, we aim to identify gaps in knowledge and areas for further research, contributing to a better understanding of the clinical potential and challenges associated with the use of bioactive glasses in various *in vivo* models.

2.2 METHOD

2.2.1 Data sources and search strategies

The Preferred Reporting Items for Systematic Reviews and Meta-Analyses (PRISMA) guidelines were used in the design and conduction of the present systematic review [31]. Two individual electronic databases were searched accurately and independently by two reviewers (Bianca Constante Guedert and Rafael Matos). The electronic databases searched for identifying the relevant studies were PubMed/Medline (National Library of Medicine, Washington, DC) and Web of Science (Clarivate Analytics, Philadelphia). The published scientific articles until April 2023 were covered, with the last research conducted on April 30, 2023. The keywords were defined through the research question: What is the current scenario of *in vivo* testing of bioactive glasses?". The keyword combination that returned the maximum number of papers was taken forward for the detailed systematic search. This way, five different combinations were applied in each electronic databases with the use of Mesh operators as shown in **Table 1**.

Table 1. Keywords combinations and results of each data base.

Keywords	**DataBase**	**Number of Results**
(bioactive glass):ti,ab,kw AND (*bioglass* OR bone regeneration OR bone defect* OR bone graft* OR animal model* OR *in vivo**):ti,ab,kw NOT (periodontal* OR metals*):ti,ab,kw	Web of Science	7
(bioactive glass* OR bioglass* OR orthopedic* AND bone graft* AND particle* AND (*in vivo** OR animal models*) NOT (periodontal*) NOT (metal*)	PubMed	59
("bioactive glass"* OR bioglass* OR orthopedic* AND bone graft* AND particle* AND (*in vivo** OR animal models*) NOT (periodontal*) NOT (metal*) NOT (titanium*) NOT (autogenous*) NOT (allo*) NOT (granules*)	Web of Science	69
(bioactive glass* AND bone regeneration* AND orthopedic* AND (*in vivo** OR animal models*) NOT periodontal* NOT metal*	PubMed	57
	Web of Science	0
(bioactive glass* OR bioglass* OR orthopedic* AND bone graft* AND granule* AND (*in vivo** OR animal models*) NOT (periodontal*) NOT (metal*)	PubMed	31
	Web of Science	0
(bioactive glass* OR bioglass* OR orthopedic* AND bone graft* AND putty* AND (*in vivo** OR animal models*) NOT (periodontal*) NOT (metal*)	PubMed	11
	Web of Science	0

In order to identify relevant studies, the following inclusion and exclusion criteria were set. We only included studies in which:

1) The bioglasses were implemented in animal models (*in vivo*);
2) With at least a brief description of the methodology used;
3) From orthopedic journals in order to focus on medium to large bones defects;
4) With a minimum contact time of 4 weeks;
5) The papers were written in English.

We therefore excluded the studies that:

1) The bioactive glasses were only tested *in vitro* or in biomechanical trials;
2) Cadaveric trials;
3) Bioglasses applied with periodontal focus (small bone defects);
4) Bioactive glasses were applied in an animal model with induced osteoporosis;
5) Failed to provide any information about the bioglass characteristics such as composition and morphology.

2.2.2 Study selection and data collection process

The articles retrieved from each combination of key terms for each database were compiled, and duplicates were removed using the Mendeley citation manager. After removing duplicates, the studies underwent a relevance screening based on title, and the abstracts of non-excluded articles were assessed. Two authors (Bianca Guedert and Rafael Matos) independently analyzed the titles and abstracts of the retrieved articles that potentially met the inclusion criteria. The next step involved evaluating the abstracts and non-excluded articles according to the eligibility criteria outlined in the abstract review. Selected articles were then individually read and analyzed in relation to the objective of the present study. Each eligible article was assigned a study nomenclature label combining the first author's name and the year of publication. The following variables were collected: authors' names, publication year, morphology and composition of the bioactive glass used, fabrication method, animal models employed, duration of the study, and number of subjects enrolled in the *in vivo* study. All the data can be accessed by contacting the author, but the relevant information is presented in **Tables 3**, **4**, and **5** throughout the paper. To ensure data accuracy and avoid duplications from multiple reports within the same study, data were directly recorded into a specific data-

collection form. This evaluation process was performed independently by two researchers, followed by a joint discussion to select the relevant studies.

2.3 RESULTS

The initial electronic search using the keywords combinations from Table 1 returned 234 articles. At the first phase of evaluation duplicate articles were excluded. The title and abstracts of the remaining 221 articles were screened and 131 papers were excluded as they were not relevant to the inclusion criteria. Finally, 90 relevant papers were scrutinized by downloading the papers and trough a consensus between the reviewers 70 papers were excluded after reading the full text. At the end of papers selection 20 papers were included in this review. A flow diagram of the selection of the studies is shown in **Figure 1**.

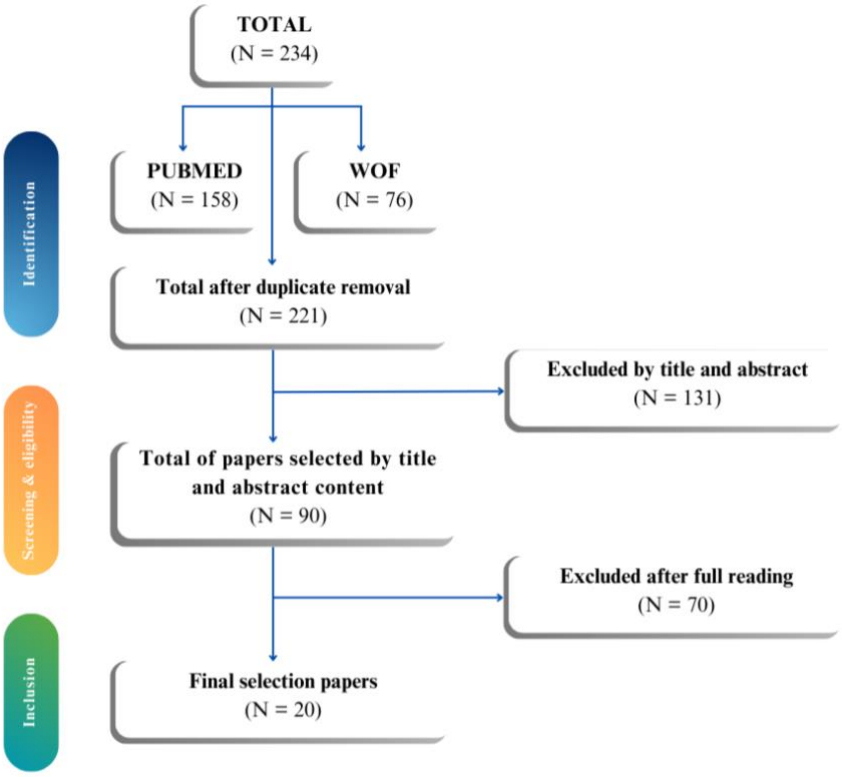

Figure 1. Flow diagram of the data selection process following the PRISMA method.

From the 20 articles included in this review, a total of 547 animal subjects were enrolled on the *in vivo* studies. Among these subjects, 433 of are rats [32–45], and 107 are rabbits [46–51]. The primary focus of all the studies was to evaluate the effect of bioactive glasses on bone defect regeneration, with a mean follow-up period of 12 weeks (ranging from 4 to 24 weeks).

The specific regions in which the bone defects were introduced varied among the studies. Eleven studies utilized the animal femur as the site for bone defect induction, seven studies targeted the calvaria region, while one study each focused on the tibia and the skull. For a comprehensive overview of the studies conducted in each specific defect region, please refer to **Table 2**

Table 2. Animal bone defect models employed for investigating the *in vivo* bone regenerating capacity of bioactive glasses used as particles and 3D scaffolds.

Scaffolds		**Particles**	
Rats	**Rabbits**	**Rats**	**Rabbits**
Femur [36,38,43]	Femur [46,47,49,50]	Femur [33,35]	Femur [48,51]
Calvaria [39–41,44,52]	-	Calvaria [34,37]	-
Skull [45]	-	Tibia [42]	-

The included articles in this review encompassed various types of bioactive glasses with different shapes and compositions. Based on the analysis of the included studies, two main groups were identified: scaffolds and particles. Thirteen studies specifically focused on evaluating bioactive glass scaffolds [36,38–41,43–47,49,50,52], while seven studies examined bioactive glass particles [33–35,37,42,48,51] (refer to **Figure 2** for a visual representation). Within the scaffolds group, eight studies utilized bioactive glasses obtained through the melted technique. Among these studies, three evaluated silicate bioactive glasses with a predominant composition based on the 13-93 nominal bioglass [39,41,50]. Additionally, four studies investigated various compositions of borosilicate bioactive glasses [36,40,45,46], and one study utilized the recognized phosphate composition known as S53P4 [47]. Four studies used bioactive glasses obtained from sol-gel method as the main raw material [38,43,49,52].

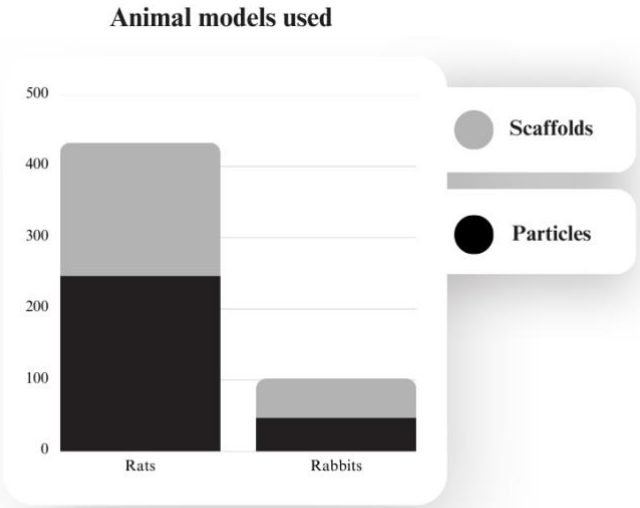

Figure 2. Animal models, rats, and rabbits, used in bioactive glass scaffolds and glass particulate group.

Various methods were employed for scaffold manufacturing in the included studies. The identified methods included thermally bonding of particles or fibers, unidirectional freezing of suspensions, polymer foam replication, sol-gel foaming, and 3D printing (for further details, refer to **Table 3**).

Table 3. Different fabrication techniques for BG scaffolds used in *in vivo* bone defects models (continue)

Fabrication method	Glass used	Advantages	Limitations
Thermally bonding of particles or fibers	– **13-93** fibrous scaffolds [40,44]. – **13-93B1** fibrous scaffolds [44]. – **13-93B3** fibrous scaffolds [40,44]. – **BAG-S53P4** rods scaffolds [47].	– Ease of Fabrication. – No need for complex machinery [16].	– Poor pore interconnectivity at low porogen concentration. – Difficult to control the porosity and pore interconnectivity [16].
Unidirectional freezing of suspensions	– **Sr** and **Li-BG** dopped Scaffolds [50]	– Formation of porous scaffolds with an oriented microstructure, resulting in higher scaffold strength in the direction of orientation. – A change of the lamellar microstructure to a columnar microstructure and a larger pore width result from the use of an organic solvent [39]	Scaffolds prepared from aqueous suspensions typically have a lamellar microstructure, with small pore width (10–4 μm) that is unfavorable support tissue ingrowth [16].
Polymer foam replication	– **^{45}Ca-MBG** scaffold [38] – **13-93** Scaffolds [39]	– Can provide a scaffold microstructure that resemble that of dry human trabecular bone. – The production of highly porous glass scaffolds with open and interconnected porosity in the range 40–95%	Low scaffold strength, typically in the range of trabecular bone, limiting its use to low- load bone sites [16].

Table 3. Different fabrication techniques for BG scaffolds used in *in vivo* bone defects models (continuation)

Fabrication method	Glass used	Advantages	Limitations
Sol-gel foaming	**nBG** and **nMBG/ChGel** Scaffolds [43]	– The scaffolds have a hierarchical pore architecture of interconnected macropores (10–500 μm) produced by the foaming process, and mesopores (2–50 nm) that are inherent to the sol–gel process, simulating the hierarchical structure of natural tissues. – Nanopores in the glass increases the specific surface area (100–200 m^2/g); compared to melt-derived glasses, resulting in faster scaffold degradation and conversion to HA [16].	Have low strength (0.3–2.4 MPa), limiting its use to substituting defects in low-load bone sites

Table 3. Different fabrication techniques for BG scaffolds used in *in vivo* bone defects models (conclusion)

Fabrication method	Glass used	Advantages	Limitations
3D printing	– **13-93** Scaffolds [41] – **MBG** Scaffolds [53] – **13-93** Scaffolds [45] – **13-93B10** Scaffolds [45] – **13-93B8Sr2** Scaffolds [45] – **13-93B5Sr5** Scaffolds [45] – **13-93B2Sr8** Scaffolds [45] – **13-93B10Sr10** Scaffolds [45]	– Its versatility through allowing the printing of a range of different materials and the fabrication of scaffolds with a range of architectures. – High compressive strengths comparable to that of human cortical bone could be achieved [16]. – A simple, versatile technique, using cheap material, with high building speed. – Heat or harsh chemicals are not required, making it a suitable tool for incorporating biologically active molecules inside the scaffolds[16].	– Optimizing the ceramic inks suitable for direct printing is a primary concern, if the ceramic powder content in the ceramic ink is too low, it will dry quickly resulting in microcracks in the assembly [16]. – The final construct has relatively low strength due to the weak bonds between particles. – Post- processing heat treatment is required to achieve higher density and better mechanical properties of the finished parts. – Limited resolution and accuracy. – A rough surface finish of the final construct due to the large size of powder particles. – In addition to the other problems like those associated with the SLS process[16]

In the particulate group, seven studies focused on the evaluation of bioactive glass particles. Five studies utilized bioactive glasses obtained from the melted-derived technique, while two studies employed the sol-gel method. The particle sizes ranged from 30 to 700 µm, and specific compositions can be found in **Table 4**

Table 4. Chemical compositions of bioactive glass particles used on tests in bone models.

Reference	Processing route	Particle size	Composition
Boyd et al. [33]	Melt derived	90-350 μm	– **BT-107** (mol %): 40SiO_2, 32ZnO, 28CaO. – **BT-108** (mol %): 40SiO_2, 32ZnO, 14CaO, 14SrO. – **BT-109** (mol %): 40SiO_2, 32ZnO, 28SrO.
Zhao et al. [34]	Melt derived	< 70 μm	– **PSC** (mol %): 0.8P_2O_5, 54.2SiO_2, 35CaO
El-Meliegy et al. [35]	Melt derived	300-355 μm	– **A** (mol%): 26.5CaO,10Na_2O,7.8MgO 4.4P_2O_5 ,50.6SiO_2 0.8TiO. – **B** (mol%): 19.5CaO, 7.9Na_2O, 15MgO, 3.4P_2O_5, 51.6SiO_2, 0.7TiO. – **C** (mol%): 15.9CaO,5.1Na_2O,0.6K_2O,19.1MgO, 2.5P_2O_5, 54SiO_2, 2.2LiF, 0.7TiO. – **D** (mol%): 12.4CaO,2.8Na_2O,1.2K_2O,23.1MgO, 1.2P_2O_5, 55.7SiO_2, 2.2LiF, 1.5TiO.
Moon et al.[37]	Melt derived	400 μm	– **BG-CaF** (mol%): 0.6CaO, 0.06CaF_2, 0.6P_2O_5, 1MgO,1ZnO
Anesi et al. [51]	Melt derived	100-500 μm	– **BGMS10** (mol%): 2.3Na_2O, 2.3K_2O, 25.6CaO, 10MgO, 10SrO, 2.6P_2O_5, 47.2SiO_2. – **Bio-MS** (mol%): 5Na_2O, 2.3K_2O, 31.3CaO, 5MgO, 10SrO, 2.6P_2O_5, 46.1SiO_2.
Lalzawmliana et al. [48]	Sol-gel	30-700 μm	– **MBWC650:** 6.65 mL TEOS, 4.25 g, $Ca(NO_3)_2{\cdot}4H_2O$, 0.65 g PEG, 0.34 mL TEP, 0.07 g citric acid. – **MBHM650:** 3.014 mL TEOS, 0.306 mL TEP, 1.98 g $Ca(NO_3)_2{\cdot}4H_2O$, 1.0 g P123 (Pluronic® P-123). – **MBCTAB650:** 3 mL TEOS, 0.13 mL TEP, 0.68 g $Ca(NO_3)_2{\cdot}4H_2O$, 0.66 g CTAB, 26.4 mL NH_4OH.
Lehman et al. [42]	Sol-gel	2-18 nm	– **BG-90** (mol%): 90SiO_2, 1P_2O_5, 3CaO

All the articles considered in this review conducted essential analytical analyses, including X-ray diffraction (XRD), Fourier-transform infrared spectroscopy (FTIR), scanning electron microscopy (SEM), and energy-dispersive X-ray spectroscopy (EDS). Additionally, *in vitro* studies, encompassing biocompatibility and toxicity testing, were performed prior to the *in vivo* studies on bioactive glasses. Moreover, all the studies consistently reported positive outcomes in terms of bone regeneration and integration, underscoring the potential effectiveness of bioactive glasses as grafts for treating bone defects. For a comprehensive assessment of the data included in this review, please refer to **Table 5**. The table provides a detailed overview of the key findings from each study, facilitating a comprehensive

understanding of the collective evidence regarding the *in vivo* application of bioactive glasses for bone defect treatment.

Table 5. Summary of selected data for the systematic review (continue)

Ref	Title	Morphology	Number° of subject	Animal model	Defect place	Time of study (weeks)
Qi et al. [36]	**Mesoporous bioactive glass-coated 3D printed borosilicate bioactive glass scaffolds for improving repair of bone defects**	Scaffold	24	Rats	Femur	8
Sui et al. [38]	**Evolution of a Mesoporous Bioactive Glass Scaffold Implanted in Rat Femur Evaluated by ^{45}Ca Labeling, Tracing, and Histological Analysis**	Scaffold	25	Rats	Femur	12
Covarrubias et al. [43]	**Bio nanocomposite scaffolds based on chitosan-gelatin and nano dimensional bioactive glass particles: *In vitro* properties and *in vivo* bone regeneration**	Scaffold	8	Rats	Femur	8
Qi et al. [53]	**Three-dimensional printing of calcium sulfate and mesoporous bioactive glass scaffolds for improving bone regeneration *in vitro* and *in vivo***	Scaffold	48	Rats	Calvaria	8
Liu et al. [39]	**Bone regeneration in strong porous bioactive glass (13-93) scaffolds with an oriented microstructure implanted in rat calvaria defects**	Scaffold	26	Rats	Calvaria	24
Gu et al. [40]	**Bone regeneration in rat calvaria defects implanted with fibrous scaffolds composed of a mixture of silicate and borate bioactive glasses**	Scaffold	10	Rats	Calvaria	12

Table 5. Summary of selected data for the systematic review (continuation)

Ref	Title	Morphology	Number° of subject	Animal model	Defect place	Time of study (weeks)
Lin et al. [41]	**Long-term bone regeneration, mineralization and angiogenesis in rat calvaria defects implanted with strong porous bioactive glass (13-93) scaffolds**	Scaffold	22	Rats	Calvaria	24
Bi et al. [44]	**Evaluation of bone regeneration, angiogenesis, and hydroxyapatite conversion in critical-sized rat calvaria defects implanted with bioactive glass scaffolds**	Scaffold	14	Rats	Calvaria	21
Ding et al. [45]	**Regulated contribution of local and systemic immunity to new bone regeneration by modulating B/Sr concentration of bioactive borosilicate glass**	Scaffold	10	Rats	Skull	8
Boyd et al. [33]	**Preliminary investigation of novel bone graft substitutes based on strontium–calcium–zinc–silicate glasses**	Particles	24	Rats	Femur	4
El-Meliegy et al. [35]	**Development and bioactivity evaluation of bio glasses with low Na_2O content based on the system Na_2O–CaO–MgO–P_2O_5–SiO_2**	Particles	24	Rats	Femur	12
Zhao et al. [54]	***In vitro* and *in vivo* evaluation of the pH-neutral bioactive glass as high-performance bone grafts**	Particles	48	Rats	Calvaria	12
Moon et al. [37]	**Bone formation in calvaria defects of Sprague-Dawley rats by transplantation of calcium phosphate glass**	Particles	60	Rats	Calvaria	8
Lehman et al. [42]	**Bioactive glass containing 90% SiO_2 in hard tissue engineering: An *in vitro* and *in vivo* characterization study**	Particles	90	Rats	Tibia	10

Table 5. Summary of selected data for the systematic review (conclusion)

Ref	Title	Morphology	Number° of subject	Animal model	Defect place	Time of study (weeks)
Gu et al. [46]	**Biodegradable borosilicate bioactive glass scaffolds with a trabecular microstructure for bone repair**	Scaffolds	3	Rabbits	Femur	8
Bjorkenheim et al. [47]	**Bone morphogenic protein expression and bone formation are induced by bioactive glass S53P4 scaffolds *in vivo***	Scaffolds	36	Rabbits	Femur	8
Niu et al. [49]	**Bioactive and degradable scaffolds of the mesoporous bioglass and poly(L-lactide) composite for bone tissue regeneration**	Scaffolds	12	Rabbits	Femur	12
Khan et al. [50]	**Influence of single and binary doping of strontium and lithium on *in vivo* biological properties of bioactive glass scaffolds**	Scaffolds	16	Rabbits	Femur	12
Lalzawmliana et al. [48]	**Potential of growth factor incorporated mesoporous bioactive glass for *in vivo* bone regeneration**	Particles	32	Rabbits	Femur	22
Anesi et al. [51]	**In-vivo evaluations of bone regenerative potential of two novel bioactive glasses**	Particles	15	Rabbits	Femur	8

2.4 SUMMARY OF *IN VIVO* STUDIES ON BIOACTIVE GLASSES

2.4.1 BGs Scaffolds: *in vivo* outcomes

Scaffolds have emerged as a promising solution for the repair and regeneration of large bone defects, as they offer a three-dimensional structure that can mimic the natural bone environment. These 3D structures are designed with a combination of desirable properties such as chemical composition, morphology, microarchitecture, degradation, and mechanical characteristics, which have a profound impact on the proliferation and differentiation of cells crucial for bone regeneration. A vast body of research has been dedicated to the development and optimization of scaffold materials, and their potential for clinical applications continues to

be explored. In this section, we will discuss the latest findings on scaffold materials and their properties, and how they can be tailored to improve bone regeneration considering the *in vivo* studies outcomes.

The reviewed articles report different types of bioactive glass scaffolds, in which the raw material was obtained by sol-gel or melt derived method, including mesoporous bioactive glass (MBG), silicate bioactive glasses, borosilicate bioactive glass and phosphate bioactive glasses offering an intriguing opportunity to examine and compare the distinctive characteristics and performance of these scaffold types.

2.4.1.1Silicate bioactive glasses

2.4.1.1.1Melt-derived 13-93 bioactive glasses

The 13–93 bioactive glass (BG) composition stands out as one of the early developments specifically engineered to withstand high temperatures without undergoing devitrification. Its composition is 54.6 SiO_2, 6 Na_2O, 22.1CaO, 1.7 P_2O_5, 7.9 K_2O, and 7.7 MgO (mol%). When subjected to simulated body fluid (SBF) tests, the formation of a hydroxycarbonate apatite (HCA) layer on the surface of 13–93 BG takes approximately 7 days, whereas particles of 45S5 BG with similar dimensions achieve this layer within a mere 8 h. The slower reactivity of 13–93 BG can be attributed to its higher network connectivity, which stems from the elevated silica content relative to 45S5 BG [55].

i) Rat model studies

In a study conducted by Liu et al. [39], the bone regeneration ability, osseointegration, and mechanical response of 13-93 BG scaffolds with an oriented microstructure were investigated in 26 rat calvaria defect model. The oriented scaffolds, fabricated using unidirectional freezing of camphene-based suspensions, exhibited 50% porosity with pore diameters ranging from 50-150 µm. Trabecular scaffolds, serving as the positive control group, were fabricated using polymer foam replication and had 80% porosity with pore sizes of 100-500 µm. The study findings showed that at 12 weeks post-implantation, defects treated with oriented scaffolds displayed new bone formation primarily on the dural side, with limited bone ingrowth into the scaffold periphery. At 24 weeks, improved bone infiltration into the periphery of the scaffolds and enhanced osseointegration were observed. In contrast, defects implanted with trabecular scaffolds exhibited bone regeneration mainly in the periphery of the implants,

with better osseointegration than the oriented implants at 12 weeks. The differences in bone infiltration and new bone formation were attributed to the distinct microstructures of the scaffolds. Despite having lower porosity and pore size compared to the trabecular scaffolds, the oriented scaffolds demonstrated higher bone in-growth and new bone formation, likely due to better pore interconnectivity and less tortuous pore channels. The study also noted an elastoplastic response of the scaffolds after *in vivo* implantation, possibly facilitated by the presence of new bone and soft tissue that provided a deformable matrix for the otherwise brittle glass and HA-like material.

Another study, conducted by Lin et al. [41] evaluate the long-term bone regeneration of osseous defects using porous 13-93 BG scaffolds. These scaffolds had a porosity of 47 ± 1% and a grid-like microstructure prepared through the robocasting method. The researchers investigated osseous healing, conversion of glass to hydroxyapatite (HA), and angiogenesis in the 13-93 BG scaffolds. They examined the scaffolds that were either pretreated in K_2HPO_4 solution for 3 days or loaded with BMP-2 (1 μg per scaffold) in non-critical sized rat calvaria defects for 12 and 24 weeks, comparing them with the as-fabricated scaffolds (control group). The findings were also compared with a study by Liu et al. [39] that used similar scaffolds implanted in the same animal model for 6 weeks.

The results demonstrated a significant increase in osseous regeneration in the as-fabricated scaffolds group as the implantation time increased from 6 to 24 weeks. The pretreated scaffolds showed enhanced bone regeneration at 6 weeks but not at 12 or 24 weeks, indicating that the observed increase in osseous regeneration at 6 weeks was a short-term effect. The rough hydroxyapatite (HCA) surface initially improved protein adsorption and cellular response. However, the as-fabricated scaffolds exhibited faster conversion to HA compared to the pretreated scaffolds, enhancing their ability for bone regeneration. Consequently, at 24 weeks, no significant difference in bone regeneration was observed between the as fabricated and pretreated scaffolds.

In contrast, the BMP-2-loaded scaffolds significantly enhanced bone regeneration at all three implantation times, resulting in the formation of marrow-rich bone, a typical outcome of BMP-2-induced bone growth. Histological analyses using H&E and periodic acid-Schiff (PAS) staining revealed a significantly greater area of blood vessels and a higher number of newly formed blood vessels infiltrating the BMP-2-loaded scaffolds at 6- and 12-weeks post-implantation, compared to the as-fabricated and pretreated scaffolds. However, there was no significant difference among the three groups of scaffolds at 24 weeks in terms of the extent of new bone formation. **Figure 3** shows a diagram of the main results found by the authors.

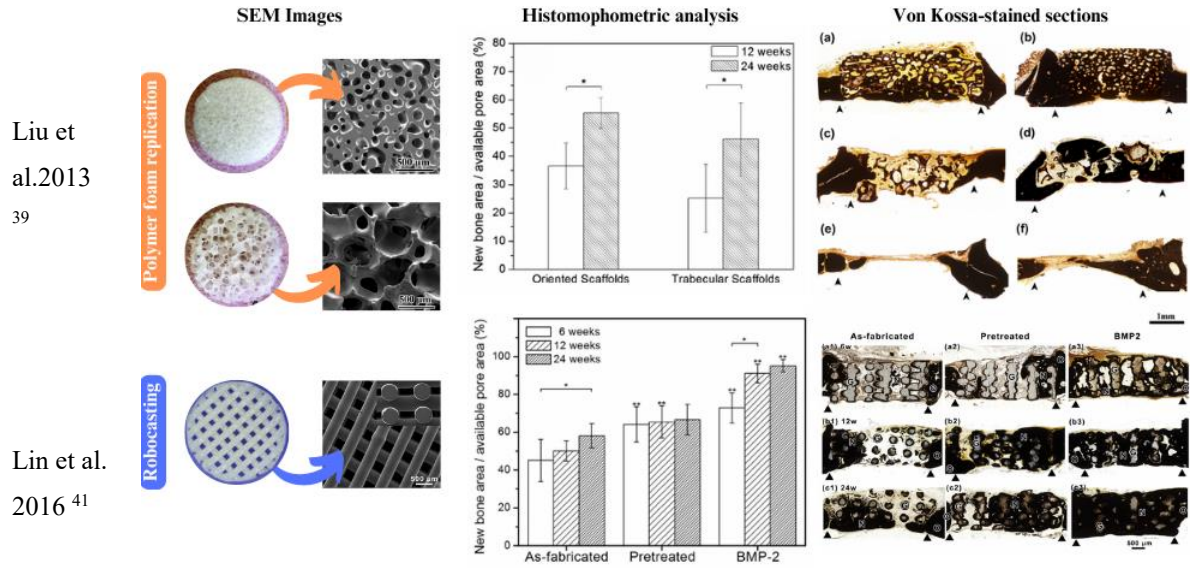

Figure 3. Diagram illustrating Optical, SEM, Histomorphometry, and Von-Kossa stained analyses of bone regeneration in rat calvaria defects using polymer foam and robocasting scaffolds. Von-Kossa stained sections demonstrate the progression of bone regeneration over time: oriented and trabecular polymer foam replication at 12 weeks (a, b), trabecular replication at 12 and 24 weeks (c, d) [39]. Robocasting-derived scaffolds display bone development at 6, 12, and 24 weeks, including as-fabricated, pretreated, and BMP2-loaded groups (a1–c3) [41]. Adapted with permission from Liu et al. 2013 [40] and Lin et al. 2016 [41]. Copyright © 2013, Elsevier.

2.4.1.2 Sol-gel derived bioactive glass

2.4.1.2.1Mesoporous bioactive glasses scaffolds

A promising candidate for local drug/protein delivery systems, the mesoporous bioactive glass, have garnered a significant attention in biomedical application since the first synthesis in 2004 [56]. The mesoporosity allow controlled release of therapeutic agents during glass dissolution, as well for bone tissue regeneration [57]. Fabricated through an evaporation-induced self-assembly (EISA) process utilizing non-ionic block copolymers as structure-directing agents, MBGs possess ordered mesoporosity, high surface area, and specific pore characteristics that contribute to their excellent bone-forming capability [15]. Furthermore, the replication method, originally developed for melt-derived bioactive glasses, has been successfully applied to create MBG scaffolds, mimicking the architecture of cancellous bone and enabling the production of porous bioceramics [16].

i) Rat model studies

Mesoporous bioactive glasses (MBG) have gained significant attention as biodegradable scaffolds with unique nanostructures. However, despite their potential, MBG

still faces certain challenges in terms of *in vivo* evaluation. Questions surrounding the in-situ degradation process, the local effects induced by degradation, and the disposition of degradation products remain unclear. In their study, Sui et al. [38] identified a series of questions that need to be addressed for considering future clinical applications of MBG based scaffolds, including the biological effect of MBG nanostructure and ion-release profile. In addition, the fate of ions released as result of the MBG degradation process, and whether they are involved in local or systemic metabolic reactions must be considered. Most importantly, the potential toxicity of MBG degradation products which can cause systemic subacute toxicity reactions needs to be studied.

Sui et al. [38] conducted a study to address these inquiries by utilizing *in situ* labeling with $^{45}CaCl_2$ during the synthesis of ^{45}Ca-MBG scaffolds, composed of $80SiO_2.15CaO.5P_2O_5$. These labeled scaffolds were then implanted into critical-sized rat femur defects for varying durations (1 day, 1 week, 4 weeks, 8 weeks, and 12 weeks). The distribution and quantitative tracing of ^{45}Ca ions were assessed using liquid scintillation counting (LSC), both locally and systemically.

In vivo, the radioactivity associated with ^{45}Ca was predominantly found in the bloodstream and various organs, including the heart, lungs, spleen, kidneys, intestines, and brain, indicating systemic circulation. The radioactivity peaked at week 1 and gradually decreased as the scaffolds degraded, becoming almost undetectable by week 12. This demonstrates a significant reduction in the risk associated with the use of MBG scaffolds over time. Additionally, ^{45}Ca was observed to accumulate in distal bone tissues such as the radius and cranium.

Interestingly, only a small fraction of the released Ca ions (less than 9.63%) during degradation contributed to new bone formation. Notably, no notable pathological changes were observed in tissues and organs at 4- and 12-weeks post-implantation, and blood chemistry analysis revealed no abnormalities, except for higher white blood cell counts in the experimental group compared to the control group. This increase was attributed to the activation of phagocytic cells involved in engulfing the degradation products.

The study also evaluated the impact of MBG scaffold extracts on the osteogenic differentiation of rat bone marrow mesenchymal stem cells (rBMSCs). Results showed a significant enhancement in the mRNA levels of osteoblast-related genes, including RUNX-2, ALP, and OCN, after 3 and 10 days of exposure to the extracts. Curiously, the mRNA expression of these genes was higher in the 50 mg/mL extract compared to the 100 mg/mL extract. This discrepancy was attributed to the higher concentration of Ca ions released from

the 100 mg/mL extract, resulting in an increased pH value of the extract (8.7), which affected the differentiation of rBMSCs and subsequently reduced mRNA expression levels. **Figure 4** shows a diagram of the main results found by the author.

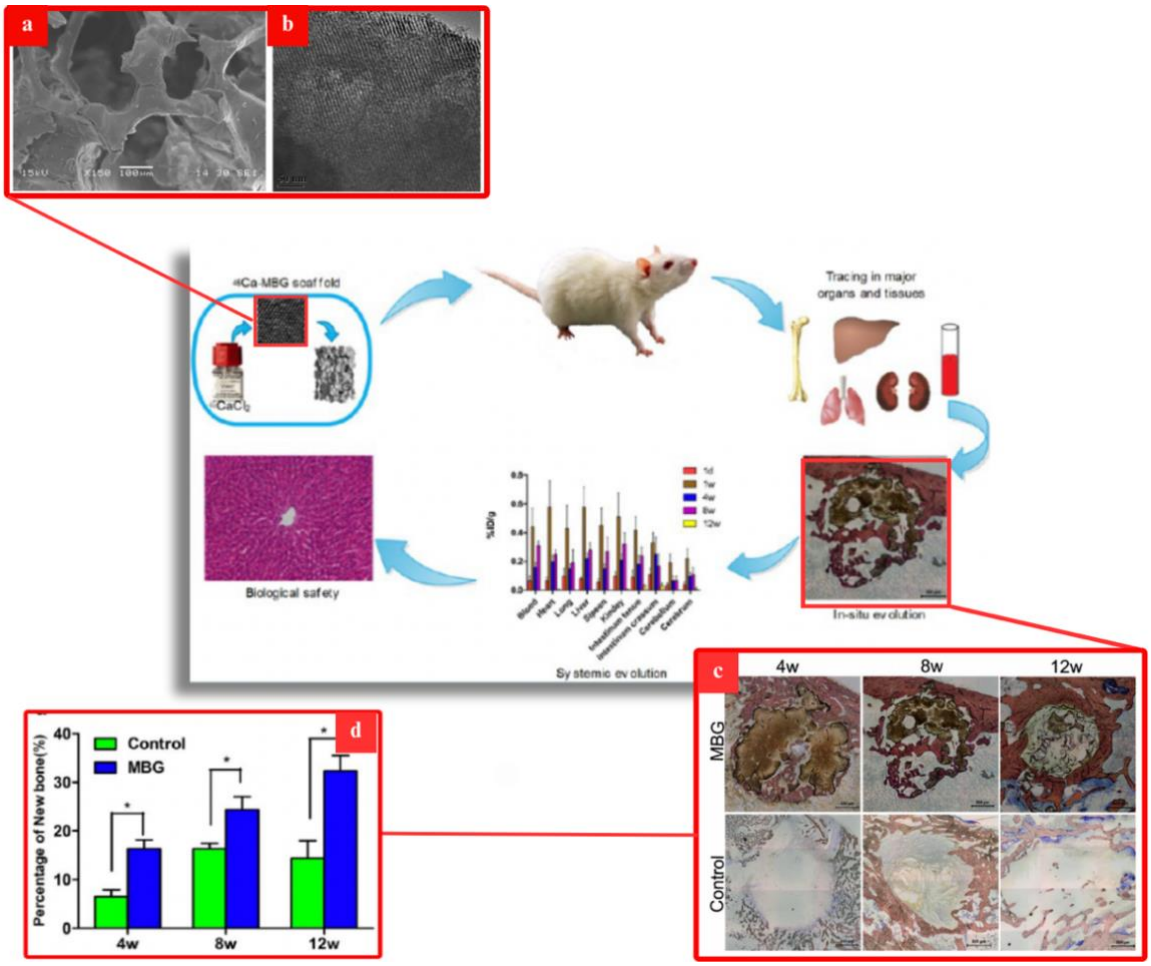

Figure 4. Flow diagram of the study showing: (a) SEM image displaying MBG scaffold surface morphology, (b) TEM images revealing the mesoporous structure, (c) Progression of new bone formation and material degradation in MBG scaffolds at 4, 8, and 12 weeks post-implantation (Red, green, and brown indicate newly formed bone, fibrous tissue, and residual material, respectively), and (d) Histomorphometry analysis indicating the percentage of newly formed bone. Adapted with permission from Sui et al. 2014. Copyright © 2014, American Chemical Society.

Coating scaffolds with bioactive glass, particularly mesoporous bioactive glasses (MBG), has also yielded promising outcomes [53, 36]. Li et al. [36] examined the impact of MBG coating with varying concentrations on borosilicate scaffolds utilizing a 3D printed extrusion method. The coating procedure consisted in immerse the sintered borosilicate bioactive scaffolds in the MBG solution for 10 min and then stirred by a centrifugation process. This

coating procedure was repeated 3, 6, 9 times resulting in three types of scaffolds named BG-3M, BG-6M and BG-9M.

Micro-CT imaging in femoral defects showed that the BG-9M scaffold group exhibited more newly formed bone, with higher local bone mineral density (BMD) and bone volume fraction (BV/TV) compared to other groups. Fluorescent labeling analysis showed the percentage of labeling for different stages of bone formation (TE, AL, and CA) at 2, 4, and 6 weeks. The BG-9M scaffold group consistently exhibited higher percentages of labeling compared to other groups, indicating enhanced bone formation and mineralization. Histological and immunohistochemical analysis confirmed extensive new bone formation in the defect areas, with significant improvements observed in the BG-9M scaffold group.

Liu et al. [53] conducted another study where MBG was used to enhance calcium silicate hydrate (CSH) scaffolds. Precise control over the scaffold architecture was achieved through 3D printing in which the finished scaffolds were named according to the mass ratios of CSH to MBG powders (CSH/MBG20, CSH/MBG40, CSH/MBG60). The results showed significant differences between CSH/MBG and CSH scaffolds in bone regeneration. Micro-CT images revealed improved new bone formation in CSH/MBG compared to CSH. Local BMD was significantly higher in CSH/MBG20, CSH/MBG40, and CSH/MBG60, indicating enhanced bone regeneration. BV/TV analysis supported these findings, confirming the positive impact of MBG incorporation into CSH scaffolds. Histological staining using Van Gieson's picric-fuchsin staining provided visual evidence of the difference in new bone formation. The CSH group showed minimal bone formation, while the CSH/MBG20 group displayed limited new bone growth. In contrast, the CSH/MBG40 and CSH/MBG60 groups exhibited more significant ingrowth of newly formed bone, with the CSH/MBG60 group showing the most active bone formation and nearly complete coverage of the defect area. Histomorphometry analysis confirmed these observations, with a significantly greater percentage of new bone area in the CSH/MBG20, CSH/MBG40, and CSH/MBG60 groups compared to the CSH group.

Covarrubias et al. [43] investigated the effect of incorporating nano bioactive glasses (nBG/70nm and nMBG/100nm) into a chitosan-gelatin (ChGel) matrix to create nanocomposite scaffolds. To fabricate the scaffolds, a nanoparticle/gelatin dispersion was prepared and mixed with a chitosan solution under stirring. The hydrogel blend was then cross-linked using a solution of sodium hexametaphosphate and sodium hydroxide dissolved in distilled water. Individual scaffolds were created by placing the crosslinked gel into 48 well plates and freezing them at -80°C for 24 h. Subsequently, the scaffolds were freeze-dried for two to three days at -45°C using a freeze dryer. The resulting nanocomposites, nBG/ChGel and nMBG/ChGel, had

a weight ratio of Ch/Gel of 1:1 and contained 5% and 25% w/w nanoparticle content, respectively. Micro-CT analysis supported the findings that the incorporation of BG nanoparticles into the ChGel polymer matrix enhanced the osteogenic properties of the nanocomposites, making them promising materials for accelerating bone reconstruction treatments.

ii) Rabbit model studies

Zheng et al. [49] conducted a study to enhance the physical, chemical, and biological properties of bioactive glass scaffolds by combining them with degradable polymers. The aim was to address the limitations of bioactive glass scaffolds, such as low mechanical strength and high dissolution leading to an elevated pH value that affects their osteogenesis and biocompatibility *in vivo*. In their study, Poly(l-lactide) (PLLA) scaffolds were fabricated using the solvent casting-particulate leaching method. These scaffolds were then coated with two different concentrations of MBG: 15 wt.% (m-BCP15) and 30 wt.% (m-BCP30), achieved through continuous stirring.

In this study, the *in vivo* osteogenesis potential of PLLA (Poly(l-lactide)) scaffolds and m-BPC30 scaffolds was evaluated through implantation into rabbit femur defects. The assessment was conducted at 4-, 8-, and 12-weeks post-implantation using Micro-CT imaging and histological evaluation (H&E staining). After 12 weeks, the m-BPC30 scaffolds demonstrated complete healing of the bone defect, with new bone formation and nearly complete degradation of the scaffold. In contrast, the PLLA scaffolds showed limited new bone formation and incomplete scaffold degradation even after 12 weeks.

Histological analysis confirmed these findings, with more new bone tissue observed in the defects filled with m-BPC30 scaffolds compared to PLLA scaffolds. At 4 weeks, minimal new bone tissue was formed in PLLA scaffolds, while m-BPC30 scaffolds exhibited substantial new bone formation. Over time, both scaffolds showed increased new bone tissue along with material degradation, but at 12 weeks, m-BPC30 scaffolds displayed a significantly higher level of newly formed bone tissue compared to PLLA scaffolds. Quantitative analysis further supported these observations, demonstrating that the m-BPC30 scaffolds had superior *in vivo* osteogenesis compared to PLLA scaffolds.

2.4.1.3 Borosilicate and borate glasses

One limitation of 45S5 bioactive glass (BG) and other silicate bioactive glasses is their relatively slow and incomplete conversion to hydroxyapatite (HA) due to the low solubility of silica. As a result, remnants of unconverted silicate glass can be detected in the body for extended periods [58]. Manipulating the composition of bioactive glasses can alter their degradation rate, and this can be achieved by partially replacing SiO_2 in silicate glasses such as 45S5 or 13-93 with B_2O_3 to produce borosilicate bioactive glass, or completely replacing SiO_2 with B_2O_3 to create borate bioactive glasses. This alteration in composition affects the degradation rate of the scaffolds across a wide range. **Table 6** provides a comprehensive summary of boron-containing 3D scaffolds developed to date, which have been tested in bone animal models. In borate-based glasses, B_2O_3 serves as the major glass former instead of SiO_2 or P_2O_5. The conversion mechanism of borate glass to HA is like that of silicate 45S5 glass, but without the formation of a SiO_2-rich layer. The HCA layer forms directly on the surface of the underlying unreacted borate glass, without the formation of a borate-rich layer, owing to the high solubility of borate in body fluids [59].

Table 6. Chemical compositions of boron-containing bioactive glass scaffolds tests in bone models

Reference	Glass Scaffold	Composition
Bi et al. [44]	**45S5** silicate glass particles and scaffolds of **13-93** silicate, **13-93B1** borosilicate, and **13-93B3** borate glass	– **45S5** (wt.%): 45.0 SiO_2, 24.5 Na_2O, 24.5 CaO and 6.0 P_2O_5. **13-93** (wt.%): 53.0 SiO_2, 6.0 Na_2O, 12.0 K_2O, 5.0 MgO, 20.0 CaO, and 4.0 P_2O_5. – **13-93B1** (wt.%): 34.4 SiO_2, 20.0 B_2O_3, 5.8 Na_2O ,11.6 K_2O, 4.9 MgO, 19.5 CaO and 3.9 P_2O_5. **13-93B3** (wt.%): 56.6 B_2O_3, 5.5 Na_2O, 11.1 K_2O , 4.6 MgO , 18.5 CaO and 3.7 P_2O_5.
Gu et al. [40]	Mixture of **13-93** and **13-93B3** glass	– **13-93** (wt.%): 53.0 SiO_2, 6.0 Na_2O, 12.0 K_2O, 5.0 MgO, 20.0 CaO, and 4.0 P_2O_5. – **13-93B3** (wt.%): 53 B_2O_3, 6 Na_2O, 12 K_2O, 5 MgO, 20 CaO, 4 P_2O_5.
Gu et al.[46]	**13-93B1** borate BG scaffold	– **13-93B1** (mol %): $6Na_2O$–$8K_2O$–8MgO–22CaO–$18B_2O_3$–36SiO2–$2P_2O_5$
Qi et al.[36]	A borate bioactive scaffold coated with a mesoporous bioglass **BG-MBG**	– **BG** (mol%): $6Na_2O$, $8K_2O$, 2MgO, 6SrO, 22CaO, $36B_2O_3$, $18SiO_2$, $2P_2O_5$. – **MBG** (mol%): $58SiO_2$, 33CaO, $9P_2O_5$
Ding et al.[45]	Borate bioactive glass with strontium **13-93; 13-93B10; 13-93B8Sr2; 13-93B5Sr5; 13-93B2Sr8** and **13-93B10Sr10**	– **13-93** (mol%): $54SiO_2$, $6Na_2O$, $8K_2O$, 8MgO, 22CaO, and $2P_2O_5$. – **13-93B10** (mol%): $6Na_2O$, $8K_2O$, 8MgO, 22CaO, $2P_2O_5$, $44SiO_2$, 10SrO. – **13-93B2Sr8** (mol%): $6Na_2O$, $8K_2O$, 8MgO, 22CaO, $2P_2O_5$, $2B_2O_3$, $44SiO_2$, 8SrO. – **13-93B5Sr5** (mol%): $6Na_2O$, $8K_2O$, 8MgO, 22CaO, $2P_2O_5$, $5B_2O_3$, $44SiO_2$, 5SrO. – **13-93B8Sr2** (mol%): $6Na_2O$, $8K_2O$, 8MgO, 22CaO, $2P_2O_5$, $8B_2O_3$, $44SiO_2$, 2SrO. – **13-93B10** (mol%): $6Na_2O$, $8K_2O$, 8MgO, 22CaO, $2P_2O_5$, $10B_2O_3$, $44SiO_2$.

i) Rat model studies

Gu et al. [40] aimed to investigate the performance of scaffolds composed of a physical mixture of silicate 13-93 and borate 13-93B3 bioactive glasses, considering their different capabilities in supporting bone regeneration and distinct degradation rates. The objective was to assess the potential of these scaffolds to promote osteogenic cell proliferation and function *in vitro* and to regenerate bone in rat calvaria defects *in vivo*.

The scaffolds had similar microstructures, with porosity ranging from 58% to 67%, and they were composed of 0%, 25%, 50%, or 100% 13-93B3 glass, fabricated by thermally bonding randomly oriented short fibers. Results showed that the silicate 13-93 scaffolds had better cell proliferation and alkaline phosphatase activity compared to the scaffolds containing borate 13-93B3 fibers. At 12 weeks, the amount of new bone formed in the 13-93 scaffolds was 31%, which was significantly higher than the values of 25%, 17%, and 20% observed in scaffolds containing 25%, 50%, and 100% 13-93B3 glass, respectively. Results indicated the rather inhibitory effect of the scaffolds containing 13-93B3 glass on cell proliferation with decreased or almost constant ALP activity of the cells, indicating poor cytocompatibility, which could be explained by toxic effects of released boron ions in static culture conditions. 13-93 scaffolds showed higher capacity to support osteogenic cell proliferation and ALP activity.

It was found that the 13-93B3 fibers were fully converted to hydroxyapatite and formed a tubular morphology, while the 13-93 fibers were only partially converted at 12 weeks. H&E-stained analysis sections revealed that the 13-93 scaffolds exhibited extensive bone growth, with new bone formation occurring at the periphery and bottom of the scaffolds. In contrast, scaffolds containing 13-93B3 glass showed less bone regeneration as the concentration of 13-93B3 increased. Higher-magnification images showed that the 13-93 scaffolds had new bone formation within their interior pores, while the 13-93B3 scaffolds mainly had fibrous tissue infiltration. Blood vessels were observed in all scaffold groups. Quantitative analysis showed that the 13-93 scaffolds had a significantly higher percentage of new bone compared to the 13-93B3 scaffolds. The von Kossa-stained sections demonstrated the presence of mineralized bone and hydroxyapatite (HA) formed by the conversion of bioactive glass. The total von Kossa-positive area did not significantly differ among the scaffold groups. SEM analysis confirmed the conversion of the 13-93 and 13-93B3 glass fibers to HA, with new bone observed within the scaffold pores but not directly bonded to the HA layer. Overall, the 13-93 scaffolds exhibited better bone regeneration compared to the 13-93B3 scaffolds, indicating their potential for promoting bone regeneration in osseous defect models. **Figure 5** shows the main results found by the authors.

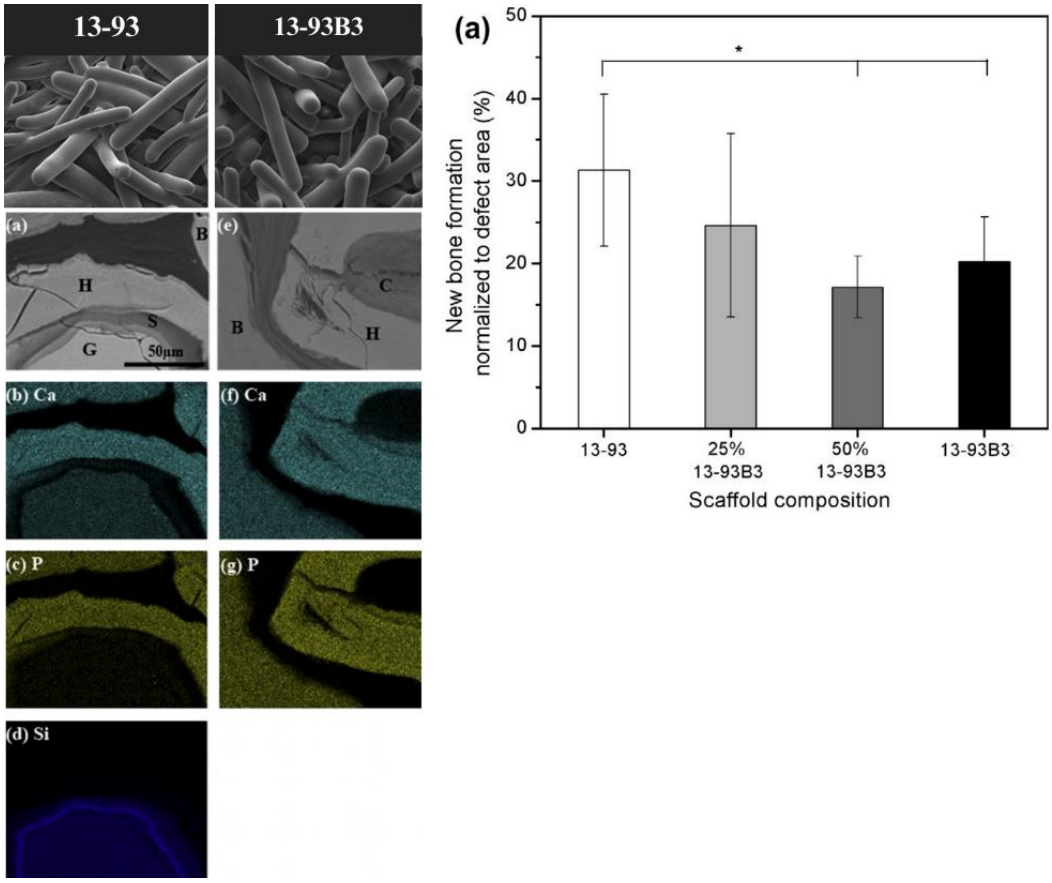

Figure 5. SEM images of the scaffolds. Backscattered electron images and X-ray maps of Ca(K), P(K), and Si(K) detail scaffolds composed of silicate 13-93 glass (a-d) and borate 13-93B3 glass (e-g), implanted for 12 weeks in rat calvaria defects. Components marked: G: unconverted glass; S: silica-rich layer; H: hydroxyapatite (HA) layer resulting from glass conversion; B: mineralized bone; C: hollow cavity in 13-93B3 fibers post conversion to HA. New bone percentage formed in rat calvaria defects over 12 weeks with four bioactive glass scaffold groups. Adapted with permission from Gu et al. 2013 [40]. Copyright © 2013, Elsevier.

In contrast to these outcomes, a separate investigation, Bi et al. [44] examined the effectiveness of 3D scaffolds made from 13-93 silicate, 13-93B1 borosilicate, and 13-93B3 borate glasses in promoting bone regeneration, angiogenesis, and hydroxyapatite (HA) conversion using a critical-sized rat calvaria defect model. The scaffolds were obtained by thermally fusing randomly oriented short fibers, with 45S5 bioactive glass particles serving as a positive control and empty defects as the negative control. After 12 weeks of implantation, defects filled with bioactive glasses exhibited bone regeneration both at the top and bottom of the implants. There was no significant difference in average bone regeneration between 13-93B3 and the positive control, 45S5 BG. The average new bone growth was 12.4% for 45S5 BG, 8.5% for 13-93 silicate glass, 9.7% for 13-93B1 borosilicate glass, and the highest amount of new bone growth was observed in 13-93B3 borate glass at 14.9%, which was significantly higher than that of 13-93 silicate glass. The incorporation of higher boron oxide content enhanced mineralization capacity and HA formation, evident from the increased von-Kossa

positive area. PAS-stained sections showed the highest percentage of blood vessel area in the 45S5 BG group, significantly surpassing all three experimental scaffolds. Empty defects consisted only of fibrous tissue and did not exhibit bone formation or von Kossa positive material. SEM-EDS analysis confirmed the complete conversion of 45S5 and 13-93B3 bioactive glasses to HA after 12 weeks, whereas 13-93 and 13-93B1 glasses were only partially converted. These findings highlight the promising potential of 13-93B3 glass scaffolds as a bone substitute material in promoting bone regeneration and the main results are shown in **Figure 6**.

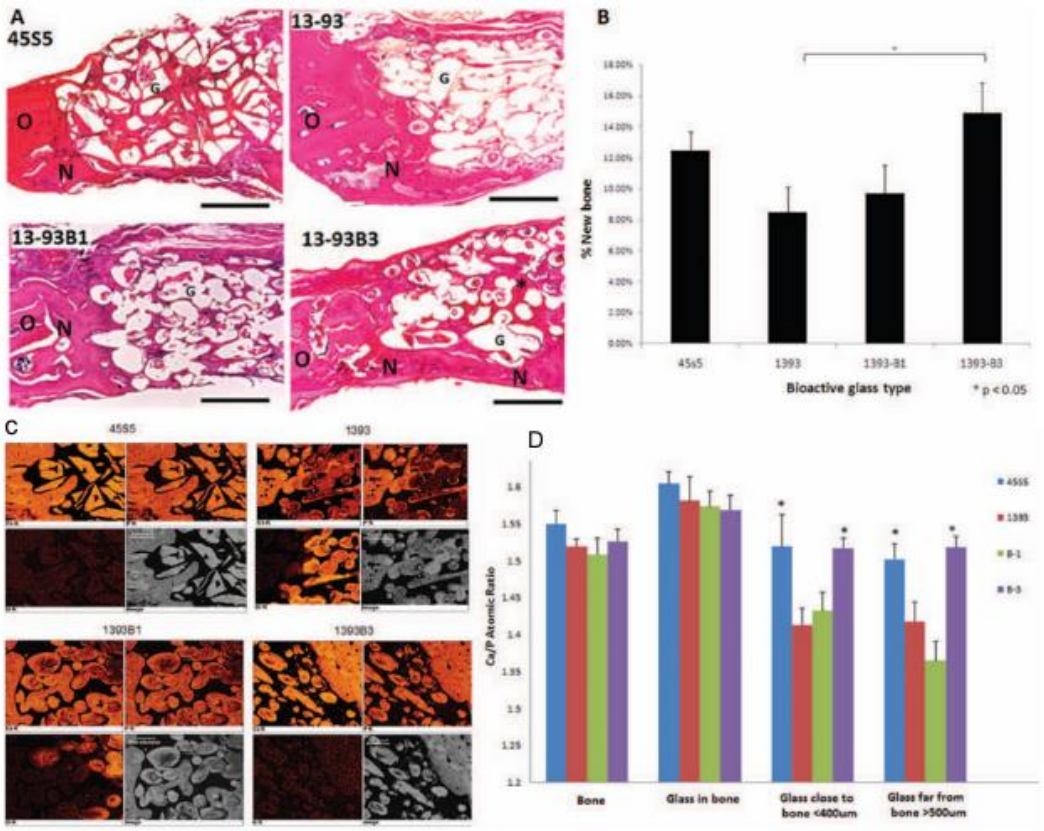

Figure 6. Bioactive glass 45S5, 1393, 1393B1, and 1393B3 outcomes at 12 weeks post-surgery: (A) H&E stained sections of rat calvaria defects, indicating old and new bone (O and N), boney islands (*), and glass (G). Scale bar: 500 µm. (B) Percentage of new bone regeneration. (C) SEM-EDS X-ray maps displaying signals of calcium, phosphorus, and silicon. (D) Atomic calcium-to-phosphorus ratio in bone and bioactive glass particles 45S5, 1393, 1393B1. Adapted with permission from Bi et al. 2012 [44]. Copyright © 2012 Wiley Periodicals, Inc.

In a pioneering study conducted by Ding et al. [45], the focus was on exploring the impact of spleen and macrophage polarization on bone regeneration using bioactive borosilicate glass. Their investigation introduced molecular dynamics (MD) simulations to replicate the structures of a specifically designed glass series, known as 1393-B-Sr. Through the analysis of various

structural parameters and descriptors, the relationship between the primary dissolution rate of boron (B) and strontium (Sr) and the structural descriptor F_{net} was examined. Following this analysis, the researchers proceeded to prepare the glass using a high-temperature melting technique, and subsequently, 3D-printed bioactive borosilicate glass (BG) scaffolds were fabricated.

The results of this study demonstrated the synergistic effects of boron (B) and strontium (Sr) in promoting vessel regeneration, modulating M2 macrophage polarization, and facilitating new bone formation both *in vitro* and *in vivo* when released from the 1393B2Sr8 bioactive glass (BG). Notably, the 1393B2Sr8 BG was found to mobilize monocytes from the spleen to the bone defects and subsequently modulate them into M2 macrophages, which then cycled back to the spleen. To investigate the necessity of spleen-derived immune cells in bone regeneration, two rat models (with/without spleen) of skull defects were established. Results revealed that rats without a spleen had fewer M2 macrophages surrounding the skull defects and slower recovery of bone tissue, indicating the beneficial effects on bone regeneration of circulating monocytes and polarized macrophages provided by the spleen. This study offers a novel approach and strategy for optimizing the complex composition of novel BG and highlights the importance of the spleen in modulating the systemic immune response to contribute to local bone regeneration. **Figure 7** shows the main findings by the author.

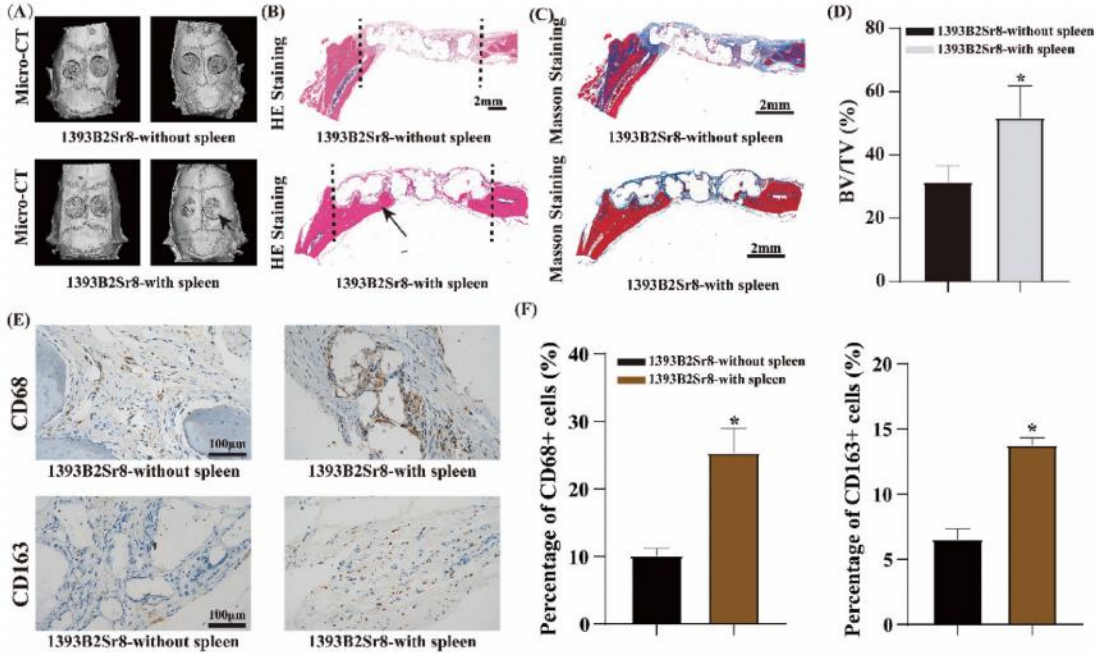

Figure 7. (A) Micro-CT evaluation of bone regeneration in rat (with/without spleen) calvaria defects at 8 weeks post-implantation of 1393B2Sr8, the left reconstructed imaged is the top view, and the right one is the upward view. (B) H&E staining and (C) Masson staining of the new bone formation surrounding scaffolds. (D) The calculated BV/TV of the skull defects of 1393B2Sr8 with/without spleen. (E) CD68 and CD163 immunostaining of local new bone tissues of 1393B2Sr8 group with/without spleen. (E) Quantification of CD68þ and CD163þ cells in rats with/without spleen. *P < 0.05. Reproduced with permission from Ding et al.2023 [45] (Creative Commons Attribution License (CC BY)).

ii) Rabbit model studies

The capacity of trabecular 13-93B1 glass scaffolds to support osseous regeneration was evaluated by Gu et al. [46]. In their study, they examined the scaffolds' effectiveness in non-critical sized rabbit femoral defects and their potential as carriers of platelet-rich plasma (PRP) to enhance osteogenesis in critical-sized segmental defects in the rabbit radii diaphysis. The scaffolds prepared using the foam replication method with porosity of 78 ± 8% and a pore size in the range of 400–650 μm, with an average of ~500 μm. *In vitro* experiments confirmed the bioactivity of the 13-93B1 scaffolds, as they degraded and formed a hydroxyapatite (HCA) layer when immersed in a simulated body fluid (SBF) solution. Histological analysis revealed superior bone healing in rabbit femoral defects implanted with the 13-93B1 scaffolds compared to the unfilled control group. In the rabbit radii defects, both unloaded, and PRP-loaded scaffolds integrated with the host bone, while no bone formation was observed in the empty defects. Furthermore, defects implanted with PRP-loaded scaffolds demonstrated accelerated

callus formation and a greater area of new bone compared to those implanted with unloaded scaffolds. Consequently, both unloaded and PRP-loaded 13-93B1 scaffolds exhibited significant potential for enhancing *in vivo* bone regeneration. **Figure 8** reveal the *in vivo* outcomes found by the author.

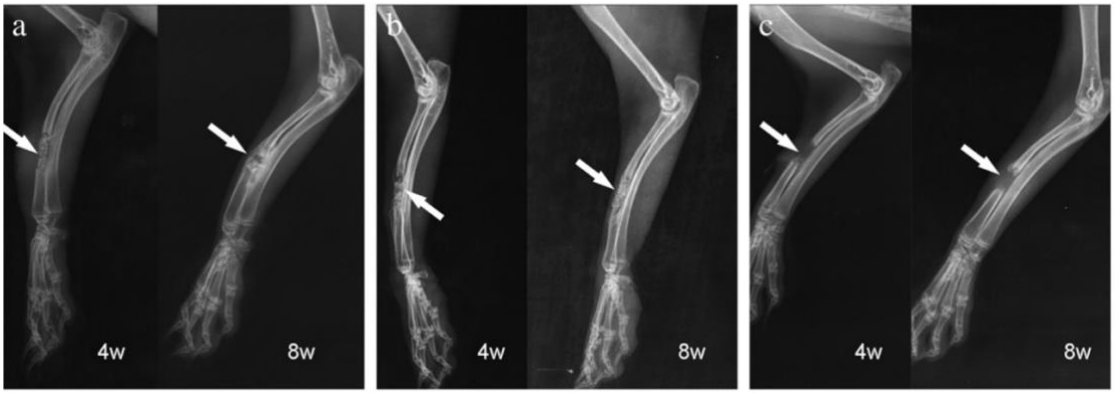

Figure 8. X-ray radiographs of rabbit radius defect sites after implantation for 4 and 8 weeks with (a) 13-93B1 scaffolds, and (b) 13-93B1 scaffolds loaded with platelet-rich plasma; (c) unfilled defect at 4 and 8 weeks. Reproduced with permission from Gu et al. 2014 [46]. Copyright © 2014, Elsevier.

Khan et al. [50] conducted a study on the effects of strontium and lithium ion doping on the biological properties of bioactive glass (BAG) obtained through the melted-derived technique. Using a rabbit femoral defect model, the researchers evaluated soft and hard tissue formation after 2 and 4 months. Histological observations demonstrated excellent osseous tissue formation in scaffolds doped with strontium and lithium ions, while scaffolds doped with lithium ions alone showed moderate bone regeneration. Fluorochrome labeling studies indicated wider regions of new bone formation in the strontium and lithium-ion doped samples compared to the samples doped with lithium ions alone. Scanning electron microscopy (SEM) analysis revealed a rich collagenous network and minimal or no interfacial gap between bone and implant in the strontium and lithium-ion doped samples, contrasting with the samples doped with lithium ions alone. Furthermore, micro-CT analysis demonstrated that the samples doped with both strontium and lithium ions exhibited the highest degree of peripheral cancellous tissue formation and increased vascularity compared to other compositions, with cortical tissues inside the implanted samples. These findings highlight that the addition of strontium and/or lithium ions modifies the physical and chemical properties of BAG, fostering early-stage *in vivo* osseointegration and bone remodeling, **Figure 9** and **Figure 10** presents the main outcomes. This research holds significant implications for the field of bone tissue engineering.

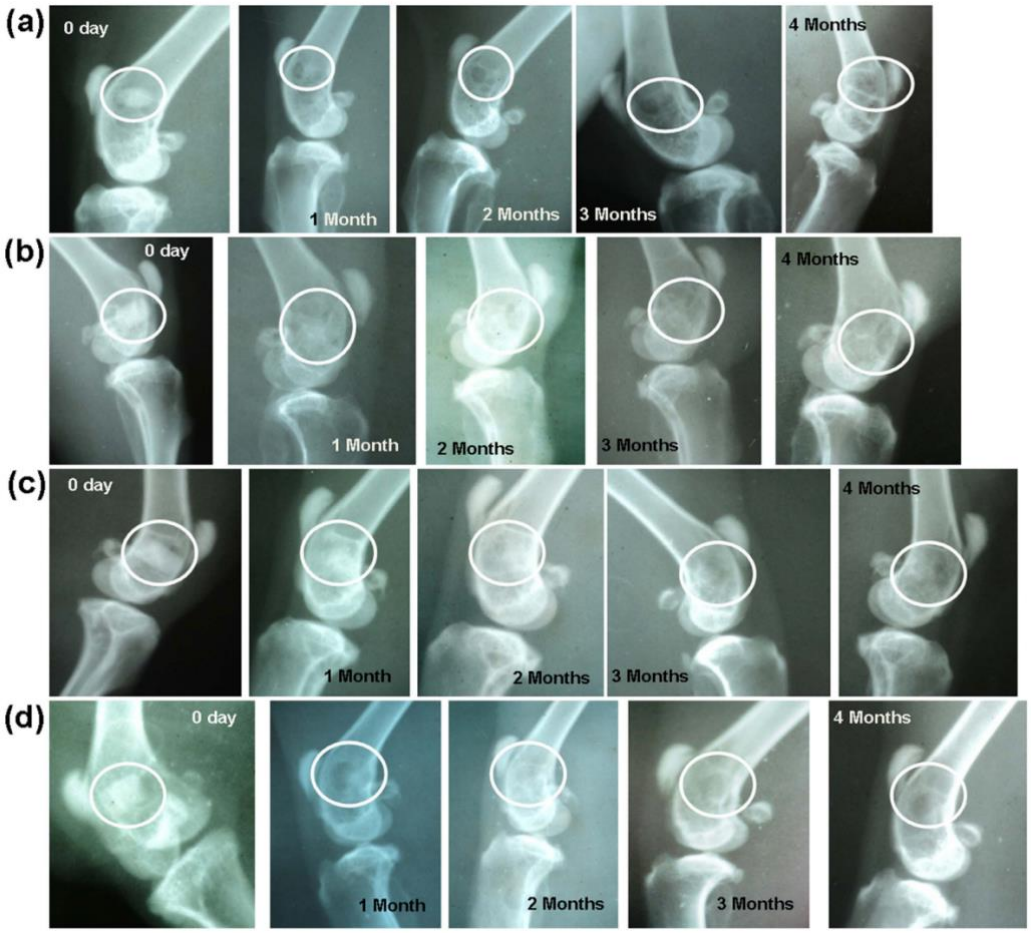

Figure 9. Radiographs taken at '0' day, 1, 2, 3 and 4 months post-operatively implanted with (a) BAG, (b) L-BAG, (c) S-BAG and (d) LS-BAG. Reproduced with permission from Khan et al. 2016 [50] (Creative Commons Attribution License (CC BY)).

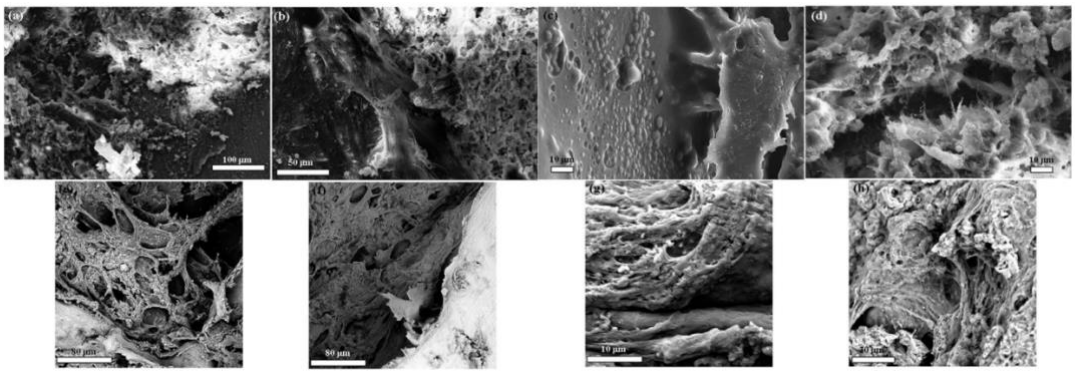

Figure 10. SEM images of bone-material (BAG, L-BAG, S-BAG and LS-BAG) interface taken after 2 months (a–d) and 4 months (e–h) post-operatively respectively. Reproduced with permission from Khan et al. 2016 [50] (Creative Commons Attribution License (CC BY)).

2.4.1.4 Melt-derived S53P4 bioactive glasses

The bioactive glass S53P4, with a specific composition of 53SiO_2, 4P_2O_5, 23Na_2O, and 20CaO (wt. %), was first developed by Anderson and Karlsson in 1990 and approved by the FDA. It is commercially known as BonAlive Biomaterials Ltd. and is used in various clinical applications, particularly in the healing of bone defects and the treatment of osteomyelitis (inflammation of the bone and/or bone marrow caused by infection). The initial reported applications of S53P4 were in craniofacial surgeries, and despite being a variant composition of 45S5, it is the most used composition in current clinical practice. One of the main advantages of S53P4 bioactive glass, in addition to its excellent bone healing properties, is its ability to protect against bacterial adhesion and colonization on its surface, possessing antimicrobial properties by hindering bacterial growth. The antibacterial properties result from a localized increase in pH caused by the exchange of alkaline ions with protons in solution (body fluid). S53P4 is primarily used in granules (0.8 - 3.5 mm) but can also be used in the form of non-porous plates or discs [8]. According to long-term study results, S53P4 bioactive glass degrades slowly, with visible remnants still present after fourteen years of implantation, and no ectopic bone was found in the surrounding soft tissue, confirming its osteoinductive nature rather than osteoconductive. Although complete resorption may not occur, the application of S53P4 has high clinical success rates and may become the standard procedure, especially in the treatment of osteomyelitis, due to its antibacterial effects. Moreover, S53P4 has been identified for its ability to offer an antimicrobial treatment solution using a distinct mechanism from antibiotics, potentially contributing to the rise of antibiotic-resistant bacteria. [7,60].

i) Rabbit model studies

Björkenheim et al. [47] conducted a study to assess the *in vivo* osteogenic potential of induced membranes (IM) made of BAG-S53P4, BAG-S53P4-PLGA, and PMMA. The bioactive glasses BAG-S53P4 were developed using the melted-derived method. They underwent crushing and sieving, resulting in granules ranging from 300 to 500µm. Subsequently, the granules were sintered to form cylindrical scaffolds. BAG-S53P4-PLGA scaffolds were obtained by coating the BG scaffold with a solution of 20 wt.% PLGA.

The results of BAG-S53P4, BAG-S53P4-PLGA, and PMMA scaffolds found significant bone in-growth and reaction layer formation already at 2 weeks after implantation

in all bag samples. The study also showed that BAG-S53P4 and BAG-S53P4-PGLA scaffold IMs showed similar or superior expression of BMP-2, -4, and -7 compared with PMMA IM. While bone ingrowth into BAG scaffolds increased over time, active bone formation occurred inside the BAG scaffolds, and the respective BMP expressions were similar or superior for the BAG IMs compared with PMMA.

In this study, the researchers observed comparable results to previous studies regarding the expression of selected bone-inducing factors. They found that the expression of BMP-2, -4, and -7 in the BAG-S53P4-PLGA induced membranes (IMs) was similar or even superior to the membranes of BAG-S53P4 and PMMA. Specifically, at 8 weeks, BAG-S53P4-PLGA showed higher expression of BMP-4 compared to BAG-S53P4.

The results showed no significant differences in BMP-2 expression during the 8-week follow-up between PMMA, BAG-S53P4, and BAG-S53P4-PLGA scaffolds, except for a peak expression at 4 weeks for BAG-S53P4. The difference in results can be attributed to the different methodologies used to detect BMP production. Stable expression of BMP-4 was observed for both PMMA and BAG-S53P4, while BAG-S53P4-PLGA IMs showed a different pattern with a high peak at 8 weeks. The reason for this high BMP-4 expression in BAG-S53P4-PLGA scaffolds remains a topic for further research. Similarly, an elevated expression of BMP-7 was observed for BAG-S53P4-PLGA compared to BAG-S53P4 and PMMA at the 8-week time point. **Figure 11** shows the main results found by the authors.

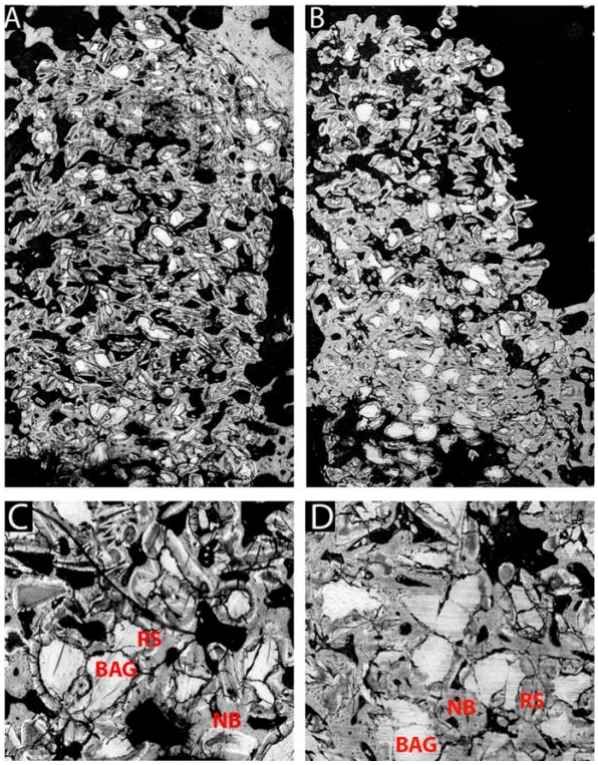

Figure 11. Representative SEM images from BAG-S53P4 (A) and BAG-S53P4-PLGA (B) scaffolds 8 weeks post implantation. Scaffold visible as highly dense (white) trabecular material surrounded by bone matrix and medullary spaces. Black areas are medullary spaces. Notice the extensive ingrowth of bone into the scaffold and replacement of BAG with bone matrix. Enlargements of representative cortical regions from 8 week samples are shown in (C) (BAG-S53P4) and (D) (BAG-S53P4-PLGA). New bone (NB), bioactive glass (BAG), and reaction surface (RS) are marked in red text to clarify the different layers seen on the SEM. Reproduced with permission from Björkenheim et al.2019 [47] . Copyright © 2018 Wiley Periodicals, Inc.

Micro-CT scans confirmed the results obtained from the study. The images showed significant bone ingrowth and reaction layer formation as early as 2 weeks after scaffold implantation. Comparisons between the two BAG scaffolds were limited due to the nature of the obtained images. However, it was observed that the BAG-S53P4-PLGA scaffolds exhibited more rapid bone formation compared to BAG-S53P4. The study suggests that the elevated expressions of BMP-4, BMP-7, and VEGF, along with the presence of capillary beds in PLGA-coated BAG-S53P4, may contribute to the more rapid bone formation. The PLGA coating did not have a significant negative effect on bone formation inside the BAG-S53P4-PLGA scaffold.

2.4.2 BG particles: *in vivo* outcomes

Bioactive glass particles are highly regarded for their unique properties and wide range of applications in the field of biomaterials. These particles are composed of glass-forming

elements such as silica (SiO_2), calcium oxide (CaO), and phosphorus pentoxide (P_2O_5). The bioactivity of these glass particles stems from their ability to form a biologically active hydroxyapatite (HA) layer on their surface when exposed to body fluids. This HA layer promotes the integration of the particles with surrounding tissues, facilitating bone regeneration and tissue healing processes. Bioactive glass particles can be tailored in terms of size, shape, and composition to meet specific requirements for various applications. They are commonly used in bone tissue engineering as fillers, coatings, or scaffolds, promoting osteogenesis and enhancing bone formation. Additionally, bioactive glass particles find application in drug delivery systems, as their porous structure allows for controlled release of therapeutic agents. Their biocompatibility, bioactivity, and versatility make bioactive glass particles a promising material for advanced biomedical applications.

The reviewed articles investigate different types of bioactive glasses, where the raw material was obtained by sol-gel or melt derived method, including mesoporous bioactive glass (MBG) and new compositions offering an intriguing opportunity to examine and compare the distinctive characteristics and performance of these bioactive glass types. For specific details regarding the compositions of bioactive glass particles, please refer to **Table 4**.

2.4.2.1Melt-derived

i) Rat model studies

Boyd et al.[33] conducted an evaluation of the *in vivo* properties of calcium-strontium-zinc-silicate glasses in rat calvaria defects. The aim was to investigate the combined release of zinc and strontium ions from the glasses and their potential to provide synergistic therapeutic effects for bone health. Three compositions were developed: BT 107, BT 108, and BT 109. The final particle size distribution ranged from 90-350μm.

Histological examination revealed that particles of the test material were visualized as small angular, pale glassy particles, typically slightly out of plane in the section. The particles were aggregated and occupied angular spaces in the medullary space and cortical bone. In most cases, particles had escaped into the surrounding soft tissue, leading to a localized foreign body reaction characterized by macrophages, scattered giant cells, and fibrosis. However, there was no evidence of inflammation in terms of increased vascularity, chronic inflammatory cells, or neutrophils.

The cortex of the femurs healed in all animals, except for one in which BT107 was implanted. Within the central medullary space, the implanted material was surrounded by new bone without intervening fibrous tissue or fibrous tissue with bone formation. BT109 induced direct bone formation in all six animals, while BT108, BT107, and Novabone showed a more mixed response with the presence of both bone and fibrous tissue. No evidence of inflammation or foreign body giant cell/osteoclast response was observed in the medullary space, and the residual marrow tissue appeared histologically normal.

In another study, Zhao et al. [34] evaluated an emerging pH-neutral bioactive glass (PSC) that was developed with a higher phosphate content (10mol% to 2mol% P_2O_5) and zero Na_2O content. The outcomes of PSC were compared to those of 45S5 and β-TCP, which are two popular artificial bone grafting materials. The powders of PSC, 45S5, and β-TCP had particle sizes smaller than 70μm and were implanted into defects in the rats' calvaria bone. The control group consisted of empty defects.

Micro-CT was used to evaluate new bone formation at 6- and 12-weeks post-operation. At 6 weeks, PSC groups showed higher levels of new bone tissue compared to 45S5, β-TCP, and control groups. The bone mineral density (BMD) of PSC groups was also higher than that of the other groups. At 12 weeks, minimal new bone formation was observed in the control groups, while PSC, 45S5, and β-TCP groups displayed gradual growth of new bone from the edge to the inside of the defect. PSC groups exhibited significantly higher BMD and larger percentages of new bone area compared to the other groups. From a histological perspective, PSC groups showed more organized and continuous new bone tissue with lamellar bone morphology. Additionally, PSC groups demonstrated a greater number of blood vessels, indicating its ability to promote blood vessel formation *in vivo*. These findings were consistent with the *in vitro* angiogenic differentiation of BMSCs. **Figure 12** illustrates the main findings.

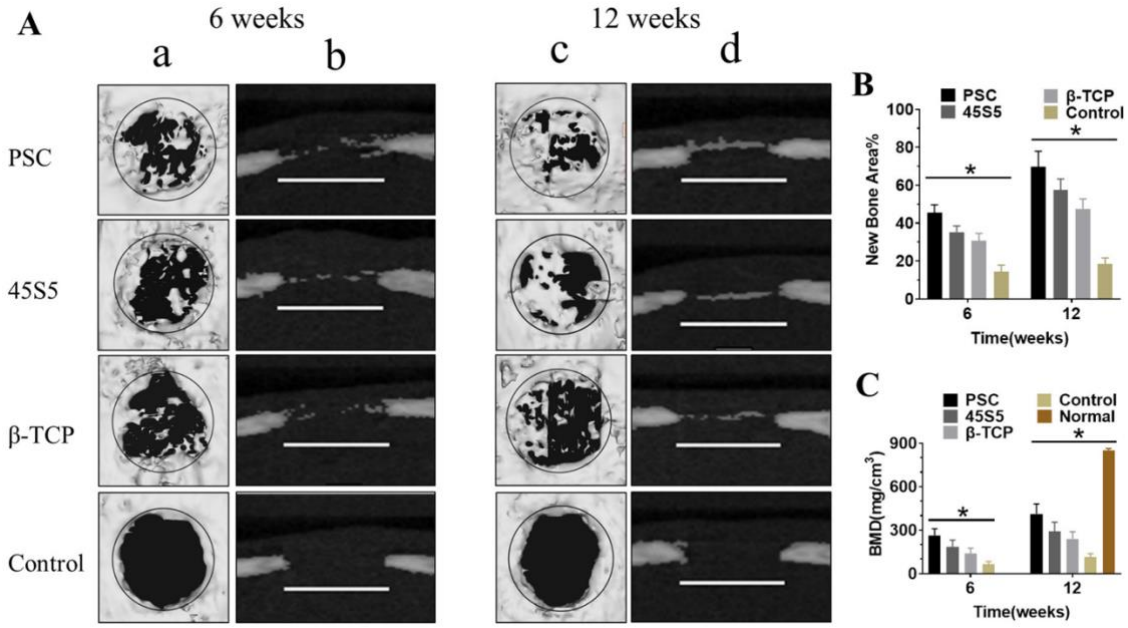

Figure 12. Micro-CT image analysis of calvaria bone regeneration. A) the horizontal plane (a, c) and the coronal plane (b, d). B) Statistical result of new bone area. C) Statistical result of BMD. Diameter of the circle 5 mm and Scale bar 5 mm. (*p < 0.05). Reproduced with permission from Zhao et al. 2020 [34] . Copyright © 2020, Elsevier.

El-Meliegy et al. [35] evaluated another four compositions with lower Na_2O content (less then 10 mol %) and free of K_2O and Al_2O_3 based on the Na_2O–CaO–MgO–P_2O_5–SiO_2 glass system, referred as A, B, C and D. The *in vivo* studies were conducted in rat femur bone defects in which the particles implanted had particle sizes in a range of 300-355µm in a period of 12 weeks. Scanning electron microscopy (SEM) analysis of the bioactive degradable glass implanted *in vivo* revealed a positive response with the host bone, with remodeling occurring at the glass-bone interface. Over a 12-week period, critical size bone defects in rat femurs grafted with glass particles A, B, and C were completely healed, filled with mineralized bone matrix. However, defects grafted with glass particles D remained open and were not fully healed.

Histological analysis showed the formation of new bone between the granules of all implanted bioglasses, without evidence of fibrous encapsulation. Osteoblasts and osteocytes were observed near the surface of the granular implants, indicating active areas of bone deposition, resorption, and remodeling between 6 and 12 weeks of implantation. Bone growth originated from the deep end walls of the defect and progressed inward for all implant compositions. Complete bone integration was observed for bioglass A at both time points, with new bone formed in continuity with the implant surface from the cortical bone at the surgical site into the marrow space. Transverse sections of the critical size bone defects at 6- and 12-

weeks post-implantation showed new bone tissue filling the spaces between the implanted particles, without a fibrous tissue layer. No signs of inflammatory cell infiltration were observed at the implantation site, and bone formation was also observed on the surface of the bioglass particles. The amount of newly formed bone depended on the composition, with bioglass A demonstrating the highest level of bone formation followed by B, C, and D.

Moon et al. [37] conducted a study to investigate the bone-regenerative effect of amorphous calcium phosphate glass powder with a mean particle size of 400μm in the CaO-CaF_2-P_2O_5-MgO-ZnO glass system. They created calvaria critical-sized defects (8mm) in 60 male Sprague-Dawley rats. Histological observations revealed the presence of thin connective tissue at the defect site in the control group after 2, 4, and 8 weeks. In the experimental group, fibrous connective tissue and residual glass particles were observed at 2 weeks, accompanied by enhanced new bone formation compared to the control group. Histomorphometry analysis demonstrated that the length and area of new bone increased with graft duration in both groups. Radio densitometric analysis indicated an increase in relative bone density with graft duration, with significant differences observed only at 8 weeks in the control group compared to 4 weeks.

2.4.2.2 Sol-gel Derived

i) Rat model studies

Lehman et al. [42] conducted a pioneering study utilizing the tibia defect model and comparing six different experimental time points to evaluate the impact of BG-90, a bioactive glass with a high content of SiO_2 (90%), on bone regeneration.

The results of *in vivo* analysis demonstrated that BG-90, a synthesized biomaterial, promoted bone formation in tibia defects and induced a mild inflammatory process throughout the experimental period. Initially, there was a delay in bone formation compared to the negative and positive control groups in the first two weeks. However, from the third week onwards, BG-90 showed sustained bone formation, which was significantly different from the positive control at four weeks. Furthermore, BG-90 was completely resorbed after four weeks, and newly formed bone trabeculae were sparsely observed, indicating that it did not disrupt the physiological bone remodeling cycle. Similar outcomes were observed for the positive control group.

The expression of BMP-2, a key protein involved in bone formation, followed a pattern consistent with the kinetics of bone formation and resorption in all groups. At the one-week

time point, all groups exhibited a peak expression of BMP-2, aligning with the higher percentage of bone formation observed during the initial grafting period. Notably, only the BG90 group showed significant expression of BMP-2 at the last experimental time, possibly due to residual ionic products released from BG90 particles.

ii) Rabbit model studies

Lalzawmlian et al. [48] perform a study with the aim to synthesize MBG using different surfactants CTAB (M1), (PEG) (M2) and Pluronic P123 (M3) and to understand their bone regeneration efficacy in combination with insulin-like growth factors (IGF-1) in bone defect of rabbit femur.

The radiological analysis revealed significant findings. In the control group, radiographs at 0 days showed a homogeneous radiodense implant filling the defect area without spillage. At 45 days, the implant remained unchanged in radiodensity, and the cortex exhibited signs of remodeling with uniform cortices. By 90 days, the implant had reduced as newly formed radiodense bony tissue filled the defect, although the remodeling process was not yet complete. In the M1 sample, the implant uniformly filled the defect at 0 days, and at 45 days, there was a decrease in radiodensity with evidence of cortical remodeling and resorption of the implant. By 90 days, the cortical defect was well filled with uniform and hyperdense osseous tissue, indicating complete remodeling. Similar patterns were observed in the M2 and M3 samples, with progressive changes in radiodensity and evidence of bone regeneration and remodeling.

The oxytetracycline labeling study further supported the findings of bone formation. At 45 days, all samples exhibited moderate coverage by newly formed bone tissue, indicating ongoing bone regeneration. At 90 days, the samples showed increased coverage and scattered regions of new bone formation, with M2 and M1 samples demonstrating greater effectiveness in bone regeneration.

Histological analysis at 45 and 90 days revealed the progression of bone healing in all samples. The control sample showed osteoblasts, osteocytes, and fibroblastic proliferation at 45 days, with well-framed osseous structures and intact cortical structures at 90 days. In the M1 sample, vascularization, fibrous tissue proliferation, and bony laminae formation were observed at 45 days, with the presence of osteoid tissues and haversian canals at 90 days. The M2 sample exhibited bony matrices and osteoblastic bony proliferations at 45 days, and neoforming osteoid with haversian canals and bony lacunae at 90 days. The M3 sample showed fibrovascular

osseous proliferation and osteoblast activity at 45 days, with haversian canals and osteoclasts present at 90 days.

Toxicological evaluation of kidney, liver, and heart tissues showed normal microstructures without major degenerative changes, indicating the biocompatibility of the materials used. Micro CT evaluation provided 3D images showing the embedded nature of the bioactive glasses within the hard bone tissue. At 45 days, complete absorption of the materials with the formation of a porous dense network was observed. By 90 days, the defect hole diameter decreased, and complete periosteum formation occurred, indicating successful new bone formation as illustrated in **Figure 13**.

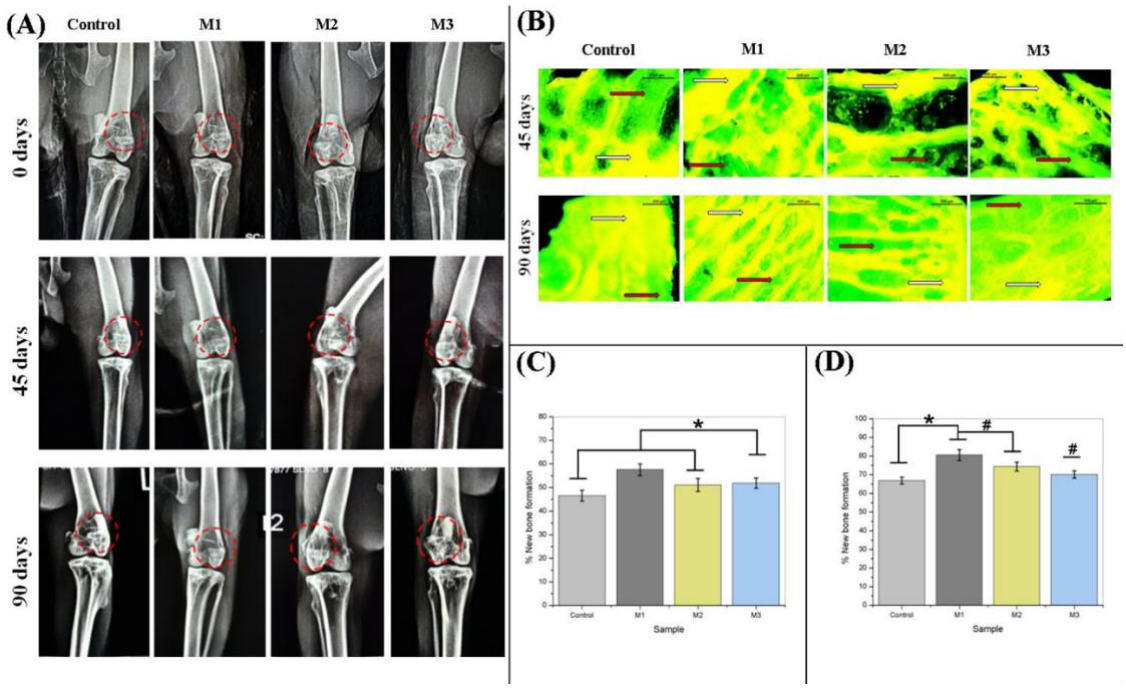

Figure 13. (A) Radiographic images of the implanted bones after '0', 45 and 90 days. The red broken circles are highlighting the area of defect and implant; (B) Fluorochrome labeling images of implanted bone taken after 45 and 90 days; Golden yellow (white arrow) represents new bone and sea green (red arrow) represents old bone. Scale bar: 500 µm; Percentage of new bone formation after (C) 45 and (D) 90 days. Data: Mean ± SD, [n =4]. Reproduced with permission from Lalzawmliana et al. 2019 [48] . Copyright © 2018, Elsevier.

In a study conducted by Anesi et al. [51] the regenerative potential of two novel bioactive glasses, BGMS10 and Bio_MS, was evaluated *in vivo*. These bioactive glasses, which contained specific therapeutic ions, were produced in granules and implanted in rabbits' femurs for a duration of up to 60 days. The particle size of the granules ranged between 100 and 500µm.

The results, supported by histomorphometry and light microscopy analysis, revealed that after 30 days, BGMS10 and Bio_MS exhibited similar performance to the well-known 45S5 bioactive glass. However, after 60 days, their behavior differed significantly. The 45S5

granules were mainly surrounded by wide and scattered bone trabeculae, with large amounts of soft tissue separating them. On the other hand, although the amount of bone formation was similar, BGMS10 and Bio_MS granules exhibited thin and uniformly distributed trabeculae around the granules.

Overall, the novel BG granules demonstrated good biocompatibility and osteoconductivity. These findings suggest that BGMS10 and Bio_MS have potential advantages over the 45S5 granules. The uniform distribution of bony trabeculae observed in BGMS10 and Bio_MS is favorable compared to the less uniform and coarse trabeculae surrounded by large soft tissue areas seen in the 45S5 granules. It should be noted that these results are preliminary, and further investigations are necessary to fully understand the potential of these novel bioactive glasses. **Figure 14** shows the main results found by the authors.

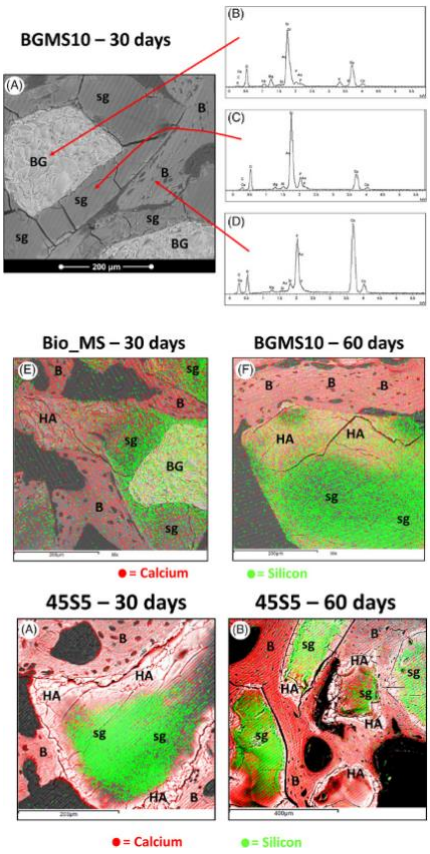

Figure 14. BGMS10 group at 30 and 60 days: representative SEM micrographs and results of the X-ray microanalysis (B–D). In particular, (E and F) and (A-B) for the 45S5 group, report the X-EDS maps showing the distribution of Si—representative of both the glass and the silica gel—and Ca—representative of both the hydroxyapatite (or the calcium phosphate rich phase) and the bone tissue—in the BGMS10 group. B, bone; BG, bioactive glass; HA, hydroxyapatite; sg, silica gel. Reproduced with permission from Anesi et al. 2023 [51] (Creative Commons Attribution License (CC BY)).

2.5 DISCUSSION

The present review aimed to investigate the *in vivo* outcomes of using bioactive glasses for bone regeneration. Since the first bioactive glass – Hench's early study in 1969 – many new bioactive glasses and clinical products had been studied and developed. However, the new research on the field still faces the bioactive glasses oldest challenges such as reliable coatings, mechanical properties, and reliable *in vitro* and *in vivo* testing. This review included 20 *in vivo* studies that evaluated the effectiveness of bioactive glasses for bone regeneration in various animal models. The present discussion will summarize the main findings of the review, discuss the clinical relevance of the results, acknowledge the limitations of the available evidence, and consider potential avenues for future research in this area.

Although *in vitro* tests provide initial insights into material performance, they have limitations in fully capturing the *in vivo* behavior and clinical relevance of the bioactive glasses such as a correct selection of the cell culture, the age of the cells and incubations times. In this regard, *in vivo* animal models offer a dynamic and physiologically relevant environment for better understanding and evaluation of these materials. Despite the extensive focus on *in vitro* characterization of BGs, there remains a scarcity of reports specifically addressing *in vivo* studies of the range of bioactive glasses in animal bone defect models.

Three-dimensional (3D) scaffolds that mimic the microstructure and porosity of native bone are highly promising for bone tissue engineering (BTE) strategies in treating critical-sized bone defects. Bioactive inorganic materials, particularly different compositions of bioactive glasses (BGs), have gained significant attention as potential BTE scaffolds due to their osteoconductive and osteoinductive properties. Continuous research efforts worldwide have led to the development of various compositions and architectures of BG scaffolds. However, before these scaffolds can be translated to clinical applications, thorough characterization tests are necessary to assess their biocompatibility and osteogenic potential.

The chemical composition of BGs plays a crucial role in determining their *in vivo* performance. Modifying the composition significantly affects scaffold degradation, bioactivity, and the ability to fabricate scaffolds with specific shapes and porosities. Different compositions also result in varying degrees of crystallinity, influencing whether the scaffolds are amorphous (glassy) or (partially) crystalline glass-ceramic structures. Therefore, understanding the impact of BG composition on scaffold properties is vital for optimizing their design and performance in bone regeneration applications. Boron-containing glasses, particularly those with higher B_2O_3 content, have shown a faster degradation rate and greater hydroxyapatite (HA) formation

when compared to silicate BGs [40,44,46,50]. However, despite these findings, the available evidence does not conclusively confirm whether this rapid conversion directly leads to increased bone formation *in vivo*.

Divergent outcomes regarding osseous regeneration were observed in the same animal model, utilizing identical scaffold compositions and a consistent implantation period of 12 weeks [40,44]. For instance, Bi et al. [44] compared the regenerative potential of 13-93 silicate, 13-93B1 borosilicate, and 13-93B3 fibrous scaffolds in critical-sized non-loaded rat calvaria defects. They discovered that the 13-93B3 borate glass yielded the highest levels of new bone growth and von Kossa-positive area, which were significantly greater than those achieved with 13-93 silicate glass. However, in a contrasting study conducted by Gu et al. [40], an inverse relationship was observed between 13-93B3 content and bone regeneration in rat calvaria defects implanted with scaffolds of fibrous microstructure. The scaffolds consisted of a blend of various ratios of silicate 13-93 and borate 13-93B3 glasses. Notably, defects implanted with 100% 13-93 scaffolds exhibited significantly enhanced new bone formation compared to scaffolds containing 50 and 100 wt.% 13-93B3 glass. These findings imply that low concentrations of boron ions are advantageous for healthy bone formation, while high boron concentrations may induce chronic toxicity.

The fabrication techniques employed in scaffold production significantly influence the scaffold architecture, pore characteristics, tissue growth, tissue regeneration, and mechanical properties. Various methods have been utilized to create 3D porous bioactive glass (BG) scaffolds for bone tissue engineering (BTE) applications. These methods include thermally bonding particles and fibers, unidirectional freezing of suspensions, polymer foam replication, sol-gel foaming, and more recently, solid freeform fabrication (SFF) or additive manufacturing techniques. The use of SFF methods enables precise control over the microstructure of the scaffolds, which was not achievable with conventional methods. Previous literature has extensively reviewed different scaffold fabrication methods for BTE applications, including a comprehensive overview presented in **Table 3**. The table summarizes the various techniques discussed in the review, highlighting their respective advantages and limitations.

Coating techniques were also explored to enhance the properties of bioactive glass scaffolds. The findings revealed a significant trend of coating scaffolds with mesoporous bioactive glasses, which can be attributed to their ability to provide controlled release of therapeutic agents, favorable nanostructure, and enhanced osteogenesis. The findings made by Li et al. [36], Liu et al. [53], and Covarrubias et al. [43], the *in vivo* results evaluating critical bone defects consistently indicated that scaffolds with higher MBG concentrations promoted

superior bone regeneration compared to scaffolds without MBG. The analysis results supported these findings, demonstrating a significantly higher percentage of new bone area in scaffolds with higher MBG concentration. However, despite the study conducted by Sui et al. [38] to address MBG in situ labeling, further investigations are needed to address lingering questions. These include understanding the biological effects of MBG nanostructure and ion-release profiles, as well as the potential long-term toxicity of degradation products.

A previous review conducted by Bocaccini et al. [16] in 2019 examined the research question of whether 3D BG scaffolds can regenerate bone. Some of the articles included in that review were also found in the present study. The findings highlighted by Bocaccini reinforce the discussion at hand. Over a span of four years since the current research began, only a limited number of studies have been published on the application of bioactive glass scaffolds *in vivo*, particularly focusing on new compositions and scaffold coatings. Additionally, in line with their study, the assessment of the osteoregenerative ability of BG scaffolds in humans remains challenging, with the rat model being the most employed, followed by rabbits. Considering this, the main question posed by Bocaccini regarding the regenerative potential of BG scaffolds is answered affirmatively, and recent studies included in this review provide further support. However, it is important to note that the scope of this research is not limited to scaffolds alone, as another group of interest, namely particles, was also evaluated for their *in vivo* application.

Similarly to scaffolds, the bioactive glass particles composition, size, and shape significantly influence bone regeneration. The tendency for crystallization of a bioactive glass also has an impact on its bioactivity and represents one of the ongoing challenges in the field of bioactive glasses. Two well-established manufacturing routes, namely melt-derived and sol-gel routes, determine a significant portion of the involved properties. Different morphological aspects are achieved, and the results obtained in this research highlight a higher number of *in vivo* studies for melt-derived bioactive glasses, with variations in glass composition.

This can be supported by the versatility, scalability, and homogeneity of the manufacturing route, which also enables easier testing of new compositions, as reported by [61]. In the studies included in this review, particles used in the *in vivo* tests ranged from 30 to 700μm, with smaller particles generally associated with better bone regeneration outcomes (Table 4). Bioactive glass particles can be tailored in terms of size, shape, and composition to meet specific requirements for various applications. In the context of bone tissue engineering, they are commonly used as fillers, coatings, or scaffolds, promoting osteogenesis and enhancing bone formation. The studies conducted in rat models by Boyd et al. [33] and Zhao et al. [34] investigated the *in vivo* properties of different compositions of bioactive glass particles. Both

studies demonstrated positive outcomes, with the particles promoting bone healing and integration with the surrounding tissue. Furthermore, the study by Zhao et al. [34] highlighted the superior performance of a pH-neutral bioactive glass composition (PSC) compared to other popular artificial bone grafting materials, such as 45S5 and β-TCP.

The reviewed studies primarily focused on the use of melt-derived bioactive glass particles, but sol-gel-derived particles were also investigated for their potential in bone regeneration. Furthermore, bioactive glass particles have applications beyond bone tissue engineering, such as in drug delivery systems. The porous structure of sol-gel-derived bioactive glasses allows for controlled release of therapeutic agents. The choice of surfactant during fabrication can influence the mesoporosity of the glass particles. For example, a study demonstrated that a bioactive glass produced using CTAB as a surfactant exhibited nano-sized particles, mesoporosity, and a high surface area, which played a crucial role in the formation of an apatite layer. Conversely, the use of PEG resulted in more calcite formation, while P123 led to enhanced HAp phase and reduced overall crystallinity after 14 days of immersion in simulated body fluid. *In vivo* studies assessing bone regeneration efficacy with the addition of IGF-1 showed high degrees of new bone formation for all mesoporous bioactive glasses: CTAB (80.7 ± 2.9%), PEG (74.4 ± 2.4%), and P123 (70.1 ± 1.9%), compared to traditional bioactive glass (66.9 ± 1.8%). The included studies of the particles' effects on *in vivo* application are detailed in **Table 4**.

After analyzing the findings from the studies discussed earlier, it is evident that the current application of bioactive glasses in *in-vivo* scenarios still encounters challenges like those highlighted by Bocaccini in their review on 3D scaffolds [16]. Various animal models, including rats, rabbits, and sheep, were utilized in these studies (**Figure 2** and **Table 2**). Each animal model possesses unique anatomical and physiological characteristics that can influence the response to bioactive glass particles. Although larger animals are more relevant for mimicking human conditions (as pigs, sheep and dogs), rats are commonly chosen as the initial option for *in vivo* material testing [17]. However, this model has limitations due to its size, which makes it unsuitable for testing multiple implants. Additionally, rats have small, long bones with thin and weak cortices and lack Haversian-type cortex remodeling seen in larger animals.

The next preferred animal model are rabbits (New Zealand white rabbit) for musculoskeletal research [17] due to their availability, relatively small size, and ease of handling and housing. Some similarities in bone mineral density and fracture toughness have been reported between rabbits and humans [62]. On the other hand, the accelerated bone turnover rate and rapid skeletal changes observed in rabbits present difficulties in extrapolating findings from

rabbit studies to the clinical scenario in humans. Consequently, utilizing larger animal models becomes a more suitable approach to bridge the gap between animal research and human conditions. However, it is crucial to carefully consider factors such as the specific animal species, defect size, and duration of implantation, as these variables can significantly influence the *in vivo* response and efficacy of bioactive glasses.

Moreover, researchers also encounter strict regulations regarding the use of animals for *in vivo* evaluation of newly developed bioactive glasses. Due to the potential pain experienced by laboratory animals during research, their usage must be justified. To minimize the number of animals used, a well-designed experiment is recommended in the literature [19]. This approach enables scientists to collect data with the minimum number of animals required. However, it is important to note that enough animals are still necessary for reliable statistical analysis and to generate significant results, thus avoiding the need for additional experiments and the use of more animals.

2.6 CONCLUSIONS

In summary, this review examined the use of bioactive glasses for bone regeneration and highlighted the persisting challenges in this field. Despite advancements, reliable coatings, mechanical properties, and comprehensive testing remain areas of concern. The review encompassed 20 *in vivo* studies across various animal models, summarizing key findings, discussing clinical relevance, acknowledging limitations, and suggesting future research directions.

While *in vitro* tests provide initial insights, *in vivo* animal models offer a more physiologically relevant environment for evaluating bioactive glasses. However, animal species, defect size, and implantation time significantly impact outcomes. Three-dimensional scaffolds that mimic native bone structure show promise, and thorough characterization is crucial for clinical translation. The chemical composition of bioactive glasses influences their performance, with boron-containing glasses showing rapid degradation and increased hydroxyapatite formation. Fabrication techniques, such as solid freeform fabrication, affect scaffold properties, while coating techniques using mesoporous bioactive glasses enhance regeneration.

Particle size, shape, and composition also affect bone regeneration, with variations depending on manufacturing routes and surfactants used. Rat and rabbit models are commonly employed, but considerations should be given to larger animal models and ethical usage.

Stringent regulations call for well-designed experiments with adequate sample sizes to minimize animal usage while obtaining reliable data.

Further research is imperative to address the challenges and optimize the design and performance of bioactive glasses. This necessitates a comprehensive approach, encompassing enhanced characterization techniques, refinement of fabrication processes, exploration of novel compositions and coatings, and the use of appropriate animal models to bridge the existing gap between preclinical and clinical applications.

The findings presented in this study offer valuable insights into the characterization analyses conducted as precursors to in vivo evaluations. They serve as a crucial reference dataset for guiding and facilitating comparisons with the experimental phase outlined in Chapter 3. This includes process parameters for the melting route, particle size and shapes typically employed for comparison, insights into sol-gel mesoporous structural order, the influence of surfactants, and parameters for characterizing physical, chemical, bioactive, and biological properties.

CHAPTER 3 - A COMPARATIVE ASSESSMENT OF BIOACTIVE GLASSES 45S5, S53P4, 58S AND MBG 58S: PHYSICAL, CHEMICAL, BIOACTIVE, AND BIOLOGICAL PROPERTIES

3.1 INTRODUCTION

Bone defects that exceed a critical size pose significant challenges in terms of regeneration and repair [1]. Traditional bone grafting procedures, while effective, have limitations such as increased risk of morbidity, potential rejection, and tissue degradation. In search of better alternatives, synthetic grafts have gained attention, with bioactive and biodegradable glasses (BGs) being prominent contenders [25,63].

The concept of utilizing bioglasses in medical contexts was first introduced in the late 1960s when researchers discovered that certain glasses could bond to living bone tissues [64]. This bioactive behavior arises from the unique composition of bioglasses, predominantly comprising silicon dioxide (SiO_2), calcium oxide (CaO), phosphorus pentoxide (P_2O_5), and sodium oxide (Na_2O). This blend of elements results in a glassy matrix with the ability to form a biologically active hydroxyapatite layer upon contact with body fluids, facilitating a strong bond with surrounding tissues [10].

Over the years, several bioglass formulations have been developed and refined, each exhibiting different physical, chemical, bioactive, and biological properties. The Bioglass 45S5, known as the "original" bioglass, has set a benchmark for subsequent formulations [65]. Initially, bioactive glasses were manufactured through the melting of relevant oxides at temperatures ranging from 1100 to 1300 °C as seen in the 45S5 composition. Furthermore, the S53P4 bioglass, developed in the 1990s also through the melt-derived method, stands out for its high silica content, improved mechanical properties, and enhanced bioactivity [6–8].

The significance of textural characteristics in influencing bioactivity levels became more pronounced with the introduction of sol-gel–derived bioactive glasses. The advent of the sol-gel method facilitated the production of glasses exhibiting heightened bioactivity compared to their melt-derived counterparts of identical composition, primarily due to the highly porous nature of the sol-gel material [20,21]. Investigations have demonstrated that sol-gel glasses formulated within three-components (SiO_2, CaO, P_2O_5), two-components (SiO_2, CaO), and even single-component (pure silica) systems can rapidly develop an apatite layer upon exposure to simulated body fluids [9–11].

The sol-gel process offers advantages such as lower processing temperatures and improved control over textural properties. Within this framework, the 58S bioglass emerged with a modified composition, exhibits improved biodegradation and ion release characteristics [22–24] . Moreover, the Mesoporous Bioactive Glasses (MBG) 58S, featuring an unique mesoporous structure, has shown immense potential in drug delivery and tissue engineering applications [12–15].

The process of glass network dissolution, which involves the formation of a silica-rich gel layer and the subsequent deposition of an apatite-like layer onto the glass surface, has been identified as a fundamental sequence for establishing a bond between glass and living tissue *in vivo* [25]. This phenomenon has been similarly observed in *in vitro* tests in which bioactive glasses are immersed in simulated body fluids [25]. The degree of bioactivity, as indicated by the rate of apatite layer formation and the thickness of the apatite-like layer, is contingent upon both the chemical composition of the glass and its morphological attributes, including surface area, pore size, and pore volume [20,21].

Understanding the specific advantages and limitations of each bioglass composition is critical for optimizing their use in various clinical scenarios. This comparative assessment aims to provide an in-depth analysis of Bioglasses 45S5, S53P4, 58S, and MBG 58S, focusing on their physical, chemical properties, bioactivity, and biological responses.

3.2 MATERIALS AND METHODS

3.2.1 BG 45S5 and S53P4 melted derived route

BG 45S5 (composition 45wt.% SiO_2, 24.5 wt.% Na_2O, 24.5 wt.% CaO, 6 wt.% P_2O_5) and BG S53P4 (composition 53 wt.% SiO_2, 23 wt.% Na_2O, 20 wt.% CaO, 4 wt.% P_2O_5) were processed via the melt technique. Raw materials in powder form were utilized, including SiO_2 (99.9% Sigma Aldrich, USA) as the silica source, sodium carbonate (Na_2CO_3) to provide sodium oxide (Na_2O) after decarbonation (99%, Lafan, Brazil), calcium carbonate (Ca_2CO_3) as the calcium oxide (CaO) source after decarbonation (98%, Lafan, Brazil), and Phosphorus pentoxide (P_2O_5) as the phosphate source (99.5%, Exôdo Científica, Brazil). The amounts of SiO_2, Na_2O, CaO, and P_2O_5 were calculated according to the proportions required for the BG 45S5 and S53P4 glasses compositions.

Subsequently, each batch was melted in a 100mL platinum crucible within the melting furnace (Jung, Blumenau -SC, Brazil) using a heating rate of 10°C/min and following a two-step process. The first step involved heating the mixture up to 900 °C for 1 h to decarbonate the

carbonates used. The second step included heating up to 1450 °C for 2 h to melt and homogenize the raw materials. To obtain the glass frits, the vitreous mass was quenched in water, sieved, and dried in a dryer (SP LABOR® - Brazil) at 100 °C for approximately 4 h.

3.2.2 BG 58S and MBG 58S sol-gel synthesis

BG 58S and MBG 58S powders (composition 58 wt.% SiO_2, 33 wt.% CaO, 9 wt.% P_2O_5) were processed using the sol-gel technique, as previously developed in a study by Galarraga et al. [14]. The composition slightly deviates from the nominal, involving a 9 wt.% addition of P_2O_5 (instead of the nominal 4 wt.% P_2O_5). The augmented P_2O_5 content is commonly employed to enhance the mechanical properties and bioactivity of the bioglass composition [66,67]. The ramifications of this modification on biological assays will be investigated.

To create the mesoporous structure, 4 g of Pluronic triblock copolymer P123 (EO20PO70EO20, 5800, Sigma Aldrich, USA) surfactant was dissolved in 50 mL of ethanol using a stirring bar at 40 °C for 1 h. Afterward, tetraethyl orthosilicate (TEOS) (98%, Sigma Aldrich, USA), triethyl phosphate (TEP) (99.8%, Sigma Aldrich, USA), and calcium nitrate tetrahydrate ($Ca(NO_3)_2 \cdot 4H_2O$) (Vetec, Brazil) were added to the solution as precursors of silicon, phosphorus, and calcium oxide. The solution was stirred at 40°C for 12 h.

To dissolve $Ca(NO_3)_2 \cdot 4H_2O$ and adjust the pH of the solution, nitric acid (HNO_3, 68%, Vetec, Brazil) was used, while ethyl alcohol (EtOH, P.A., Synth, Brazil) was used to dissolve P123, TEOS, and TEP. The molar ratios of SiO_2, P_2O_5, and CaO were calculated according to the 58S BG glass composition. TEOS and TEP were placed in a glass recipient containing EtOH under magnetic stirring at 25 °C for 10 min. $Ca(NO_3)_2 \cdot 4H_2O$ was dissolved in 2M HNO_3 and then added to water at a molar ratio of TEOS: H_2O of 1:4. The solution was then dried in a chamber at 70 °C for 24 h. Subsequently, the dried gel was thermally treated at 600 °C for 6 h at a heating rate of 1°C/min to remove the organic agents and the surfactant template. For the BG 58S glass composition, there is no need to use the surfactant P123.

3.2.3 Physical and chemical characterization

The particle size distribution was measured using a laser scattering analyzer (Mastersizer 3000, Malvern Instruments, UK). The powder was introduced into a wet

dispersion unit with low water rotation (~1200 rpm) to prevent significant particle agglomeration.

Semi-quantitative chemical analysis of the samples was performed using energy dispersive X-ray spectroscopy (EDS, VEGA 3, Tescan, Czech Republic). The melt derived (BG 45S5 and S53P4) glass samples were ground in high-energy ball mill for 10 min at 300 rpm (Retsch PM 100, Verder, US) and all samples were subsequently coated with a thin layer of gold to allow the electron conduction for SEM analysis. The compound composition was obtained by rearranging the quantity of oxygen to calculate the weight percentage of oxides using the most stable stoichiometric arrangement, resulting in a reliable semi-quantification of the respective oxides. The bioglasses morphological aspect were analyzed by scanning electron microscope (SEM, VEGA 3, Tescan, Czech Republic) at different magnifications applying an acceleration potential of 10 and 15 kV.

The functional groups of the powder samples were identified by Fourier transform infrared spectroscopy (FTIR, Cary 600 Series, Agilent technologies, USA), performed using the KBr pellet technique [68]. Pellets were prepared by mixing 1 mg of each sample powder with 300 mg of KBr at infrared grade under vacuum. The infrared spectra were recorded in the wavenumber range of 400-4000 cm^{-1} in transmission mode with 32 scans and a resolution of 4 cm^{-1}.

Density analysis was conducted using a non-aqueous medium by the Helium gas pycnometer method (Micro Ultra pycnometer, ULTRAPIC 1200e T, v5.04, England). The automatic method took five readings for each sample to evaluate the actual volume and density obtained for the mass inserted in a known volume, using a cell of 58.3872 cm^3. The test temperature was 26.3°C with an automatic purge of 1 min. The thermal behavior was characterized by Heating microscope using (Misura 3.32 Microscope, TA Instruments), with a heating rate of 10°C/min up to 1200°C.

MBG textural analysis was performed by N_2 adsorption and desorption isotherms measured by a porosity analyzer (AUTOSORB-1-1 C, Quantochrome) at -203.85°C. Pore size distribution and volume were determined from the isotherm adsorption branch using the Barrett-Joyner-Halenda (BJH) method, while the specific surface area was determined by the Brunauer-Emmett-Teller (BET) method. The morphological aspects of the MBG particles were analyzed by transmission electron microscopy (TEM, Zeiss Leica, Germany) at an acceleration potential of 100 kV.

3.2.4 Bioactive characterization: apatite-forming assays

Simulated body fluid (SBF) was used for conducting the *in vitro* tests. The SBF solution was prepared following Kokubo's method [69], and its chemical composition is presented in **Table 7.** Melt-derived particles that have passed through a 325-mesh sieve are utilized. Across all four compositions, 75mg of powder were placed in 50mL of sterilized SBF solution within sanitized flasks. These flasks were then placed in a glycerin container set at 37°C. The solution was stirred at 90 rpm using a magnetic stirrer (C-MAG HS 7 Control, IKA, USA) for 8, 24, and 72 h. After each specified time period, the samples were removed by filtration, and then dried in a vacuum oven at 37°C for 24 h [69].

Subsequently, the HCAp-forming ability of all samples was evaluated using SEM (VEGA 3, Tescan, Czech Republic), EDS (Swift 2000, Hitachi, Japan), and FTIR analysis following the methodologies as before described. Additionally, to determine the hydroxyapatite crystallinity of the samples, X-ray Diffraction analysis was performed (XRD, Rigaku MiniFlex 600 (Rigaku, Japan).

Table 7. Chemical composition of the SBF solution. [69]

ORDER	REAGENT	AMOUNT (g/l)
1	**NaCl**	8.035
2	**NaHCO**	0.355
3	**KCl**	0.225
4	**K_2HPO_4 $3H_2O$**	0.231
5	**$MgCl_2$ $6H_2O$**	0.311
6	**HCL 1M**	38mL
7	**$CaCl_2$ $2H_2O$**	0.386
8	**Na_2SO_4**	0.072
9	**Tris**	6.118

3.2.5 Biological characterization: *in vitro* biocompatibility

3.2.5.1 Materials

Murine cell line of fibroblasts (L929, Thermo Scientific, Brazil), PBS (PBS, for *in vitro* cell culture were cultivated in a culture medium containing sodium carbonate (Sigma Aldrich), penicillin-streptomycin (pens/strep), Dulbecco's Modified Eagle's medium (DMEM),

fetal bovine serum (FBS). TrypLE Express Enzyme, phosphate buffered saline (PBS), CellTiter 96® Aquous One Solution (MTS [3-(4,5-dimethylthiazol-2-yl)-5-(3-carboxymethoxyphenyl)-2-(4-sulfophenyl)-2H-tetrazolium]) (Promega Biotecnologia do Brasil, Brazil), glutaraldehyde and formaldehyde were also used in several assays.

3.2.5.2 Sample preparation

The samples were sterilized in an autoclave at 121 °C at 1 ATM of pressure, were ressuspend in DMEM medium and diluted in medium at different concentration quadruplicate (0-1000 µg/mL). For the direct contact assay, the different concentrations were plated directly on the cells. For the extract test, the different concentrations were placed in contact with the medium for 24 h at 37 °C. The samples were centrifuged and the supernatant was added over the cells.

3.2.5.3 Cell preparation

Cell viability was evaluated with a murine cell line of fibroblasts (L929, Thermo Scientific, Brazil) seeded in 96-well cell culture plates (Corning Life Sciences). Cells were kept under a moist atmosphere at 37 °C with 5% CO_2 and cultured in DMEM, supplemented with 10% FBS and 1% penicillin/streptomycin. Cell culture medium was refreshed every 2 days until cells reached 85–90% confluence. Cells were detached using Tryplex, and placed in 96-well plates at a density of $1 \cdot 10^4$ cells/well. After 24 h, different concentrations were added to the cell wells. Subsequently, the cells were washed twice in PBS and cell viability (MTS) was evaluated.

3.2.5.4 MTS assay (Metabolic activity)

The cells were then incubated for 24, 48 and 72 h at 37 °C, 5% CO_2 and 90% humidity. The control wells containing culture medium only were also incubated. After the time, the cells were rinsed with PBS (PBS, Gibco® USA), and cell viability was measured with AQueous One solution proliferation assay (CellTiter 96, MTS, Promega). In each well, a mixture of 20 µL cell MTS reagent (Promega Corporation® USA) and 100 µL medium was added and cultured in an incubator (Ultrasafe HF 212UV, Brazil) at 37 °C for 2 h with 5% CO_2. Afterward, the

remaining medium was transferred into 96-well plates for optical density measurements at 490 nm wavelength. The analyses were performed on a spectrophotometer (Molecular Devices, Spectra Max Plus 348) with four parallel replicates for each sample. The culture medium was used as a control group and the results show metabolic activity (Melgar Aguilar et al., 2021).

3.2.5.5 Statistical analysis

Metabolic activity of L929 cells were analyzed using OriginPro® (OriginLab Corporation, Northampton, Massachusetts, USA) expressed as the mean ± standard error from three independent assays and their triplicates. Statistical evaluation was performed using one-way analysis of variance (ANOVA), followed by Tukey's test with $p < 0,05$ considered as statistically significant.).

3.3 RESULTS

3.3.1Characterization of BG and MBG particles

Melt derived BG 45S5 and S53P4 showed a particle size ranging from 188 μm up to 890 μm with the mean particle size around 548 μm. Sol gel derived BG 58S showed a range from 11 μm up to 287 μm, with the mean particle size around 96 μm and MBG 58S showed a particle size range from 2 μm up to 42 μm and mean particle size around 14 μm as shown on **Table 8**. A Gaussian-like distribution was shown for all samples. However, the sol-gel derived showed a larger monomodal distribution than the melted derived glasses as shown in **Figure 15**.

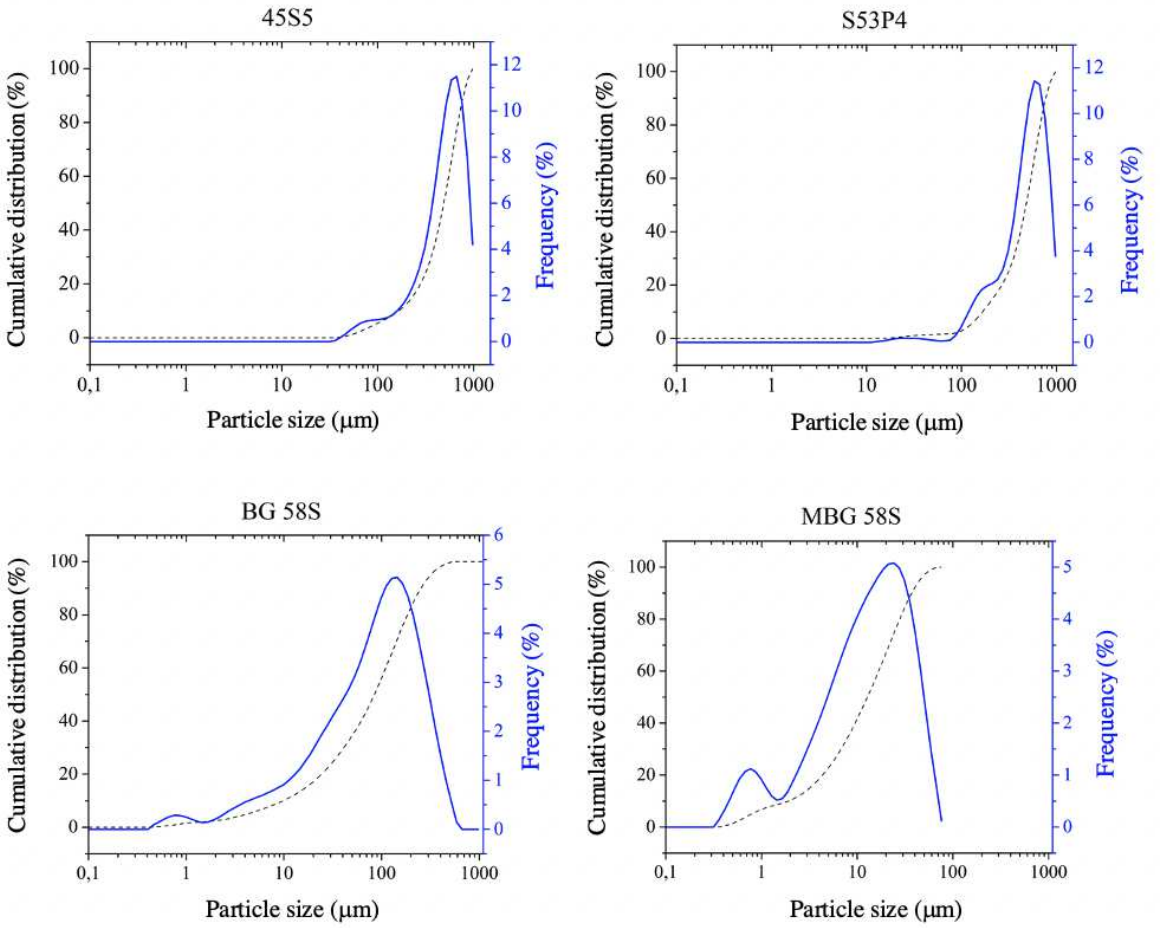

Figure 15. Particle size distribution of BG 45S5, S53P4, 58S and MBG 58S glass powders.

Table 8. Data of powder characterization: equivalent spherical diameter at the cumulative volume percentage of 10% (D10%); 50% (D50%) and 90% (D90%) measured by laser spectrometry.

Sample	$D_{10\%}$ (µm)	$D_{50\%}$ (µm)	$D_{90\%}$ (µm)
45S5	188	554	890
S53P4	189	543	876
58S	11.1	95.9	287
MBG 58S	2.16	14.5	42.2

The results of skeletal density measured by helium pycnometer varied within the range of 2.64 to 2.79 g/cm^3 regardless of the particle size or composition and close to the values reported in literature[23], as shown in **Table 9**.

Table 9. Data of skeletal density of developed bioactive glasses.

Sample	Density (g/cm^3)
BG 45S5	2,80± 0,006
BG S53P4	2,71± 0,004
BG 58S	2,66± 0,022
MBG 58S	2,64± 0,023

The porous structure analysis of the MBG 58S regarding N_2 adsorption-desorption isotherms, BJH pore size distribution and volume are shown in **Figure 16**. According to the International Union of Pure and Applied Chemistry (IUPAC) classification the MBG 58S have N_2 adsorption-desorption isotherms of type IV curve with H1-type hysteresis loops (Figure 16A). The initial part of this curve can be associated to monolayer-multilayer adsorption. Also, the limiting uptake over a range of high P/P_0 was noted. In addition, both branches of adsorption/desorption isotherms show sharp steps in the P/P_0 region of 0.70-0.80 which are associated with capillary condensation taking place in mesopores, and the limiting uptake over a range of high P/P_0 [70] . The BJH method revealed that MBG particles had a mean narrow pore diameter at 14.29 nm, as shown in Figure 4B, and a porosity volume of about 0.20 cm3g. The MBG specific surface area was 77.20 m^2/g according to BET analysis.

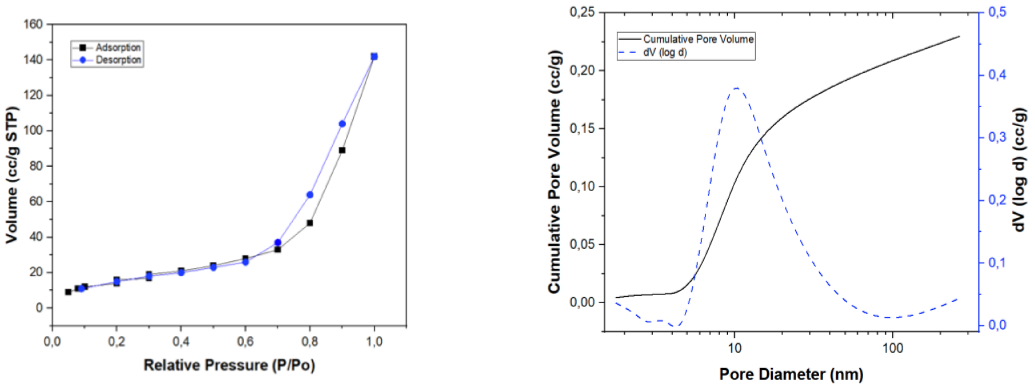

Figure 16. (A) N_2 adsorption (black) and desorption (blue) isotherms and (B) BJH pore diameter distribution curves for 58S mesoporous bioactive glass particles.

The FTIR analysis showed BG characteristic peaks of Si-O-Si in which the main absorption bands for the sol-gel derived bioactive glasses were at 1080, 810 cm^{-1}, and 1060, 900 cm^{-1} for the melted derived BGs, attributed to the Si-O-Si asymmetric stretching (range 1175-710)[71], and at 460 cm^{-1} attributed to Si-O-Si bending, as showed in **Figure 17**.

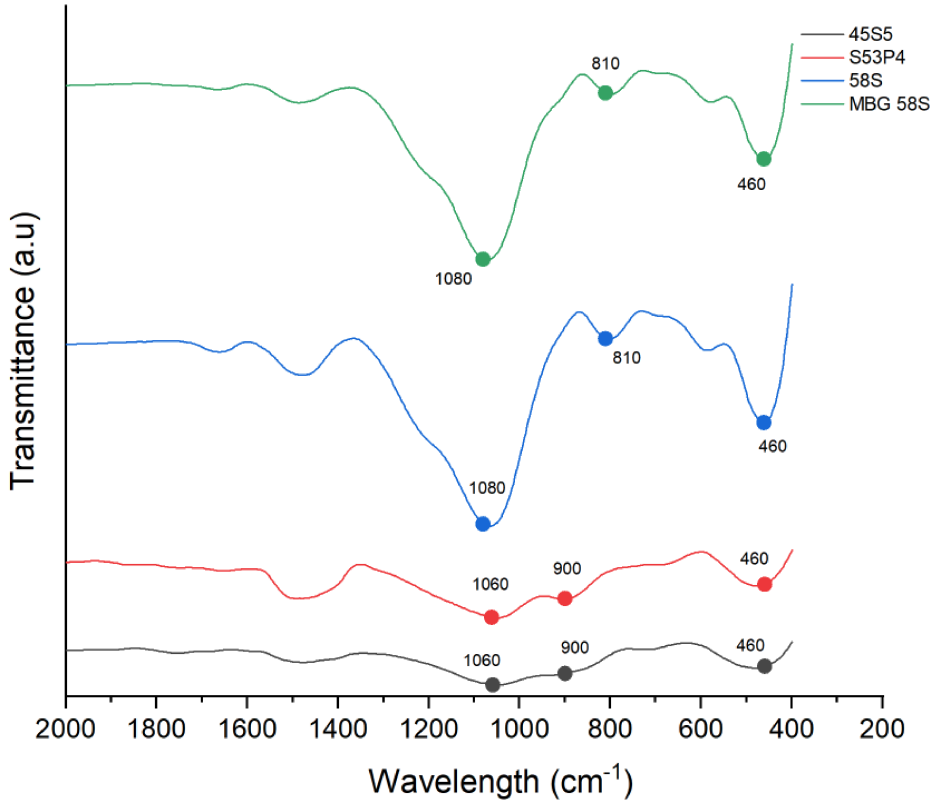

Figure 17. FTIR spectrum obtained for the prepared bioactive glasses (relevant Si-O-Si peaks are indicated and discussed in the text).

Thermal analysis provides valuable insights into the temperature behavior of bioactive glasses, including sintering, softening and melting points. These temperatures are linked to the glass's viscosity and represent a crucial factor in determining the forming and shaping procedures that can be used for a particular composition [72]. **Table 10** presents approximated viscosity values (in dPas) for bioactive glass forming process, as predicted by Vedel et al. [73] .

Table 10. Approximate viscosity values (dPas) for bioactive glass forming processes

Processing	**Viscosity (η) in dPas**
Melting	$10…10^2$
Pressing	$10^4…10^6$
Drawing of continuous fibers	$10^{2.5}…10^{3.5}$
Sinter glass powder to porous body	$10^8…10^9$
Annealing	$10^{12}…10^{13}$

The thermal behavior data are presented in **Figure 18** and **Table 11.** As anticipated, compositions featuring higher SiO_2 concentrations displayed elevated characteristic temperatures. Regarding sol-gel derived BGs (58S and MBG 58S), they exhibited reduced sensitivity to temperature fluctuations, leading to minimal alteration in the sample's shape. However, a marginal volumetric reduction might have transpired due to the release of residual liquid compounds into the particle porosity during the sol-gel route. The extensive porosity inherent in the mesoporous structure of MBG contributed to the lower temperatures observed for BG 58S. In contrast, melt-derived glasses manifested heightened temperature sensitivity, with BG 45S5 revealing lower characteristic temperatures in comparison to BG S53P4, as expected due to its lower SiO_2 content. The recorded temperatures were close to those previously reported in the literature [50].

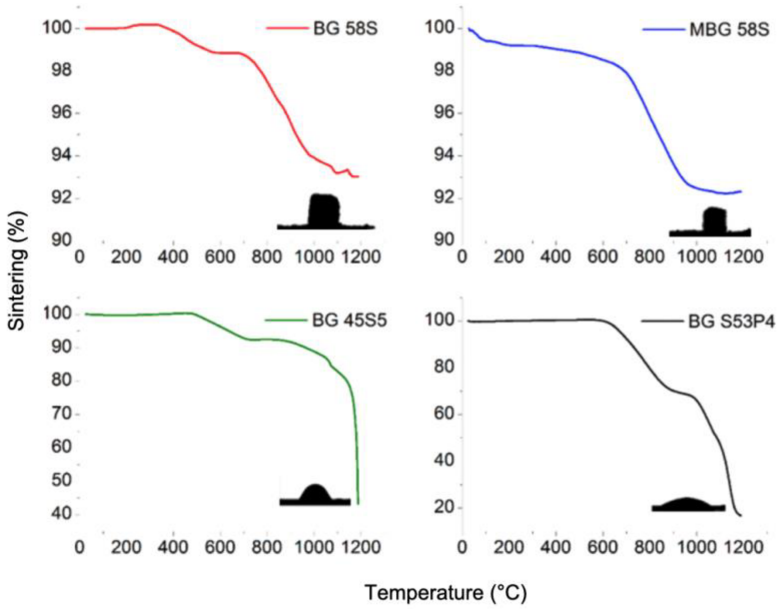

Figure 18. Thermal behavior of the produced bioactive glasses (powder compacts) until 1200 °C on a 10 °C/min heating rate.

Table 11. Thermal behavior and characteristics temperatures of the developed bioactive glasses

Sample	**Sintering (°C)**	Softening (°C)	Melting (°C)
BG 45S5	607	642	1110
BG S53P4	721	722	1134
BG 58S	900	-	-
MBG 58S	831	-	-

SEM micrographs show a uniform and well-defined appearance of all bioactive glass particles, as depicted in **Figure 19**. The samples exhibit angular shapes. In particular, the MBG particles display a non-smooth microporous structure with noticeable porosity, as showed in Figure 5D.

TEM images of MBG particles further confirm the mesoporous structure, which is evident from the lighter areas within the particles, representing empty regions, as shown in **Figure 20**.

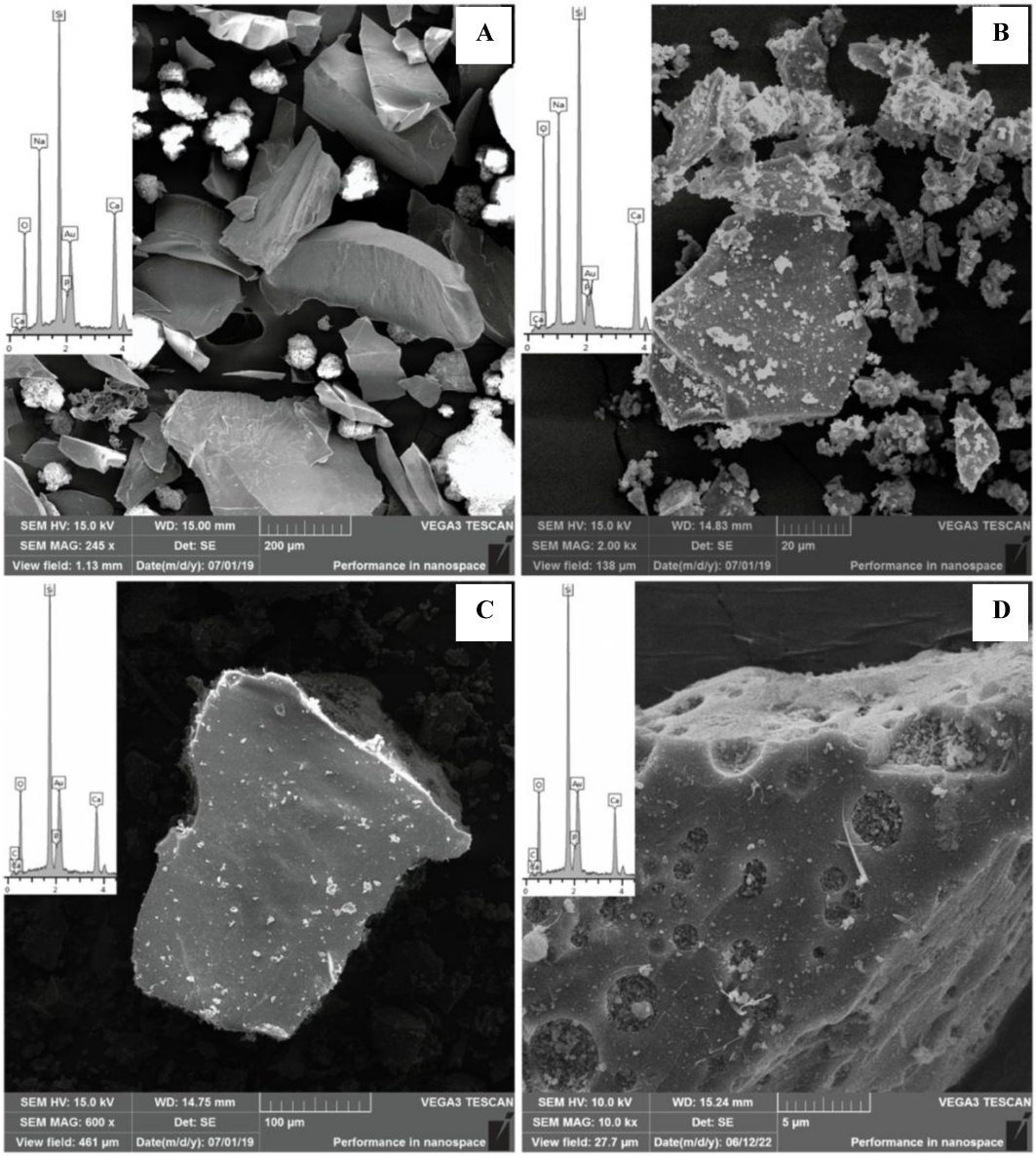

Figure 19. SEM images of BG 45S5 (A), S53P4 (B), 58S (C) and MBG 58S (D) particles at different magnifications.

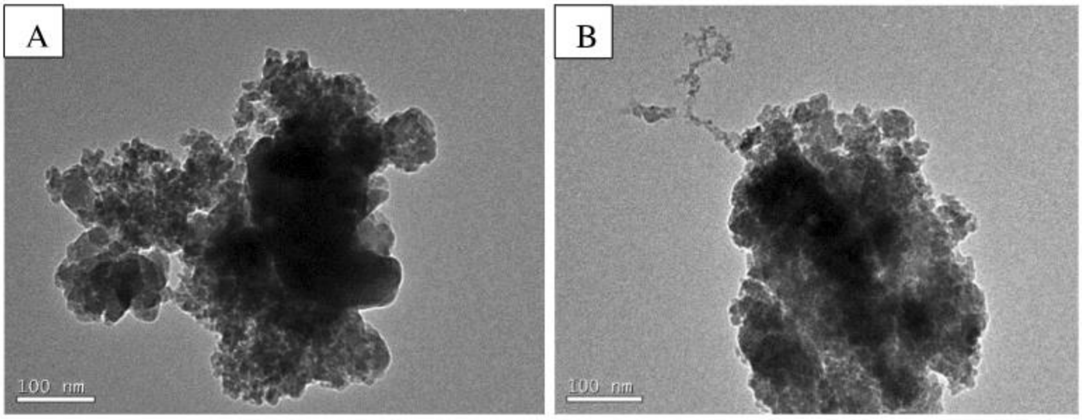

Figure 20. TEM image of the MBG 58S revealing the mesoporous structure.

3.3.2 Bioactivity outcomes: apatite-forming assays

SEM images revealed that the surface of all samples appeared relatively smooth before immersion in SBF, with some precipitates present. However, a significant change in surface morphology was observed after immersion in SBF for 8 h, indicating the formation of hydroxy-carbonate apatite (HCAp), as depicted in **Figure 21** This HCAp formation appeared to increase after 24 h of immersion. Notably, the changes in surface morphology for the samples immersed for 72 h closely resembled those immersed for 24 h, with more pronounced differences observed in the samples derived from the sol-gel route.

Regarding the melted-derived samples (BGs 45S5 and S53P4), a layer formation was evident, and this layer showed a considerable increase from 8 h to 72 h, as showed in **Figure 21**. Additionally, the bioactive glasses derived from the melt route exhibited HCAp nucleation over this layer, displaying a more granular morphology. After 72 h of immersion in SBF, the surface of BG 58S and MBG 58S glass particles displayed a thick layer of HCAp with spherical, needle-like, and polygonal crystals.

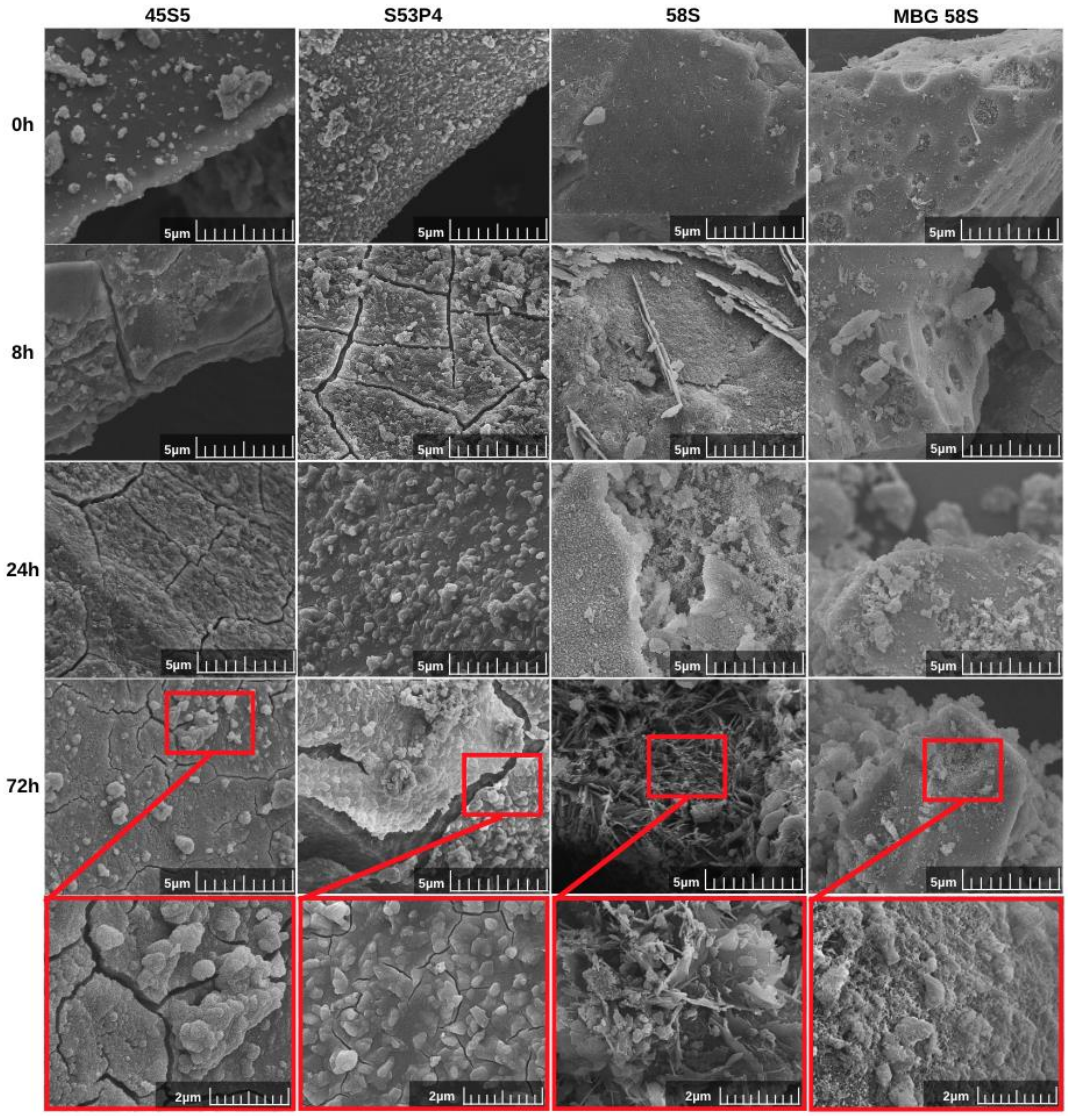

Figure 21. SEM micrographs at 10,000x recorded on BG 45S5, S53P4, 58S and MBG 58S glasses after immersion in SBF for 0,8,24 and 72h. The r*ed square* regions are shown in separate micrographs at higher magnification (*20,000x*).

The atomic Ca/P ratio of the samples was calculated using the results obtained from the EDS analysis. The semi-quantitative chemical analysis was repeated 10 times per sample to determine representative values of mean and standard deviation after 0h, 8h, 24h, and 72h of immersion in SBF fluid, as presented in **Table 12**.

Table 4 shows that all samples reached a Ca/P ratio of approximately 2.00 after 72 h of immersion in SBF, which is close to the reference value of the non-stoichiometric biological apatite molar ratio of 1.67 Ca/P [74].

Table 12. Ca/P elemental concentrations ratios of samples before and after SBF immersion for 0, 8, 24 and 72h obtained by EDS analysis.

Time SBF (h)	BG 45S5	BG S53P4	BG 58S	MBG 58S
0	7.2 ± 0.4	7.9 ± 0.1	6.0 ± 0.8	5.4 ± 0.7
8	2.1 ± 0.4	2.0 ± 0.1	2.9 ± 0.6	2.3 ± 0.6
24	2.1 ± 0.4	1.9 ± 0.2	2.1 ± 0.4	2.3 ± 0.5
72	1.9 ± 0.2	1.9 ± 0.2	2.1 ± 0.5	2.0 ± 0.2

The EDS spectra analysis did not reveal a significant change between the different types of bioactive glasses after 8h of immersion. After 24h of immersion one can observe the increase in Ca and P content (wt.%) and the decrease of Si content in all samples. All the bioglasses showed a noticeable loss in Si content (wt.%) and a significant increase in P content (wt.%) after 72 h of immersion in SBF as shown in **Figure 22**. However, this behavior seems to be more expressive in bioactive glasses obtained from the melting route. This behavior may be related to the presence of the HCAp layer presented in the images obtained by SEM.

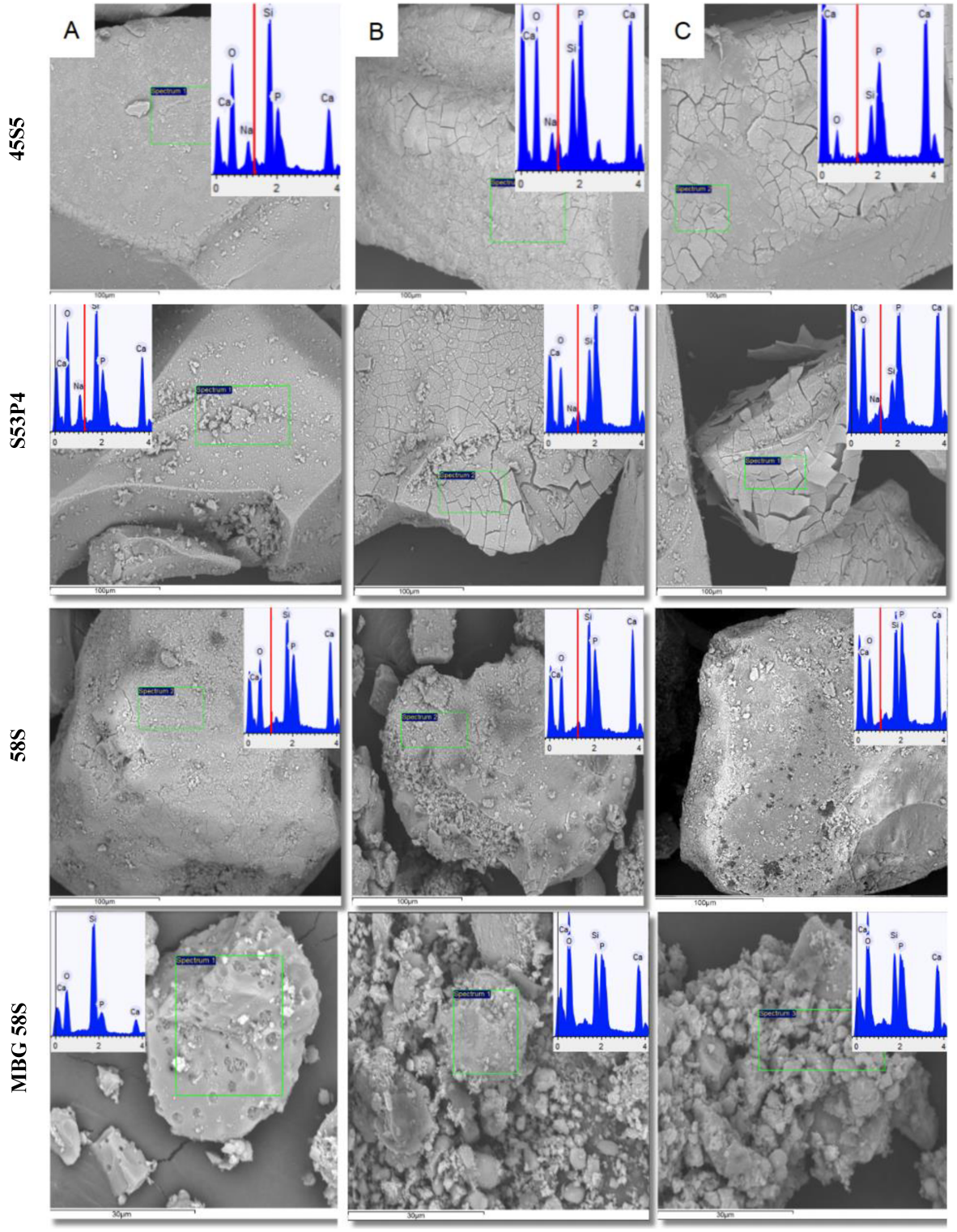

Figure 22. SEM micrographs captured at 500x magnification and EDS analysis conducted on BG 45S5, S53P4, 58S, and MBG 58S glasses at 1000x (A) and 2000x (B-C) magnifications with acceleration energy of 15kV. These samples were immersed in an SBF solution after (A) 8 h, (B) 24 h, and (C) 72 h.

The FTIR spectra of all samples exhibited characteristic peaks associated with the formation of the HCAp layer, **Figure 23**. These peaks appeared as a doublet at approximately ~600 cm^{-1}, representing the bending mode of crystalline phosphate P-O, and at ~1050 cm^{-1}, corresponding to the P-O stretching mode. Notably, the resonance at ~1050 cm^{-1} was more pronounced, especially in the spectrum of pure BGs. Prior to immersion in SBF, the spectra of all samples did not display the mentioned double peak, but the resonances attributed to the phosphate group were present. Additionally, a narrowed band around 820 cm^{-1} indicated the bending mode of C-O, while a peak at around 1400 cm^{-1} represented the C-O stretching mode in all samples' spectra. Moreover, the resonance at ~1680 cm^{-1} suggested the presence of C-O in CO_3^{2-}, indicating the formation of a carbonated HAp due to the presence of CO_2 in SBF.

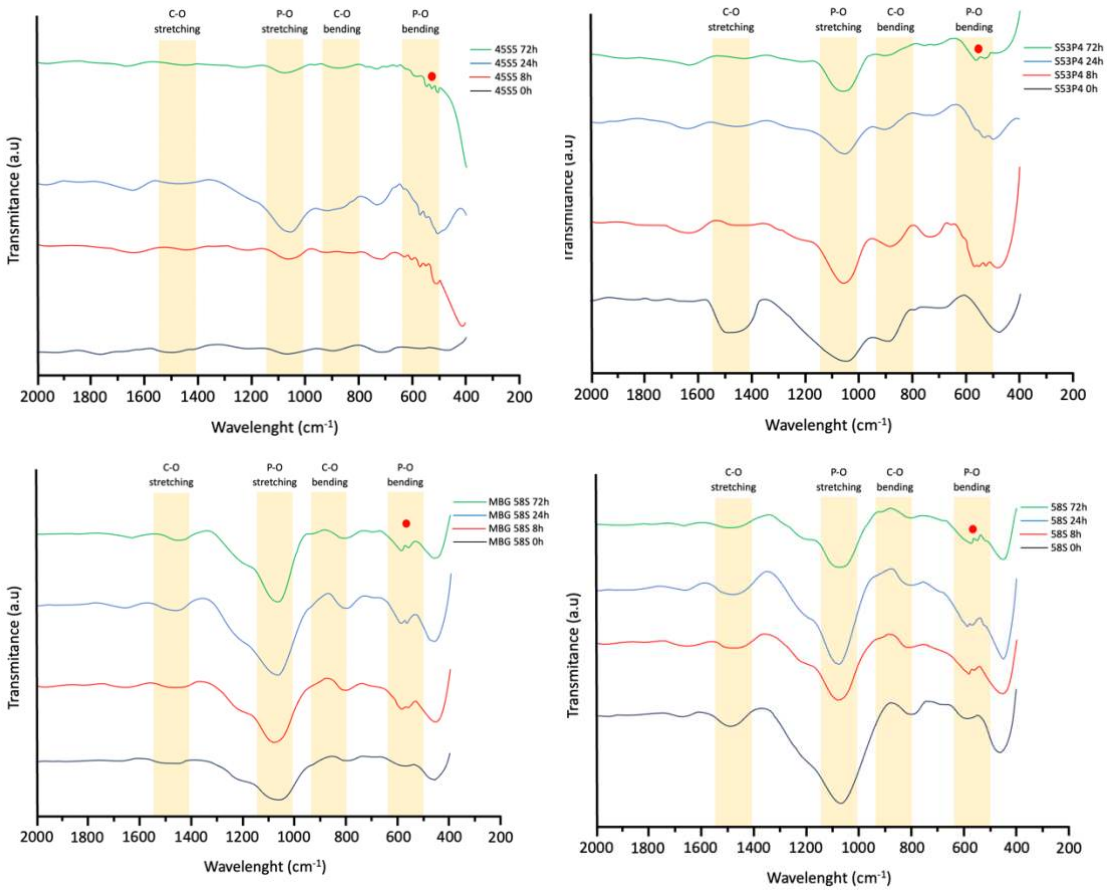

Figure 23. FTIR spectra obtained for developed bioactive glasses samples (45S5, S53P4, 58S and MBG 58S glasses) before and after 8h, 24h and 72h of SBF immersion. (The red circle identifies the double peak characteristic of HCAp formation).

Figure 24 displays the XRD patterns used to determine HCAp formation. After 72 h of SBF immersion, all samples reveal an amorphous nature, with identifiable HCAp crystal planes (ISCD no. 180315). The sol-gel-derived samples exhibit peaks at 31.8°, 25.9°, and 29.0°,

corresponding to (211), (002), and (210) crystal planes, respectively. The melt-derived samples, on the other hand, show a peak at 33.0° assigned to (300) crystal plane.

The 58S XRD patterns after 72 h of SBF immersion exhibit high-intensity diffraction peaks at 31.8° (211) and low-intensity peaks at 25.9° and 29.0°, corresponding to (002) and (210) crystal planes, respectively. The MBG XRD patterns are similar, with an additional high-intensity peak at 32.3° assigned to the (112) crystal plane.

Similarly, the 45S5 BG patterns after 72 h of SBF immersion show high-intensity diffraction peaks at 33.0° and 32.3°, corresponding to (300) and (112) crystal planes, respectively. Additionally, low-intensity peaks are observed at 16.8°, 18.8°, 28.2°, 34.4°, 35.5°, 39.3°, 42.1°, 45.4°, and 51.4°, assigned to (101), (110), (102), (202), (301), (212), (302), (202), and (410) crystal planes. However the absence of the diffraction peak at (211) crystal plan may suggest a different phase formation.

The S53P4 BG patterns after 72 h of SBF immersion also display high-intensity peaks at 31.8° and 33.0°, corresponding to (211) and (300) crystal planes, respectively. Additionally, low-intensity peaks at 22.9° and 46.8° are assigned to (111) and (222) crystal planes.

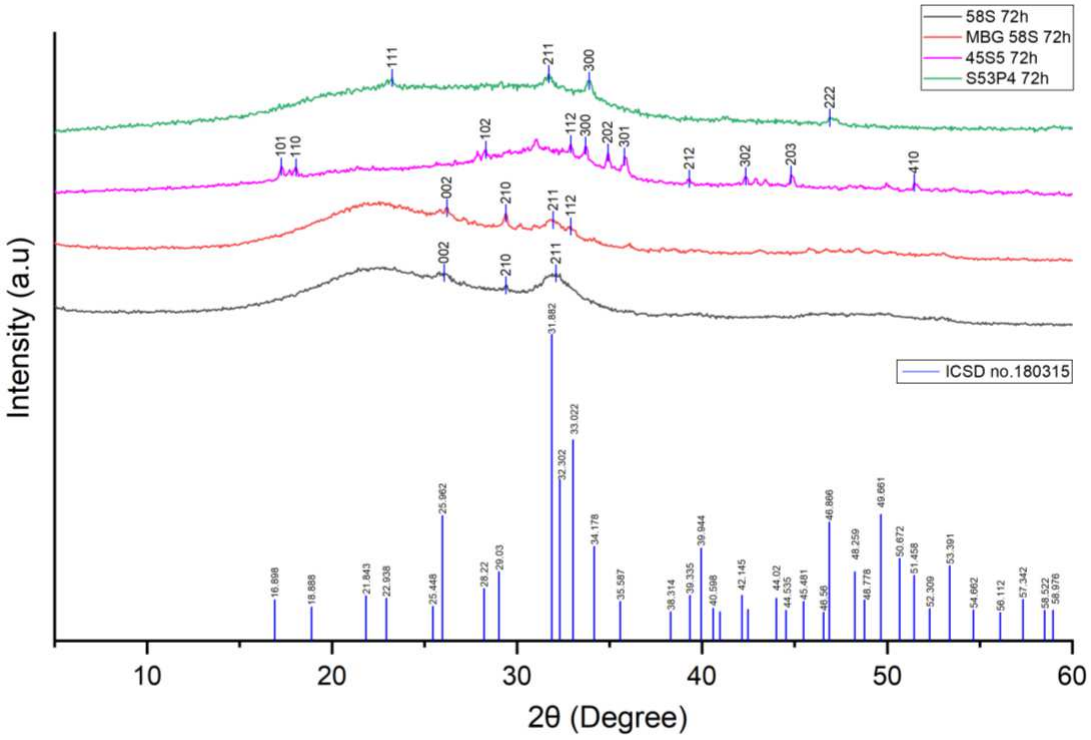

Figure 24. XDR patterns of samples after SBF immersion for 72h. The indicated planes identify HCAp crystal planes according to ICSD no.180315.

3.3.3 Biological outcomes: *in vitro* bioactivity

The metabolic assay outcomes were evaluated through both direct and indirect contact with murine fibroblast cell lines. This evaluation aimed to assess the interaction of 45S5, S53P4, 58S, and MBG 58S bioglasses. The purpose was to understand their immediate effects on target cells (direct contact) and their behavior when physically separated from the cells (extract contact).

Bioglasses 45S5 and S53P4 exhibited no cytotoxic effects in direct contact with cells across all concentrations and tested periods (24, 48, and 72 h). Notably, S53P4 bioglass demonstrated a 20% reduction in metabolic assay at 72 h and a concentration of 100 ug/mL.

Similarly, 58S and MBG 58S bioglasses displayed no decrease in metabolic activity upon direct contact with cells at 24 h for lower concentrations (10 and 100 ug/mL). However, after 48 h, a decline in metabolic activity was observed, reaching 58.63% ± 1.74 for 1000 ug/mL. When the material remained in contact with the cell for 72 h, concentrations of 500 and 750 ug/mL also showed reduced viability: 45.16% ± 1.11 and 34.43% ± 0.74, respectively, while 17.34% ± 0.82 viability was recorded.

Following the guidelines of ISO 109993/5, a decrease in cell metabolic activity of less than 70% indicates that the material causes some cell injury, and cytotoxicity should be confirmed through other assays. **Figure 25** shows the cytotoxic effect of direct contact on fibroblast proliferation for all samples across different concentrations and time intervals.

After 8, 24, and 48 h of indirect contact, all samples exhibited no cytotoxic effects on the cells at any concentration. **Figure 26** shows the cytotoxic effect on fibroblast proliferation at various concentrations and time points. The extraction process involved maintaining contact between the bioglasses and the cells for 24 h.

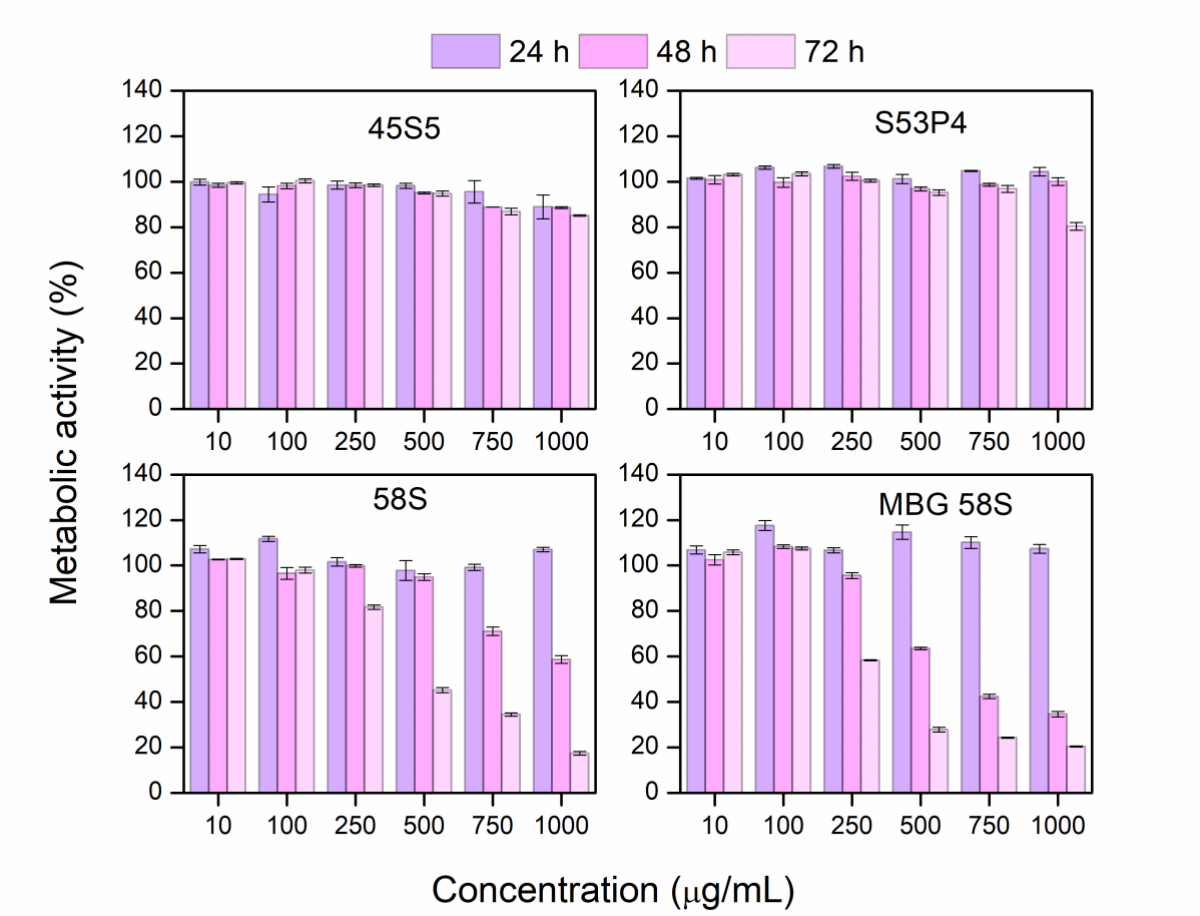

Figure 25. Metabolic activity of samples in direct contact with fibroblast cells was assessed after 24, 48, and 72 h at various concentrations (0, 10, 100, 250, 500, 750, and 1000 μg/mL).

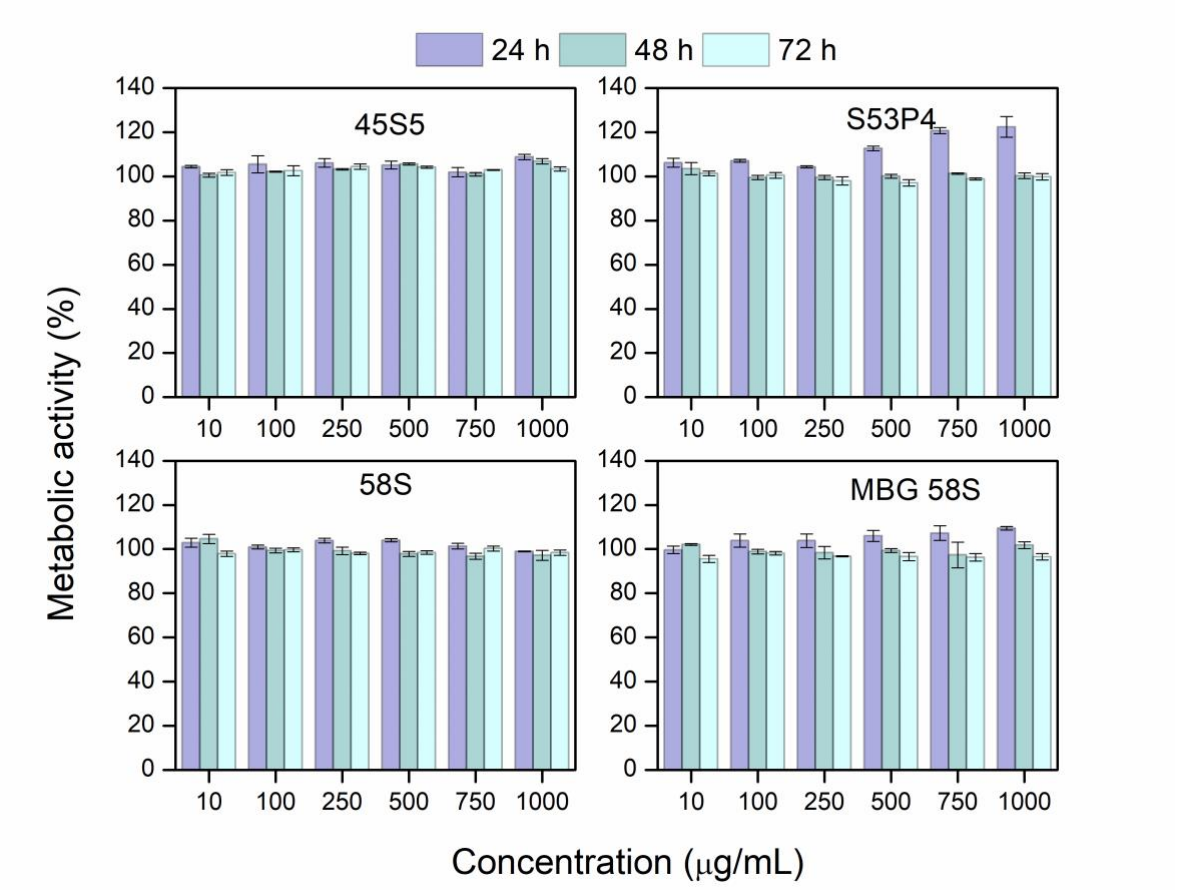

Figure 26. Metabolic activity of fibroblast cells was assessed after 24, 48, and 72 h of exposure to extracts at various concentrations (0, 10, 100, 250, 500, 750, and 1000 ug/mL).

3.4 DISCUSSION

The present study aimed to conduct a comparative assessment of four different types of Bioglasses, namely Bioglass 45S5, S53P4, 58S, and MBG 58S. The evaluation encompassed a comprehensive analysis of their physicochemical, bioactive, and biological properties. Properties that are known to influence the glass dissolution and subsequent mechanisms leading to hydroxycarbonate layer formation. Many *in vivo* studies using bioactive materials to fill bone defects have demonstrated that the rate of formation of biological apatite on the surface of these materials controls the bone in growth rate and the rate of new bone formation [25,75–77].

It is established that the processing routes, specifically melt-derived (45S5, S53P4) and sol-gel derived (58S, MBG 58S) powders, play a crucial role in influencing the physical properties of bioactive glasses. These physical properties, in turn, affect the dissolution behavior of the glasses and subsequent mechanisms leading to the formation of a hydroxycarbonate layer [23].

The synthesis route significantly influenced the physical properties of the bioactive glasses, such as particle size and thermal behavior. Sol-gel derived BGs (58S and 58S MBG) demonstrated lower temperature sensitivity and smaller particle size range compared to the melt-derived glasses (45S5 and S53P4). The composition also played a crucial role, with higher SiO_2 content resulting in higher characteristic temperatures. However, particle size analysis may have limitations, especially for small particles like those from the sol-gel method, where results could be affected by particle agglomeration. Dynamic Light Scattering (DLS) could have provided information on particle size changes due to aggregation or agglomeration, but this analysis was not included in this work. Nevertheless, SEM images supported the presented particle size range. Regarding skeletal density, all samples showed consistent results regardless of particle size or composition [23].

The mesoporous structure of the synthesized MBG could be determined by its IV type N_2 adsorption and desorption isotherm curve with a H1-type hysteresis loop at high relative pressure according to the International Union of Pure and Applied Chemistry (IUPAC) classification [12]. The present study is supported by previous investigations showing the same type of hysteresis loop in the N_2 isotherms for mesoporous materials further confirmed by TEM. To confirm the ordered mesoporous induced structure by P123 surfactant a TEM 200 need to be performed[15].

When comparing with previous works, MBG 58S exhibited a relatively lower BET surface area of $77 m^2/g$ [14]. This could be attributed to various factors during synthesis or sample preparation, including potential pore collapse or particle aggregation [13]. Previous study have reported that the increase P_2O_5 concentration could influence the particle morphology, potentially leading to a reduction in pore volume [66]. Notably, the presence of micropores, which were not effectively detected in the BET analysis, could also contribute to the observed lower surface area[12]. However, the pore volume and diameter of MBG 58S remained consistent with the literature, suggesting that overall porosity remained unaffected [78].

The simulated body fluid test, despite facing criticism for its poor *in vivo* relevance [79], is widely accepted for evaluating material bioactivity (bioreactivity). This test assesses the material's ability to induce the formation of HCAp on its surface, which is considered a marker of its bonding capacity to bone tissue [80]. The mechanism of bioactive glass apatite formation involves several steps. Initially, an ionic exchange leads to the formation of silanol groups on the biomaterial's surface, which then polymerize to create an amorphous silica gel. Subsequently, calcium and phosphate ions migrate to the newly formed silica gel and start

generating an HCAp layer, which eventually crystallizes, forming needle and cauliflower-shaped structures that are reported to promote bone cell attachment [81].

FTIR analysis showed the presence of intense peaks in the P-O stretching and C-O bending bands indicates the presence and concentration of phosphate ions and carbonate (CO_3^{2-}) in the glass matrix, respectively. These findings serve as good indicators for hydroxyapatite formation when the bioactive glasses are exposed to biological fluids and tissues[9]. A significant difference after immersion in SBF was identified at ~600 cm^{-1}. As depicted in **Figure 23**, FTIR spectra for all samples exhibited characteristic peaks associated with the formation of a hydroxyapatite layer, which has been reported in other studies as well [14,82].

XRD patterns obtained from the surfaces of the particles after 72 h of SBF immersion revealed the amorphous nature of all samples. The sol-gel derived bioglasses exhibited high-intensity crystalline peaks at 2 theta values of 31.8°, 25.9°, and 29.0°, corresponding to (211), (002), and (210) reflections of crystallized hydroxyapatite. In contrast, the melt-derived samples showed a peak at 33.0°, assigned to the (300) crystal plane. Additionally, the melt-derived samples exhibited more low-intensity peaks compared to the sol-gel derived ones. These results are consistent with previous studies that reported XRD analysis for HCAp formation [14,57,83] . As reported, the intensity of these major reflections increases with higher concentrations of Ca^{+2} and PO_4^{3-} ions on the surfaces of the bioglasses when in contact with SBF.

Moreover, the melt-derived samples showed the most defined and intense peaks, suggesting a higher crystalline quality in the hydroxyapatite crystals. However, when comparing different processing routes, the composition and morphology must be considered, such as the smaller and porous particle size of the sol-gel derived particles. The porous characteristics of these particles can preferentially promote crystal nucleation, leading to the formation of smaller hydroxyapatite crystals with a higher dispersion. Consequently, one of the limitations of the present study is the relatively short SBF immersion time, as a longer immersion period might have allowed more time for crystallization and higher formation of HCAp on the sample surfaces.

After 8 h of SBF immersion, all samples showed a decrease in the Ca/P ratio, stabilizing around 2.0 after 72 h, in line with the non-stoichiometric biological apatite molar ratio of 1.67 Ca/P [74]. The biomineralization process occurs when bioactive materials interact with SBF, where excess calcium ions from the material combine with phosphate ions from SBF, forming a hydroxyapatite (HCAp) layer on the material's surface. This process leads to a decrease in the Ca/P ratio [84]. EDS spectra supported these findings, revealing increased calcium

and phosphorus peaks and reduced silicon content (wt.%). SEM images also confirmed the presence of a hydrated silica layer on all samples' surfaces, along with precipitates indicating HCAp formation.

The shape of HCAp crystals varied depending on the processing routes, likely influenced by the porous characteristics and higher surface area of sol-gel derived glasses [12,13]. However, these images had limitations in magnification, and FESEM images could better represent the shape and morphology of HCAp formations. Variations in texture were found to be more significant in determining the dissolution and bioactive behavior of sol-gel–derived glasses than in melt-derived glasses [11,20,21]. The highly porous texture of sol-gel–derived glasses promote a higher degree of surface hydroxylation, forming a silica-rich gel layer (SiO-H), providing more nucleation sites for calcium phosphate (apatite precursor) layer [10].

Despite the extensive analysis, a limitation of this work is the lack of traceability of dissolution ions in the developed bioactive glasses. As noted by Hupa et al [72], controlled dissolution and ion release are crucial criteria for selecting novel compositions. To study the early-stage dissolution kinetics of bioactive glass without interference from HA formation, inductively coupled plasma analysis (ICP) following the TC04 (Technical Committee 4 of the International Commission on Glass) is commonly used for ion analysis. The concentrations of ions released from the glass can be used to assess its potential to activate cellular processes in tissue regeneration, compared to well-established glass compositions.

Finally, a biological *in vitro* evaluation was conducted to assess and address this behavior. The bioactive glasses derived from the melt-derived route (45S5 and S53P4) exhibited non-cytotoxic effects on fibroblast proliferation during direct contact. This outcome remained consistent across different time intervals and concentrations. In contrast, bioglasses obtained through the sol-gel method displayed a significant reduction in metabolic activity, especially at elevated concentrations and prolonged contact periods (72 h). This decline surpassed the ISO 109993/5 threshold of 70%, indicating potential cell injury and cytotoxicity.

This observed behavior in sol-gel-derived bioglasses might be linked to their higher dissolution rates, a phenomenon previously associated with inducing cytotoxic effects [85] . The alteration in pH and ion concentration within the surrounding media, due to glass dissolution, was identified as a key factor contributing to this effect. Elevated dissolution rates led to a decrease in pH and an increase in ion concentration in the media, ultimately resulting in heightened cytotoxicity. This acidification of the media was attributed to ion dissolution, particularly in glasses containing high P_2O_5 concentrations [66,67]. The distinct behavior accentuates the heightened sensitivity to sample concentration and time, implying that in future

biological assessments, it would be prudent to employ lower quantities of sol-gel-derived particles. A limitation of this study is the assessment of P_2O_5 sensitivity in biological assays when contrasted with the BG 58S nominal composition (4wt.%) under identical conditions.

The interplay between "bioactivity" assessment and cytocompatibility evaluation holds significance, even though bioactivity assessment demands more rigorous methods. For a comprehensive risk evaluation of such materials, the connection between these two assessments must be acknowledged.

For the first time, we conducted a comprehensive assessment comparing four different bioactive glasses produced through distinct processing routes, evaluating their physicochemical, bioactivity, and biological properties. It was essential to utilize consistent instrumental analysis methods to compare the physical properties of the melt-derived glasses (45S5 and S53P4) with the sol-gel-derived glasses (58S and MBG 58S). Notable variations were observed in particle size, porosity, and the morphology of hydroxyapatite layer formation – a crucial factor in nucleation site preferences. While bioactivity properties were generally similar among all glass compositions, special attention was directed toward characterizing the mesoporous structure of the 58S composition. Although the dissolution behavior was not covered in this study and was reported elsewhere [10,72], the biological assays yielded valuable insights for future applications. These results underscore the significance of processing routes in influencing outcomes, as evidenced by the observed differences in cytotoxicity among the various glasses.

All four glasses are well-known for their high level of bioactivity both *in vitro* and *in vivo*, and their selection should consider the application site. Overall, with sufficient data, glass compositions can be tailored to meet specific properties required for different applications. The development of these distinct bioactive glasses provides a promising outlook for a wide range of biomedical applications, offering opportunities to enhance tissue regeneration and clinical outcomes. However, further research and in-depth investigations are necessary to fully comprehend the potential and limitations of each glass composition, enabling their optimal utilization in diverse biomedical fields.

3.5 CONCLUSION

In conclusion, this study compared four bioactive glasses with different processing routes, assessing their physicochemical, bioactive, and biological properties. The synthesis route significantly influenced physical properties, dissolution behavior, and hydroxycarbonate layer formation. The sol-gel derived glasses showed lower temperature sensitivity and smaller particle size ranges, while the melt-derived glasses had higher temperature sensitivity. Both glasses exhibited similar bioactivity, but further research is needed to fully understand their potential and limitations. 58S and MBG58S with 9 wt.% P_2O_5 are promising candidates for biomaterial applications, with distinct advantages such as rapid hydroxyapatite formation and enhanced bioactivity due to their unique mesoporous structure and composition. The differences between route process serve to illustrate the importance in understanding the material properties to predict their biological performance. For the continuation of this work, we suggest the following:

- Assess static and dynamic dissolution behavior and ion concentration release through ICP-OES analysis.
- Measure the pH of the samples upon contact with SBF.
- Conduct a comparison to gain a deeper understanding of the biological sensitivity towards changes in P_2O_5 concentration.
- Undertake additional biological assays.
- Conduct further clinical trials, including *in vivo* evaluations.

CHAPTER 4 - FINAL REMARKS

Bioactive glasses have been developed to address the needs of tissue bonding, necessitating a comprehensive understanding of their properties for specific applications and product manufacturing. To address the complex and unpredictable load-bearing conditions, 3D scaffolds have been designed, incorporating bioactive glasses either for enhanced drug delivery or in combination. The selection of glass composition demands a deep understanding of how major components influence relevant properties, considering both end use and manufacturing. *In vitro* studies offer a reliable means of predicting bioactive glass behavior *in vivo*, despite limitations in appropriate animal models that bridge preclinical and clinical applications. This study presents a thorough systematic review of *in vivo* evaluation scenarios for bioactive glasses, with a focus on critical bone defects. Moreover, a comparative analysis of four distinct bioactive glasses—45S5, S53P4, 58S, and MBG 58S—from both melt and sol-gel routes has been conducted. All compositions demonstrated the capability to develop a hydroxyapatite (HCAp) layer and exhibited positive biological outcomes, such as non-cytotoxicity *in vitro*. However, further investigations are essential to assess dissolution behavior and conduct *in vivo* studies for a comprehensive understanding.

REFERÊNCIAS

1. Schemitsch EH. Size Matters: Defining Critical in Bone Defect Size! *J Orthop Trauma*. 2017;31(10):S20-S22. doi:10.1097/BOT.0000000000000978
2. Mirabello L, Troisi RJ, Savage SA. Investing in workforce literacy pays : building employer commitment to workplace language, literacy and numeracy programs : [summary report]. *Internal Journal of Cancer*. 2011;125(1):229-234. doi:10.1002/ijc.24320.International
3. Dimitrou, Rozalia; Jones, Elena; McGonale DGVP. Bone regeneration: current concepts and future directions. *BMC Med*. 2011;6(66):1741-7015.
4. Jones JR, Brauer DS, Hupa L, Greenspan DC. Bioglass and Bioactive Glasses and Their Impact on Healthcare. *Int J Appl Glass Sci*. 2016;7(4):423-434. doi:10.1111/ijag.12252
5. Hench LL. Genetic design of bioactive glass. *J Eur Ceram Soc*. 2009;29(7):1257-1265. doi:10.1016/j.jeurceramsoc.2008.08.002
6. Liu I, Karlsson KH. *In Vivo Behaviour of Glasses in the SiO_2-Na_20-CaO-P_2Q. ;-AI203-B203 System*.; 1990.
7. Lindfors NC, Hyvönen P, Nyyssönen M, et al. Bioactive glass S53P4 as bone graft substitute in treatment of osteomyelitis. *Bone*. Published online 2010. doi:10.1016/j.bone.2010.05.030
8. Van Gestel NAP, Geurts J, Hulsen DJW, Van Rietbergen B, Hofmann S, Arts JJ. Clinical Applications of S53P4 Bioactive Glass in Bone Healing and Osteomyelitic Treatment: A Literature Review. *Biomed Res Int*. 2015;2015. doi:10.1155/2015/684826
9. Kim CY, Clark E, Hench LL. *Stages of calcium-phosphate layer formation in bioglasses*. Vol 113.; 1989.
10. Pereira MM, Hench LL. *Mechanisms of Hydroxyapatite Formation on Porous Gel-Silica Substrates*. Vol 7. Kluwer Academic Publishers; 1996.
11. Li R, Clark AE, Hench LL. *An Investigation of Bioactive Glass Powders by Sol-Gel Processing*.
12. Vallet-Regí M, Balas F, Arcos D. Mesoporous materials for drug delivery. *Angewandte Chemie - International Edition*. 2007;46(40):7548-7558. doi:10.1002/anie.200604488
13. Zhao L, Yan X, Zhou X, et al. Mesoporous bioactive glasses for controlled drug release. *Microporous and Mesoporous Materials*. 2008;109(1-3):210-215. doi:10.1016/j.micromeso.2007.04.041
14. Galarraga-Vinueza ME, Mesquita-Guimarães J, Magini RS, Souza JCM, Fredel MC, Boccaccini AR. Mesoporous bioactive glass embedding propolis and cranberry antibiofilm compounds. *J Biomed Mater Res A*. 2018;106(6):1614-1625. doi:10.1002/jbm.a.36352
15. Wu C, Chang J. Mesoporous bioactive glasses: Structure characteristics, drug/growth factor delivery and bone regeneration application. *Interface Focus*. 2012;2(3):292-306. doi:10.1098/rsfs.2011.0121
16. El-Rashidy AA, Roether JA, Harhaus L, Kneser U, Boccaccini AR. Regenerating bone with bioactive glass scaffolds: A review of in vivo studies in bone defect models. *Acta Biomater*. 2017;62:1-28. doi:10.1016/j.actbio.2017.08.030
17. Pearce AI, Richards RG, Milz S, Schneider E, Pearce SG. Animal models for implant biomaterial research in bone: A review. *Eur Cell Mater*. 2007;13:1-10. doi:10.22203/eCM.v013a01
18. Azevedo VVC, Chaves S a, Bezerra DC, Fook MVL, Costa a CFM. Quitina e Quitosana: aplicações como biomateriais. *Revista Eletrônica de Materiais e Processos*. 2007;2.3:27-34.

19. Baino F, Hamzehlou S, Kargozar S. Bioactive glasses: Where are we and where are we going? *J Funct Biomater*. 2018;9(1). doi:10.3390/jfb9010025
20. Li R, Clark AE, Hench LL. Effects of structure and surface area on bioactive powders by sol-gel process. *Fifth Ultrastructure Processing Conference* . Published online February 1991:627-633.
21. Pereira MM, Clark AE, Hench LL. *Effect of Texture on the Rate of Hydroxyapatite Formation on Gel-Silica Surface*. Vol 78.; 1995.
22. Silver IA, Deas J, Erecińska M. Interactions of bioactive glasses with osteoblasts in vitro: Effects of 45S5 Bioglass(®), and 58S and 77S bioactive glasses on metabolism, intracellular ion concentrations and cell viability. *Biomaterials*. 2001;22(2):175-185. doi:10.1016/S0142-9612(00)00173-3
23. Sepulveda P, Jones JR, Hench LL. Characterization of melt-derived 45S5 and sol-gel-derived 58S bioactive glasses. *J Biomed Mater Res*. 2001;58(6):734-740. doi:10.1002/jbm.10026
24. Pereira R do V. *Desenvolvimento de scaffolds biodegradáveis de PLDLA/biovidro 58S produzidos por sinterização seletiva a laser*. Universidade Federal de Santa Catarina; 2013.
25. Hench LL, West JK. Biological applications of bioactive glasses. *Harwood Academic Publishers*. Published online 1996.
26. Stevens MM. Biomaterials for bone tissue engineering. *Materials Today*. 2008;11(5):18-25. doi:10.1016/S1369-7021(08)70086-5
27. Civinini R, Macera A, Nistri L, Redl B, Innocenti M. *The Use of Autologous Blood-Derived Growth Factors in Bone Regeneration*. Vol 8.; 2011.
28. Ya-dong ZHAnG GWaYSCQZha. Combination of platelet-rich plasma with degradable bioactive borate glass for segmental bone defect repair. *Acta Orthop Belg*. 2011;77:110-115.
29. Gothard D, Smith EL, Kanczler JM, et al. Tissue engineered bone using select growth factors: A comprehensive review of animal studies and clinical translation studies in man. *Eur Cell Mater*. 2014;28:166-208. doi:10.22203/eCM.v028a13
30. Park J, Lakes RS. *Biomaterials: An Introduction: Third Edition*.; 2007. doi:10.1007-978-0-387-37880-0
31. Page MJ, McKenzie JE, Bossuyt PM, et al. The PRISMA 2020 statement: An updated guideline for reporting systematic reviews. *The BMJ*. 2021;372. doi:10.1136/bmj.n71
32. Wang H, Zhao S, Xiao W, et al. Three-dimensional zinc incorporated borosilicate bioactive glass scaffolds for rodent critical-sized calvarial defects repair and regeneration. *Colloids Surf B Biointerfaces*. 2015;130:149-156. doi:10.1016/j.colsurfb.2015.03.053
33. Boyd D, Carroll G, Towler MR, Freeman C, Farthing P, Brook IM. Preliminary investigation of novel bone graft substitutes based on strontium-calcium-zinc-silicate glasses. *J Mater Sci Mater Med*. 2009;20(1):413-420. doi:10.1007/s10856-008-3569-0
34. Zhao H, Liang G, Liang W, et al. In vitro and in vivo evaluation of the pH-neutral bioactive glass as high performance bone grafts. *Materials Science and Engineering C*. 2020;116. doi:10.1016/j.msec.2020.111249
35. El-Meliegy E, Hamzawy EMA, El-Kady AM, Salama A, El-Rashedi A. Development and bioactivity evaluation of bioglasses with low Na_2O content based on the system Na_2O-CaO-MgO-P_2O_5-SiO_2. *J Mater Sci Mater Med*. 2012;23(9):2069-2080. doi:10.1007/s10856-012-4681-8

36. Qi X, Wang H, Zhang Y, et al. Mesoporous bioactive glass-coated 3D printed borosilicate bioactive glass scaffolds for improving repair of bone defects. *Int J Biol Sci*. 2018;14(4):471-484. doi:10.7150/ijbs.23872
37. Moon HJ, Kim KN, Kim KM, et al. Bone formation in calvarial defects of Sprague-Dawley rats by transplantation of calcium phosphate glass. *J Biomed Mater Res A*. 2005;74(3):497-502. doi:10.1002/jbm.a.30408
38. Sui B, Zhong G, Sun J. Evolution of a mesoporous bioactive glass scaffold implanted in rat femur evaluated by 45Ca labeling, tracing, and histological analysis. *ACS Appl Mater Interfaces*. 2014;6(5):3528-3535. doi:10.1021/am4056886
39. Liu X, Rahaman MN, Fu Q. Bone regeneration in strong porous bioactive glass (13-93) scaffolds with an oriented microstructure implanted in rat calvarial defects. *Acta Biomater*. 2013;9(1):4889-4898. doi:10.1016/j.actbio.2012.08.029
40. Gu Y, Huang W, Rahaman MN, Day DE. Bone regeneration in rat calvarial defects implanted with fibrous scaffolds composed of a mixture of silicate and borate bioactive glasses. *Acta Biomater*. 2013;9(11):9126-9136. doi:10.1016/j.actbio.2013.06.039
41. Lin Y, Xiao W, Liu X, Bal BS, Bonewald LF, Rahaman MN. Long-term bone regeneration, mineralization and angiogenesis in rat calvarial defects implanted with strong porous bioactive glass (13-93) scaffolds. *J Non Cryst Solids*. 2016;432:120-129. doi:10.1016/j.jnoncrysol.2015.04.008
42. Lehman LFC, de Noronha MS, Diniz IMA, et al. Bioactive glass containing 90% SiO_2 in hard tissue engineering: An in vitro and in vivo characterization study. *J Tissue Eng Regen Med*. 2019;13(9):1651-1663. doi:10.1002/term.2919
43. Covarrubias C, Cádiz M, Maureira M, Celhay I, Cuadra F, von Marttens A. Bionanocomposite scaffolds based on chitosan–gelatin and nanodimensional bioactive glass particles: In vitro properties and in vivo bone regeneration. *J Biomater Appl*. 2018;32(9):1155-1163. doi:10.1177/0885328218759042
44. Bi L, Jung S, Day D, et al. Evaluation of bone regeneration, angiogenesis, and hydroxyapatite conversion in critical-sized rat calvarial defects implanted with bioactive glass scaffolds. *J Biomed Mater Res A*. 2012;100 A(12):3267-3275. doi:10.1002/jbm.a.34272
45. Ding J, Zhao J, Wang L, et al. Regulated contribution of local and systemic immunity to new bone regeneration by modulating B/Sr concentration of bioactive borosilicate glass. *Mater Today Bio*. 2023;19. doi:10.1016/j.mtbio.2023.100585
46. Gu Y, Wang G, Zhang X, et al. Biodegradable borosilicate bioactive glass scaffolds with a trabecular microstructure for bone repair. *Materials Science and Engineering C*. 2014;36(1):294-300. doi:10.1016/j.msec.2013.12.023
47. Björkenheim R, Strömberg G, Ainola M, et al. Bone morphogenic protein expression and bone formation are induced by bioactive glass S53P4 scaffolds in vivo. *J Biomed Mater Res B Appl Biomater*. 2019;107(3):847-857. doi:10.1002/jbm.b.34181
48. Lalzawmliana V, Anand A, Kumar V, et al. Potential of growth factor incorporated mesoporous bioactive glass for in vivo bone regeneration. *J Mech Behav Biomed Mater*. 2019;91:182-192. doi:10.1016/j.jmbbm.2018.12.012

49. Niu Y, Guo L, Liu J, et al. Bioactive and degradable scaffolds of the mesoporous bioglass and poly(l-lactide) composite for bone tissue regeneration. *J Mater Chem B*. 2015;3(15):2962-2970. doi:10.1039/c4tb01796j
50. Khan PK, Mahato A, Kundu B, et al. Influence of single and binary doping of strontium and lithium on in vivo biological properties of bioactive glass scaffolds. *Sci Rep*. 2016;6. doi:10.1038/srep32964
51. Anesi A, Ferretti M, Salvatori R, et al. In-vivo evaluations of bone regenerative potential of two novel bioactive glasses. *J Biomed Mater Res A*. Published online March 6, 2023. doi:10.1002/jbm.a.37526
52. Zhao S, Zhang J, Zhu M, et al. Three-dimensional printed strontium-containing mesoporous bioactive glass scaffolds for repairing rat critical-sized calvarial defects. *Acta Biomater*. 2015;12(1):270-280. doi:10.1016/j.actbio.2014.10.015
53. Qi X, Pei P, Zhu M, et al. Three dimensional printing of calcium sulfate and mesoporous bioactive glass scaffolds for improving bone regeneration in vitro and in vivo. *Sci Rep*. 2017;7. doi:10.1038/srep42556
54. Zhao H, Liang G, Liang W, et al. In vitro and in vivo evaluation of the pH-neutral bioactive glass as high performance bone grafts. *Materials Science and Engineering C*. 2020;116. doi:10.1016/j.msec.2020.111249
55. Brink M. *The Influence of Alkali and Alkaline Earths on the Working Range for Bioactive Glasses*.; 1997.
56. Yan X, Yu C, Zhou X, Tang J, Zhao D. Highly Ordered Mesoporous Bioactive Glasses with Superior In Vitro Bone-Forming Bioactivities. *Angewandte Chemie*. Published online 2004. doi:10.1002/ange.200460598
57. Xia W, Chang J. Well-ordered mesoporous bioactive glasses (MBG): A promising bioactive drug delivery system. *Journal of Controlled Release*. 2006;110(3):522-530. doi:10.1016/j.jconrel.2005.11.002
58. Bi L, Rahaman MN, Day DE, et al. Effect of bioactive borate glass microstructure on bone regeneration, angiogenesis, and hydroxyapatite conversion in a rat calvarial defect model. *Acta Biomater*. 2013;9(8):8015-8026. doi:10.1016/j.actbio.2013.04.043
59. Ege D, Zheng K, Boccaccini AR. Borate Bioactive Glasses (BBG): Bone Regeneration, Wound Healing Applications, and Future Directions. *ACS Appl Bio Mater*. 2022;5(8):3608-3622. doi:10.1021/acsabm.2c00384
60. Zhang D, Leppäranta O, Munukka E, et al. Antibacterial effects and dissolution behavior of six bioactive glasses. *J Biomed Mater Res A*. Published online 2010. doi:10.1002/jbm.a.32564
61. Kaur G, Pickrell G, Sriranganathan N, Kumar V, Homa D. Review and the state of the art: Sol–gel and melt quenched bioactive glasses for tissue engineering. *J Biomed Mater Res B Appl Biomater*. 2016;104(6):1248-1275. doi:10.1002/jbm.b.33443
62. Wang X, Mabrey JD, Agrawal CM. An interspecies comparison of bone fracture properties. *Biomed Mater Eng*. 1998;8 1:1-9.
63. Jones JR. Review of bioactive glass: From Hench to hybrids. *Acta Biomater*. Published online 2013. doi:10.1016/j.actbio.2012.08.023
64. Hench LL. The story of Bioglass®. In: *Journal of Materials Science: Materials in Medicine*. ; 2006. doi:10.1007/s10856-006-0432-z
65. Hench LL. Chronology of Bioactive Glass Development and Clinical Applications. *New Journal of Glass and Ceramics*. 2013;03(02):67-73. doi:10.4236/njgc.2013.32011

66. Ahmadi SM, Behnamghader A, Asefnejaad A. *Sol-Gel Synthesis, Characterization, and in Vitro Evaluation of $SiO_2-CaO-P_2O_5$ Bioactive Glass Nanoparticles with Various CaO/P_2O_5 Ratios*. Vol 12.

67. Kaur G, Pickrell G, Sriranganathan N, Kumar V, Homa D. Review and the state of the art: Sol–gel and melt quenched bioactive glasses for tissue engineering. *J Biomed Mater Res B Appl Biomater*. 2016;104(6):1248-1275. doi:10.1002/jbm.b.33443

68. Madejová J. *FTIR Techniques in Clay Mineral Studies*.

69. Kokubo T, Takadama H. How useful is SBF in predicting in vivo bone bioactivity? *Biomaterials*. 2006;27(15):2907-2915. doi:10.1016/j.biomaterials.2006.01.017

70. Sing KSW. Reporting physisorption data for gas/solid systems with special reference to the determination of surface area and porosity (Recommendations 1984). *Pure and Applied Chemistry*. 1985;57(4):603-619. doi:doi:10.1351/pac198557040603

71. Filho OP, Latorre GP, Hench2 LL. *Effect of Crystallization on Apatite-Layer Formation of Bioactive Glass 45%*.

72. Hupa L. Composition-property relations of bioactive silicate glasses. *Bioactive Glasses*. Published online 2018:1-35. doi:10.1016/b978-0-08-100936-9.00001-0

73. Vedel E, Arstila H, Ylänen H, Hupa L, Hupa M. Predicting physical and chemical properties of bioactive glasses from chemical composition. Part 1: Viscosity characteristics. *Glass Technology: European Journal of Glass Science and Technology Part A*. Published online 2008.

74. Stanciu GA, Sandulescu I, Savu B, et al. Investigation of the Hydroxyapatite Growth on Bioactive Glass Surface. *Journal of Biomedical & Pharmaceutical Engineering*. 2007;1:34-39.

75. Wheeler DL, Stokes KE, Hoellrich RG, Chamberland DL, Mcloughlin SW. *Effect of Bioactive Glass Particle Size on Osseous Regeneration of Cancellous Defects*. Vol 41.; 1998.

76. Ohgushi H, Okumura M, Yoshikawa T, et al. *Bone Formation Process in Porous Calcium Carbonate and Hydroxyapatite*.

77. Gauthier O, Bouler JM, Weiss P, Bosco J, Aguado E, Daculsi G. *Short-Term Effects of Mineral Particle Sizes on Cellular Degradation Activity After Implantation of Injectable Calcium Phosphate Biomaterials and the Consequences for Bone Substitution*.; 1999.

78. Lu JX, Flautre B, Anselme K, et al. *Role of Interconnections in Porous Bioceramics on Bone Recolonization in Vitro and in Vivo*. Vol 10.; 1999.

79. Bohner M, Lemaitre J. Can bioactivity be tested in vitro with SBF solution? *Biomaterials*. 2009;30(12):2175-2179. doi:10.1016/j.biomaterials.2009.01.008

80. Maçon ALB, Kim TB, Valliant EM, et al. A unified in vitro evaluation for apatite-forming ability of bioactive glasses and their variants. *J Mater Sci Mater Med*. 2015;26(2):1-10. doi:10.1007/s10856-015-5403-9

81. Goh YF, Alshemary AZ, Akram M, Abdul Kadir MR, Hussain R. Bioactive Glass: An In-Vitro Comparative Study of Doping with Nanoscale Copper and Silver Particles. *Int J Appl Glass Sci*. 2014;5(3):255-266. doi:10.1111/ijag.12061

82. Zhang X, Zeng D, Li N, et al. Functionalized mesoporous bioactive glass scaffolds for enhanced bone tissue regeneration. *Sci Rep*. 2016;6. doi:10.1038/srep19361

83. Lombardi M, Gremillard L, Chevalier J, et al. A comparative study between melt-derived and sol-gel synthesized 45S5 bioactive glasses. *Key Eng Mater*. 2013;541:15-30. doi:10.4028/www.scientific.net/KEM.541.15

84. Lu J, Descamps M, Dejou J, et al. The biodegradation mechanism of calcium phosphate biomaterials in bone. In: *Journal of Biomedical Materials Research*. Vol 63. ; 2002:408-412. doi:10.1002/jbm.10259

85. Sepulveda P, Jones JR, Hench LL. *In Vitro Dissolution of Melt-Derived 45S5 and Sol-Gel Derived 58S Bioactive Glasses*.; 2002.